The Dissertation Committee for Clément Cros Certifies that this is the approved version of the following dissertation:

The Use of Selective Materials to Reduce Human Exposure to Ozone and Oxides of Nitrogen

Committee:

Richard L. Corsi, Supervisor

Maria G. Juenger, Co-Supervisor

Atila Novoselac

Ying Xu

David T. Allen

The Use of Selective Materials to Reduce Human Exposure to Ozone and Oxides of Nitrogen

by

Clément Cros, B.S.E.; M.S.E.

Dissertation

Presented to the Faculty of the Graduate School of

The University of Texas at Austin

in Partial Fulfillment

of the Requirements

for the Degree of

Doctor of Philosophy

The University of Texas at Austin

May 2013

Dedication

To my family, for supporting me through anything.

Acknowledgements

I would like to acknowledge my advisors Dr. Richard Corsi and Dr. Maria Juenger for giving the chance to pursue my Ph.D. and supporting and guiding me through this work with patience, and kindness. I would also like to thank Dr. Neil Crain, who made so much of my research possible, for his great expertise in the laboratory and for his priceless advice. A big thank you to Dori Eubank, Susan McCoy and Steve Orwick for always being on top of things, efficient and making our lives so much easier, while being the nicest people anyone could ever hope to work with. I would also like to thank my fellow graduate students in the air research group for making my transition to the U.S. easy, for their help and for making things enjoyable in and out of the lab: Priscilla Guerrero, Erin Darling, Matt Earnest, Alexandra Terpeluk, Rachel Cano, Lisa Beck, Elliot Gall, James Lo, Brent Stephens, Brandon Boor, Jordan Clark, Yuiri Lang, Shichao Liu, Jorge Urquidi.

I would like to acknowledge my funding sources, including the Norm Hackerman Advanced Research Program, Texas Higher Education Coordinating Board grant 003658-0279-2007, the United States Green Building Council grant 00021625, and the Texas Department of Transportation (project #6636).

Finally, I would like to thank my family – maman, papa, mamy, papy, Florent, Pierre, Michel, Véronique, Solène – and my dear friends – Marion, Johanna, Sabrina, Laura, Aude, Mathilde, Stéphanie, Maëlle, Catherine, Corin, Kieran, Cédric, Éléna, Natalia, Fernando, Mateo, Anne, Aurore, Jordan, Fi, Danny, Joe, Laurène, Laure, Claire, Gaëlle, Arielle, Carolina – for their unconditional support.

The Use of Selective Materials to Reduce Human Exposure to Ozone and Oxides of Nitrogen

Clément Cros, Ph.D.

The University of Texas at Austin, 2013

Supervisors: Richard L. Corsi, Maria G. Juenger.

Ozone (O_3) and oxides of nitrogen (NO_x) are ubiquitous pollutants in many urban areas around the world. Though they mostly originate outdoors, human inhalation exposure to these pollutants largely occurs indoors, because of the large fraction of our time spent inside buildings. Exposure to O_3 and nitrogen dioxide (NO_2) has been associated with decreased respiratory function, onset of asthma, and cardiovascular events. Through laboratory testing, field exposure and modeling, this study evaluates the feasibility and long-term efficiency of using passive removal materials (PRMs) both indoors and outdoors for removal of O_3 and NO_x.

Three photocatalytic coatings used outdoors and four indoor building materials were tested for their capacity to remove NO_x and O_3. Since materials outdoors experience a wider range of environmental conditions than indoors, their effects on NO_x removal by photocatalytic coatings were evaluated through full factorial experiments representative of summertime outdoor conditions in Southeast Texas. Photocatalytic coatings were also exposed to real outdoor environments for a year to assess their long-term viability. Indoor materials were exposed to real indoor environments for a six-month period and tested monthly for their capacity to remove O_3. Carbonyl emissions from these materials before and after exposure to O_3 were also tested at regular intervals during the six-month period.

Finally, removal capacity of NO and NO_2 by new indoor building materials was tested as well.

For outdoor PRMs, results suggest that the effect of certain environmental parameters (contact time, relative humidity, temperature) on NO_x removal effectiveness are consistent across different photocatalytic coatings, while other effects are coating specific. The type of semiconductor used and resistance to wear of the coating are important factors in its ability to retain removal efficacy over time. For indoor PRMs, two of the four materials tested, an activated carbon mat and perlite-based ceiling tiles, exhibited consistent O_3 removal effectiveness over time with low carbonyl emissions, both before and after ozonation. All materials except for activated carbon mat had higher post-ozonation than pre-ozonation emissions. Post-ozonation emissions were dominated by nonanal.

Simulation of the use of indoor and outdoor PRMs on a model building through multi-zone/CFD modeling showed that indoor PRMs alone could lead to concentration reductions up to 18 % for O_3 and 23 % for NO_2 in rooms of the model building selected. Addition of PRMs on the outside of the building led to small reductions in pollutant concentrations in the air infiltrating into the building, leading to negligible changes in indoor concentrations.

Table of Contents

List of Tables

List of Figures

1. Introduction

1.1. PROBLEM STATEMENT

Oxides of nitrogen (NO_x) and ozone (O_3) are inter-related pollutants originating mostly outdoors. Oxides of nitrogen are products of combustion processes taking place in power production facilities, industries and road vehicles [1] and are present at elevated levels in most urban areas. They are precursors to the formation of O_3 [2] through photochemical processes. Exposure to O_3 and nitrogen dioxide (NO_2) has been associated with a range of adverse health effects such as decreases in respiratory functions [3-9], onset of asthma [10-12] and cardiovascular events [13-15]. In the absence of indoor sources, levels of these pollutants are usually lower indoors than outdoors, due to homogeneous and heterogeneous reactions indoors [16, 17]. However, since people in developed countries spend most of their time indoors [18], a large fraction of their exposure to pollutants of outdoor origin occurs indoors. Weschler [19] estimated that about half of the U.S. population's exposure to O_3 occurs indoors. Similarly, Levy et al. [17] noted that personal exposures to NO_x were more strongly correlated to indoor concentrations than outdoor concentrations. When indoor sources of these pollutants, such as gas stoves for NO_x [20] or certain types of air cleaners for O_3 [21], are present, the fraction of exposure occurring indoors is even higher.

Finding innovative ways to reduce concentrations of these pollutants in the indoor environment could have beneficial health effects. Conventional strategies for reducing pollutant levels indoors include source control, ventilation and use of active engineered systems (e.g. devices integrated in the HVAC system or portable air cleaners). Since O_3 originates mostly outdoors and the primary source of NO_x in many homes is outdoor air, source control requires control of their sources outdoors. This has been the focus of

legislation related to these pollutants in the past decades, e.g. in North America, Europe and Asia [22]. Emission reductions have been generally successful [23, 24]. However, concentrations of these pollutants remain high and several urban areas are still in non-attainment in the United States. Providing more outdoor air to buildings is not an appropriate solution for pollutants originating outdoors. On the other hand, reducing ventilation has been the trend in new and retrofitted buildings in order to reduce energy consumption due to heating and air conditioning. In the case of O_3, reducing building air exchange rates leads to increased exposure to the products of ozone-initiated chemistry [25], some of which may be even more harmful than O_3 itself [26]. Finally, the use of engineered systems can be applied to reduce levels of contaminants inside buildings but often involves a tradeoff associated with increased energy usage.

The use of existing building surfaces indoors has been investigated as a way to passively remove pollutants [27, 28], with a recent focus on O_3 [29-32]. This is a passive solution that can be implemented to improve indoor air quality while precluding any energy penalty. The surface-to-volume ratio indoors is large, which is an advantage for heterogeneous removal of pollutants as it increases the probability of pollutant molecules coming in contact with reactive surfaces. Hence, using properly selected indoor building materials that have the ability to remove O_3 while emitting no to low levels of by-products appears to be an attractive solution if it is viable for long-term applications.

In addition to indoor surfaces, outdoor surfaces might also be useful for pollutant removal. Air flows around a building before penetrating the building envelope through openings. Reactive materials placed on the building envelope might capture some pollutants before they can reach the indoor environment. Materials placed outdoors are subject to environmental conditions (e.g., temperature, relative humidity, air speeds) that usually vary in a wider range than they vary indoors, and effects of these parameters

should be taken into account when evaluating effectiveness of outdoor building materials for pollutant removal. However, the outdoor environment also presents opportunities for use of renewable, e.g., solar, energy that can increase removal through surface reactions. The use of outdoor surfaces has been investigated for passive removal of NO_x by photocatalytic materials [33-37]. These materials contain a semiconductor that, once activated by UV light, can catalyze water molecules adsorbed at the material surface to form hydroxyl radicals [38], which in turn react with pollutant molecules adsorbed at the material surface [39]. Hence, using properly selected materials applied on building façades that have the ability to remove NO_x in a wide range of environmental conditions is an attractive solution if it is viable for long-term applications.

1.2. RESEARCH OBJECTIVES

The general objective of this dissertation is to evaluate the feasibility and long-term effectiveness of solutions involving passive removal of pollutants on building material surfaces and surface coatings. Such materials are hereafter referred to as passive removal materials (PRMs).

Specific objectives are to:

1. Determine the NO_x removal capacity of photocatalytic paints and coatings.
2. Determine important environmental parameters influencing the removal effectiveness of NO_x by photocatalytic paints and coatings.
3. Determine kinetic parameters for removal of NO_x by photocatalytic paints and coatings.
4. Determine the capacity of a select group of building materials to remove O_3 and NO_x from indoor air.

5. Determine by-products resulting from O_3 reactions on the surfaces of these indoor materials.
6. Model O_3 and NO_x concentration reductions by use of reactive materials indoors and a combination of both indoors and outdoors for a representative building.

1.3. SCOPE OF RESEARCH

This research was completed in three major phases as follows, summarized schematically in Figure 1.1:

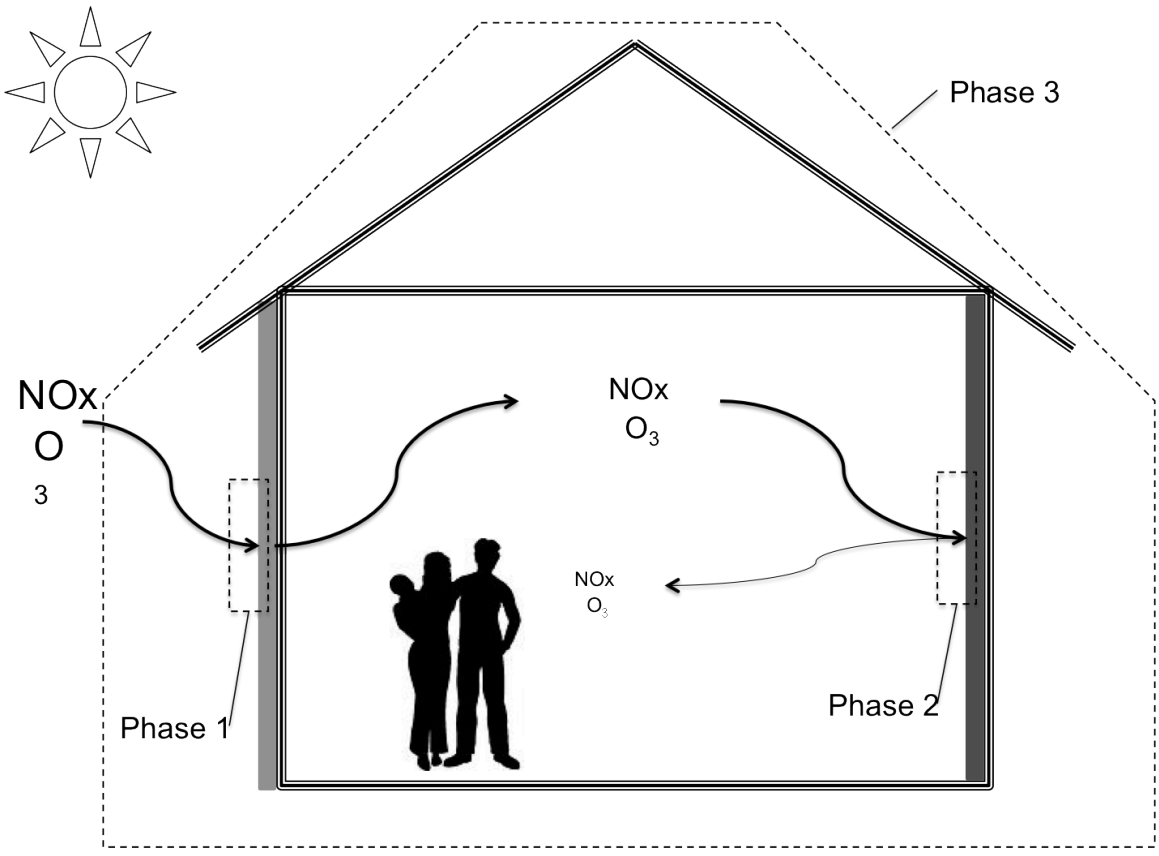

Figure 1.1. Graphical summary of research phases

- **Phase 1: Outdoor PRMs.** The first phase consisted of laboratory experiments on photocatalytic coatings to determine the effects of environmental parameters on deposition of NO_x on these coatings outdoors. The parameters considered were temperature, light intensity, relative humidity (RH), contact time, and inorganic and organic pollutant concentrations. The experiments were completed in a stainless-steel reactor with a flow-through design equipped with UV lights and thermal and humidity regulation. Pollutants included in the air mixture were ozone, nitric oxide (NO), nitrogen dioxide, propane and propylene. Oxidation of volatile organic compounds can lead to the formation of intermediate and stable reaction products, e.g., carbonyls, that are photo-chemically reactive or themselves detrimental to outdoor air quality. The reaction products associated with photocatalytic oxidation of VOCs were not evaluated in this study. A total of 244 experiments were completed for Phase 1. Material samples were also exposed to real outdoor conditions for a year at two roadside sites in Austin and Houston, Texas and a field site at the J.J. Pickle Research Campus in Austin. Exposed samples were tested after a year to evaluate the influence of outdoor exposure on their NO_x removal capacity.
- **Phase 2: Indoor PRMs.** The second phase of the study consisted of a field study and laboratory experiments involving four indoor materials, including three certified as green materials. Samples of the materials were tested in laboratory experiments before, during and after placement at field sites for a six-month period. Field sites included an institutional building, an unoccupied test house and two homes. Testing of the samples occurred on a monthly basis. Samples were brought back to the laboratory where they were tested in a system of three parallel, stainless-steel, flow-through chambers (48 L). Ozone deposition was evaluated monthly and pre and post-

ozonation VOC emissions were evaluated every three months. Deposition of NO_x on new materials was also evaluated in the same test reactor.

- **Phase 3: Modeling of the combined effect of PRMs.** The third phase involved computer-based modeling to determine possible reductions in O_3 and NO_x concentrations in a residential building through the use of outdoor and indoor PRMs. The UTest House on the J.J. Pickle Research Campus served as a model building. Scenarios including various combinations of PRMs were compared to a base case scenario (conventional building materials). The best photocatalytic coating from Phase 1 and the two best indoor materials from Phase 2 were included in the model. Material characteristics pertaining to removal of pollutants experimentally measured during Phases 1 and 2 were used as inputs to the model.

1.4. ORGANIZATION AND LIST OF JOURNAL PAPERS

This dissertation is presented as an executive summary in conjunction with the full text of four journal articles presented in appendices A through D. These articles are already published, submitted or ready for submission as described below:

Paper 1: Clement J. Cros, Alexandra L. Terpeluk, Neil E. Crain, Maria G. Juenger, Richard L. Corsi. Influence of environmental factors on removal of oxides of nitrogen by a photocatalytic coating. Submitted to *Atmospheric Environment* on March 20th 2013.

Paper 2: Clement J. Cros, Alexandra L. Terpeluk, Neil E. Crain, Richard L. Corsi, Maria G. Juenger. Removal of oxides of nitrogen by photocatalytic coatings: influence of environmental parameters and material properties. Ready for submission to *Construction and Building Materials*.

Paper 3: Clement J. Cros, Glenn C. Morrison, Jeffrey A. Siegel, Richard L. Corsi. Long-term performance of passive materials for removal of ozone from indoor air. *Indoor Air* (2011), 22, 43-53.

Paper 4: Clement J. Cros, Atila Novoselac, Richard L. Corsi. Screening model to assess the use of indoor and outdoor reactive materials for lowering indoor levels of ozone and oxides of nitrogen. Ready for submission to *Building and Environment*.

2. Literature review

2.1. Sources of NO_x

Oxides of nitrogen are composed of NO and NO_2. Both NO and NO_2 are products of combustion. Nitrogen dioxide is also formed in the atmosphere from the reaction of NO with O_3. Major sources of NO_x are processes that include the burning of fossil fuels: power production facilities, industrial facilities and road vehicles [1, 40]. Indoors, combustion sources can also increase NO_x concentrations. For example, gas stoves have been shown to be responsible for elevated NO_2 levels in homes [20].

2.2. Health effects of NO_x

The health effects of NO_x have been studied for decades. Several clinical studies have been conducted to elucidate the effects of NO_x exposure. Mohsenin [8] exposed 10 people with asthma to 500 ppb NO_2 for an hour. Airway reactivity was increased for the exposed subjects but no other significant changes were noted in other lung functions after NO_2 exposure. Bauer et al. [7] exposed 15 subjects with asthma to 300 ppb NO_2 during both resting and exercise periods. Nitrogen dioxide exposure produced significant decrements in forced expiratory rates after exercise periods but not after resting periods. Frampton et al. [9] tested pulmonary function and airway reactivity of 39 healthy subjects exposed to various NO_2 concentrations: continuous exposure to 600 and 1500 ppb NO_2 and exposure to 50 ppb with 15-minute peaks at 2000 ppb. Only subjects exposed continuously to 1500 ppb NO_2 showed signs of airway reactivity. No other symptoms were observed.

Epidemiological studies have also been conducted by researchers around the world. Several researchers have studied effects of early life and childhood exposure to NO_x and found links with respiratory symptoms and onset of asthma [11, 12, 41]. Pilotto

et al. [41] studied schoolchildren in Australia in classrooms with electric versus gas heating. During the heating period, children in classrooms with high NO_2 concentrations had increased symptoms of sore throat and colds, as well as increased absences. Clark et al. [12] used data from a cohort study of 37,041 children in British Columbia, Canada, and estimated their exposure to NO_x in utero and during the first year of life. They found an association between exposure to NO and NO_2 and onset of asthma with odds ratios of 1.08 and 1.12, respectively, for a $10\,\mu g\,m^{-3}$ increase in pollutant concentration. Gauderman et al. [11] followed 208 children in southern California, USA, and measured NO_2 concentrations outside their homes for periods of two consecutive weeks, once in the summer and once in the winter. They found an association between doctor-diagnosed asthma and average NO_2 concentration measured over four weeks, with an odds ratio of 1.83 for a 5.7 ppb increase in NO_2.

Other researchers have linked exposure to NO_x with cardiovascular incidents. Perters et al. [15] studied 100 patients implanted with cardioverter-defibrillators. During follow-up visits they downloaded data from the devices and were able to collect information about detected arrhythmias. Correlating these data with air pollution data they found an association between arrhythmia and exposure to NO_2 with an odds ratio of 1.8 for a 26 ppb increase in NO_2. Andersen et al. [42] correlated hospital admissions for stroke and air quality data and found a weak association between NO_2 exposure and stroke incidence and between fatal strokes and NO_2 exposure.

Some researchers have also found associations between exposure to NO_x and lung cancer [43-45].

2.3. ENVIRONMENTAL EFFECTS OF NO_x

Beyond adverse health effects, NO_x in urban air are also responsible for acid rain. Two possible pathways have been established for formation of nitric acid (HNO_3) [2]. The first one is a simple reaction between water and NO_2 to form nitrous and nitric acid:

$$2NO_{2\,(g)} + H_2O_{(aq)} \rightarrow HNO_{2\,(g)} + HNO_{3\,(aq)} \quad (1)$$

The second one involves three reactions leading to the formation of nitric acid:

$$NO_{2\,(g)} + O_{3\,(g)} \rightarrow NO^{\bullet}_{3\,(g)} + O_{2\,(g)} \quad (2)$$

$$NO^{\bullet}_{3\,(g)} + NO_{2\,(g)} \rightleftharpoons N_2O_{5\,(g)} \quad (3)$$

$$N_2O_{5\,(g)} + H_2O_{(aq)} \rightarrow 2HNO_{3\,(aq)} \quad (4)$$

NO_x are also precursors to the formation of O_3 through the following reactions [2]:

$$NO_2 + h\nu \rightarrow NO + O \quad (5)$$

$$O + O_2 + M \rightarrow O_3 + M \quad (6)$$

The second reaction in this system is the only significant source of O_3 in the atmosphere [2], making the role of NO_x particularly important for O_3 formation in urban areas.

2.4. HEALTH EFFECTS OF O_3

The health effects of O_3 have been studied for decades and are now fairly well understood. Ozone is a strong oxidant and can damage the lungs when inhaled. Several clinical studies have been conducted to elucidate the effects of O_3 exposure [4-6, 46, 47]. Clinical studies use fairly elevated O_3 concentrations (80 ppb to 400 ppb) and usually expose the subjects for several hours, with or without physical activity. Several researchers have reported reduction in pulmonary function after exposure to O_3 [4, 5]. Lavage fluids collected after exposure have also shown signs of inflammation of the

lungs [5, 6, 47] and cell damage [6, 46]. Auten et al. [48] reviewed several studies on the effect of post-natal exposure to O_3 and concluded that exposure to O_3 during specific periods of development could lead to changes in innervation of airways that could increase chronic sensitivity to other oxidants and allergens. Pre-natal exposure of mothers to O_3 was also associated with reduced birth weight [49].

Epidemiological studies have been conducted on the effects of O_3 around the world, and have led to well-documented associations between exposure to O_3 and increased respiratory symptoms [50], increased blood pressure [14], reduced pulmonary function [14] and asthma [13]. Finally, increases in O_3 concentrations have been associated with increased mortality, especially cardio-vascular and respiratory deaths: a 5 ppb increase in daily O_3 was associated with a 0.33 % increase in mortality in a study of 23 cities across Europe [51], 0.96 % in a study in Lisbon, Portugal [52], 1.09 % in a study in Moscow, Russia [53]; and a 10 ppb increase in daily O_3 was associated with a 0.87 % increase in mortality in a study across 95 urban areas in the United States [54].

2.5. PASSIVE REMOVAL MATERIALS

Ozone concentrations are typically higher outdoors than indoors. However, people in developed countries tend to spend much more time indoors than outdoors [18]. Weschler [19] showed that 43 to 76 % of exposure to O_3 occurs indoors. Moreover, the numerous surfaces and products that are present in indoor environments can react with O_3: furniture, building materials, cleaning and personal care products, furnishings to name a few [26]. Some of the resulting reaction products may be even more harmful than O_3 itself [26]. And this issue is becoming even more predominant with current efforts to build and retrofit buildings with tighter envelopes to save energy: reactions that were too slow to compete with air exchange rates in leakier buildings have become more relevant.

Several researchers [55-59] have shown that building materials, especially those covering large surfaces indoors, can significantly influence O_3 concentrations indoors. Pollutant uptake to surfaces is usually quantified in terms of deposition velocity, which is defined as the flux of pollutant to a surface divided by its concentration in bulk air:

$$v_d = \frac{J}{c_{bulk}} \tag{7}$$

where v_d is the deposition velocity (m h^{-1}), J is the flux of pollutant to the surface (μg m^{-2} h^{-1}) and c_{bulk} is the pollutant concentration in bulk air (μg m^{-3}).

The inverse of the deposition velocity can be expressed as an overall resistance to heterogeneous reactions, and is equal to two resistances in series:

$$\frac{1}{v_d} = r_t + r_s = \frac{1}{v_t} + \frac{4}{\gamma < v >} \tag{8}$$

where r_t is the transport limited resistance (h m^{-1}), r_s is the surface resistance (h m^{-1}), v_t is the transport-limited deposition velocity (m h^{-1}), γ is the reaction probability (-), and $<v>$ is the Boltzman velocity (m h^{-1}). The reaction probability, γ, is the fraction of collisions between the gas molecules and the reactive surface that lead to chemical reactions.

Ozone-initiated emissions from building materials have also been studied. Researchers have found that O_3 reactions with building materials almost always lead to the formation of carbonyls, with heavier n-aldehydes (C_5-C_{10}) being most predominant [59-63]. Ozone-initiated emissions from building materials can be characterized in terms of yields, calculated as the molar (or mass) emission rate of by-product normalized by the molar (or mass) uptake rate of O_3.

The concept of Passive Removal Materials (PRMs) involves materials that can be placed indoors and that can scavenge targeted pollutants that come in contact with them,

without resulting in appreciable by-product emissions or energy use. In the case of O_3, PRMs may be beneficial for two reasons: (1) PRMs can reduce exposure to O_3 itself, and (2) PRMs make O_3 less available to other materials that might otherwise lead to the formation and release of harmful reaction products. Darling et al. [31] conducted experiments in environmental chambers to test O_3 uptake and by-product emissions from carpet in the absence and presence of a PRM, a clay-based wall plaster. It was observed that O_3 concentrations as well as aldehyde emissions from the carpet were reduced in the presence of the PRM. The PRM concept was also tested for O_3 removal in both experimental chambers and in the UTest House [29], but ozone-initiated emissions were not evaluated. Kunkel et al. [29] estimated that total daily O_3 exposure could be reduced by 25 – 50 % through the use of PRMs strategically placed in the indoor environment. Using Monte Carlo simulation for a subset of homes in Houston, TX, Gall et al. [30] showed that median O_3 removal effectiveness ranging from 22 to 68 % could be achieved through the use of activated carbon mats or gypsum wallboard as PRMs. In this study, a few selected green building materials were tested to evaluate if they could be used as PRMs for indoor O_3 removal, by testing their O_3 uptake and pre and post-ozonation emissions.

The potential use of PRMs for NO_x removal was also studied. Oxides of nitrogen removal to building materials has not received as much attention as O_3 removal. However, NO_x levels can be elevated indoors, especially when combustion sources are present in the building [20].

Most researchers reported whole building or room removal rates instead of removal by specific materials. Nazaroff and Cass [64] reported results from several of these studies and found deposition velocities ranging from 0.029 to 0.061 m h^{-1} and 0.22 to 0.65 m h^{-1} for NO and NO_2 , respectively. More recently, Yang et al. [65] reported

deposition velocities for NO_2 for whole houses and found an average of 0.33 m h^{-1} for 37 houses tested in Seoul, South Korea. Grontøft and Raychaudhuri [66] reported deposition velocities of NO_2 to a variety of conventional indoor building materials ranging from 3.3 m h^{-1} for wool carpet to 0.1 m h^{-1} for painted wood. A deposition velocity 5.0 m h^{-1} was also reported for deposition of NO_2 to an activated carbon cloth. Little literature on deposition velocity of NO to indoor building materials was available but one study reported deposition velocities ranging from 0.01 to 0.12 m h^{-1} for conventional flooring and ceiling materials [67].

2.6. OUTDOOR PRM: PHOTOCATALYTIC MATERIALS

Previous results for PRM use indoors suggest that PRMs may also be applied outdoors in order to remove pollutants that have distributed sources. Ideally, any surface outdoors could help remove pollutants emitted into the atmosphere and before they enter buildings.

Photocatalytic materials are materials that contain a semi-conductor. Photocatalysis is a process that occurs at the surface of a semi-conductor exposed to light. When a photon with energy equal or larger than the band gap of the semiconductor is absorbed, an electron (e^-) from the valence band is promoted to the conduction band. The result is the presence of a "hole" in the valence band (h^+). These h^+ and e^- are strong oxidizing and reducing agents, respectively. The electron-hole pair may react with electron donors or acceptors adsorbed on the semi-conductor surface. If reaction does not occur, the electron-hole pair recombines and the energy is dissipated as heat [38, 68, 69]. Oxygen and water, adsorbed at the semi-conductor surface, are catalyzed to form reactive species, superoxide anions (O_2^-) and hydroxyl radicals ($OH^\bullet$):

$$h^+ + H_2O \rightarrow OH^\bullet + H^+ \quad (9)$$

$$e^- + O_2 \rightarrow O_2^- \quad (10)$$

Hydroxyl radicals and superoxide anions are strong oxidizing and reducing agents, respectively. They can react with pollutant molecules adsorbed to the photocatalytic surface. In the case of NO_x, the product of the photocatalytic oxidation is nitric acid [33, 70-72]:

$$NO_{ads} + OH^\bullet \rightarrow HNO_2 \quad (11)$$

$$HNO_2 + OH^\bullet \rightarrow NO_{2,ads} + H_2O \quad (12)$$

$$NO_{2,ads} + OH^\bullet \rightarrow NO_{3,ads}^- + H^+ \quad (13)$$

Titanium dioxide is the most widely used semi-conductor for photocatalysis applications. It is inexpensive, chemically and biologically inert and stable with respect to photo and chemical corrosion [69]. Of its three crystalline forms (anatase, rutile and brookite), anatase is the preferred photocatalyst because it has the highest photoactivity [68].

Researchers have previously studied the use of photocatalytic materials for removal of NO_x. However, most researchers employed air mixtures that only contained NO or NO_2 instead of more realistic mixtures containing other inorganic and organic gases.

Researchers have also studied the effect of environmental parameters on the removal of NO_x by various types of photocatalytic materials (paving stones, TiO_2 slurry, paints, concrete). There is discrepancy in the results, which might be due to the wide range of materials tested. Humidity was found by numerous researchers to have a strong effect on NO_x removal. Most have found that NO_x removal decreased almost linearly with relative humidity in the 20 % to 80 % RH range [33, 36, 37, 73-75]. Others have found

different behaviors, with Bengtsson et al. [76] finding constant removal up to 40 % and decreasing for RH > 40 % and Devahasdin et al. [77] finding removal increasing with RH up to 50 % and staying constant up to 75 %.

The effect of pollutant concentration has also been studied. Bengtsson et al. [76] and Laufs et al. [33] found that, for NO or NO_2 concentrations up to 1 ppm, the removal rate did not vary. On the other hand, Lim et al. [78] and Husken et al. [36] found that removal rate decreased with increasing NO and NO_2 concentration.

The influence of light intensity shows reasonable agreement between studies. It has generally been found that removal increases non-linearly with increasing light intensity [70, 74-76, 78-80].

The effect of temperature in a reasonable range for outdoor conditions was studied by Bengtsson et al. [76]. They found a slight linear decrease in removal with increasing temperature in the 21-30°C range.

Finally, a few researchers have studied possible interactions between VOCs and NO_x removal. Ao et al. [81] and Poulston et al. [82] observed that VOCs can influence NO conversion, but Ao et al. found that the presence of VOCs (benzene, toluene, ethylbenzene, o-xylene) decreased removal while Poulston et al. reported increased NO removal in the presence of VOCs (ethane, ethene, propane, n-butane) except in the case of propylene.

3. Summary of experimental methods

3.1. TESTING OF PHOTOCATALYTIC COATINGS

3.1.1. Materials

3.1.1.1. Concrete samples

Two types of concrete samples were used throughout the experimental program for application of the tested photocatalytic coatings. Highway barriers provided by Tricon Precast (New Braunfels, TX, USA) were divided in four sections: three sections were coated with each test coating while the fourth was left uncoated. Barriers were placed at field sites described in section 3.1.5.1. Concrete slabs were made using the same materials and mix proportions used by Tricon Precast to make highway barriers. The slabs were used for laboratory testing of pollutant removal. Some coated slabs were also placed at field sites for pollutant removal testing after exposure. More details on the concrete mix are presented in Appendix A.

3.1.1.2. Photocatalytic coatings

Three commercially available coatings were used during the experimental program. The first was a white paint, which was a silica sol and water glass-based exterior paint appropriate for mineral substrates. It contained 9.7 % TiO_2 by weight, mostly in the rutile crystalline form. It was applied on concrete samples using a brush. The second coating was a clear paint, obtained as a water-based photocatalytic spray that could be applied to virtually any surface. It contained 1 % TiO_2 by weight, in the anatase crystalline form. It was applied using a paint sprayer. The third coating was a stucco made from portland cement, a proprietary mix of admixtures and 5 % by weight of TiO_2, primarily in the anatase crystalline form. It was applied in a 5 mm thick layer, using a

hand trowel. Some concrete samples were also left uncoated for comparison with the coated samples.

3.1.2. Experimental apparatus

A testing system was designed and constructed in order to test pollutant removal capacity of the concrete slabs coated with photocatalytic coatings (Figure 3.1). The system consisted of a 150-L stainless-steel chamber equipped with UV lights, RH and temperature controls.

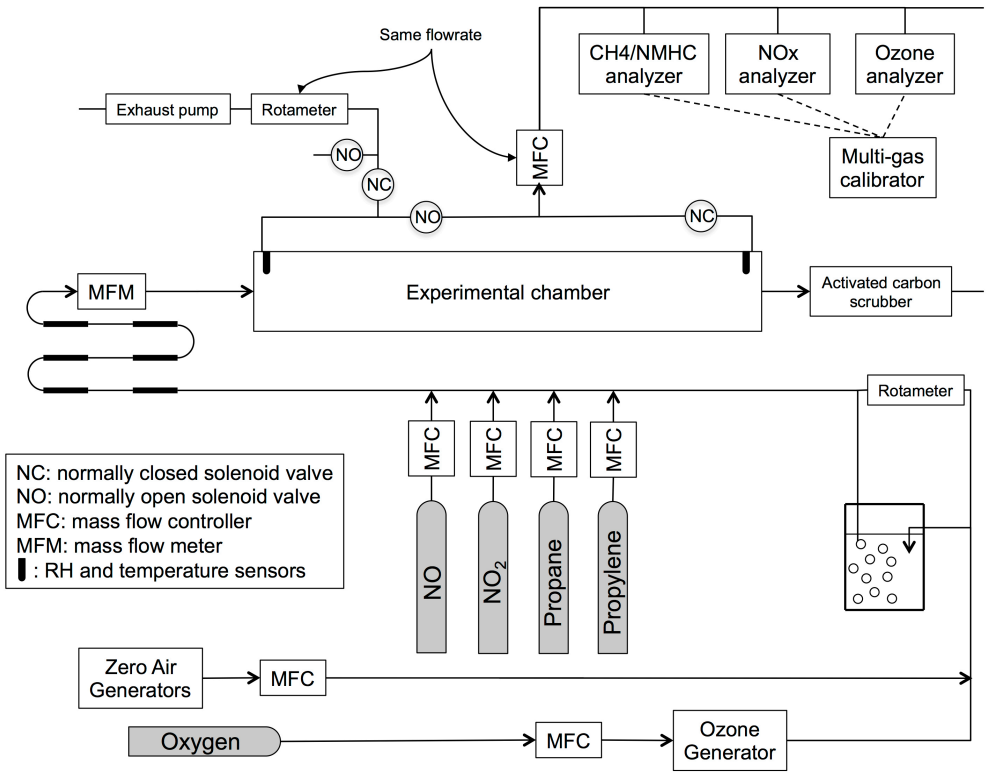

Figure 3.1. Experimental system for testing of outdoor PRMs

The inlet airstream was provided by two zero air generators and was humidified using an impinger. Pollutant species mixed in nitrogen were obtained in gas cylinders: nitrogen oxide, nitrogen dioxide, propane (as a surrogate for VOCs) and propylene (as a surrogate for highly reactive VOCs). Ozone was produced by passing pure oxygen through a UV-based ozone generator. Pollutant species were introduced through mass flow controllers. The air stream then passed through a mixing zone consisting of a succession of sections of tubing of different diameters and a mixing chamber separated from the main chamber by a baffle.

A system of solenoid valves was used to automatically switch sampling between the inlet and outlet of the chamber at regular time intervals. Pollutant concentrations were measured using a UV-absorbance ozone monitor, a chemiluminescence NO_x analyzer and a direct methane/non-methane hydrocarbon analyzer. These instruments were calibrated daily using concentration-certified gas standards. A more detailed description of the system and instrumentation is provided in a journal article presented in Appendix A.

3.1.3. Preliminary testing

Preliminary tests were completed in order to eliminate photocatalytic coatings that were inefficient and to identify efficient coatings for more intensive testing. Preliminary tests were run under conditions that, according to the published literature on photocatalytic materials, should be beneficial to NO_x removal. As such, if a coating did not perform well under such conditions, it was eliminated from further testing. The preliminary tests were run at a contact time of 7.5 minutes and pollutant concentrations of 135 ppb NO_x, 85 ppb O_3, 3 ppm hydrocarbons (2.5 ppm propane, 0.5 ppm propylene). Temperature was set at 38°C, RH at 6 % and light intensity at 2 mW cm^{-2}. Removals of

NO and NO_2 were calculated using steady-state concentration data obtained during the tests.

3.1.4. Full factorial testing

The two best performing coatings out of the preliminary tests (the clear paint and the stucco) were put through full factorial testing in order to determine which environmental parameters significantly affected their NO_x removal. Six environmental parameters were varied according to Table 3.1.

Table 3.1. Full factorial testing parameters and their low and high levels

	Low level	**High level**
Contact time	1.5 minutes	15 minutes
Relative humidity	20 %	65 %
Temperature	30°C	40°C
Organic pollutants		
- propane (VOC)	0.25 ppm	2.5 ppm
- propylene (HRVOC)	0.05 ppm	0.5 ppm
Inorganic pollutants	"morning"	"afternoon"
- NO	150 ppb	
- NO_2	20 ppb	50 ppb
- O_3		150 ppb
Lights	1 mW cm^{-2}	2 mW cm^{-2}

Samples were rinsed with distilled every eight experiments to remove products of the photocatalytic process that might have remained adsorbed on the material surface. More details on the full factorial testing are presented in Appendix B.

It should be noted that, in the afternoon condition, O_3 was present as an additional inorganic pollutant, and its removal to the photocatalytic coating was evaluated, along with NO_2 removal.

3.1.5. Field exposure

3.1.5.1. Exposure sites

Three field sites were set up to expose the coated concrete samples to real outdoor conditions and evaluate how that affected their pollutant removal efficiency. Two sites were established within 30 m of a major roadway, near I-10 in Houston and near I-35 in Austin, as shown in the digital images in Figure 3.2.

(a) (b)

Figure 3.2. Field site in (a) Austin and (b) Houston.

The third field site was set up on the J.J. Pickle Research campus of the University of Texas at Austin. It was about 400 m from a major roadway, Loop 1 in Austin. Each field site was equipped with a weather station to record temperature, relative humidity and precipitation (Hobo U-30 NRC; Onset, Bourne, MA, USA; GRWS100; Campbell Scientific, Logan, UT, USA).

3.1.5.2. Post-exposure testing

Concrete slabs coated with the best performing coating out of full factorial testing (the stucco), and that had spent one year in the Austin, Houston and J.J. Pickle field sites were returned to the laboratory for pollutant removal testing. These tests were run at conditions realistic of outdoor conditions during the ozone season in Southeast Texas: 50 % RH, 35°C, 1.5 minute contact time, low organic pollutant (0.25 ppm propane, 0.05 ppm propylene), and high UV light intensity (2 mW cm^{-2}). The tests were run for both "morning" and "afternoon" conditions (Table 3.1).

When returned from the field sites, samples were tested three consecutive times. For the first test, the sample was tested without any treatment. For the second test, the sample was rinsed with distilled water. Finally, for the third test it was rinsed with a soap and water solution. Details of the rinsing methods are presented in Appendices A and B. Samples of uncoated concrete, with newly applied photocatalytic stucco coating and with newly applied stucco coating without TiO_2 were tested under the same conditions for comparison.

3.1.6. Data analysis

3.1.6.1. Pollutant removal

Removals of NO and NO_2 were calculated using steady-state concentration data obtained during full factorial tests. Removal obtained with the uncoated sample was subtracted from the removal obtained with the coated sample in order to calculate the incremental pollutant removal that would be observed after coating existing concrete surfaces:

$$R = 100\times\left(1-\frac{c_{out}}{c_{in}}\right)-100\times\left(1-\frac{c_{out,b}}{c_{in,b}}\right)=100\times\left(\frac{c_{out,b}}{c_{in,b}}-\frac{c_{out}}{c_{in}}\right) \quad (14)$$

where $c_{in,b}$ is the pollutant concentration measured in the chamber inlet for the test run with uncoated concrete (ppb), $c_{out,b}$ is the pollutant concentration measured in the chamber outlet for the test run with uncoated concrete (ppb), c_{in} is the pollutant concentration measured in the inlet of the chamber for the test run with coated concrete (ppb), c_{out} is the pollutant concentration measured in the outlet of the chamber for the test run with coated concrete (ppb), R is the pollutant removal by the coated concrete (%).

The uncertainty associated with R was determined using standard error propagation techniques. The uncertainty on the concentration measurements was taken as two standard deviations of measured values for all calibrations run during the experimental program. Relative uncertainties were determined to be 8.0 % for NO measurements and 9.8 % for NO_2 measurements.

3.1.6.2. Data analysis for full factorial experiments

The results from the full factorial experiments were analyzed using JMP software (JMP 9; SAS, Cary, NC, USA) to determine the most important factors affecting NO_x removal, using analysis of variance (ANOVA) techniques. ANOVA allows testing whether the means of different groups are statistically different. Main factors as well as two-factor interactions were taken into account. Higher level interactions were not considered. Given the large number of experiments that needed to be run, it was not possible to complete replicates for all experiments. Ten percent of the experiments were replicated. The Lenth method was used to provide approximate tests of significance [83]. The Lenth method provides an estimate of the standard error, called the Lenth pseudo standard error (PSE), where:

$$PSE = 1.5 \times Median(|\theta_i| : \theta_i < 2.5 \times \tau_0) \quad (15)$$

$$\text{and } \tau_0 = 1.5 \times Median(|\theta_i|) \quad (16)$$

where θ_i is the i^{th} contrast.

The Lenth t-ratio was calculated as the ratio of the contrast for a factor over the PSE [84]. The t-statistic for each factor was compared to critical values provided by Mee [84]. Factors with a Lenth t-ratio larger than the critical value were deemed significant. A significance level $\alpha = 0.15$ was used to determine the critical value. Outliers were determined by using the studentized residuals test described by Mee [84].

3.1.6.3. Determination of reaction probabilities

Reaction probabilities of NO, NO_2 and O_3 on the coated concrete were determined for use in a model of PRM performance for reducing human inhalation exposure to these pollutants (Research Phase 3). As described earlier:

$$\frac{1}{v_d} = \frac{1}{v_t} + \frac{4}{\gamma < v >} \quad (17)$$

where v_d is the pollutant deposition velocity on the reactive surface (m h^{-1}), v_t is the transport-limited deposition velocity (m h^{-1}), γ is the reaction probability (-), and $<v>$ is the Boltzman velocity (m h^{-1}). The reaction probability, γ, is the fraction of collisions between the gas molecules and the reactive surface that lead to chemical reactions.

In order to determine the reaction probability, which is a constant for the material/pollutant pair, it was necessary to obtain both the deposition velocity, v_d, and the transport-limited deposition velocity, v_t, in the reactor used for testing.

The transport-limited deposition velocity in the reactor was calculated using O_3 deposition to a highly reactive surface: concrete coated with a potassium iodide solution

(125 mg KI / 100 mL distilled water, [85]). In this specific case, the surface resistance to the deposition of O_3 on the material was assumed to be negligible so that the transport resistance is the only resistance to deposition. In this case, the deposition velocity on the potassium iodide-coated concrete was:

$$\frac{1}{v_{d,O3,KI}} = \frac{1}{v_{t,O3}} + \frac{4}{< v > \gamma_{O3,KI}} \qquad \lim_{\gamma_{O3,KI} \to 1} \frac{1}{v_{t,O3}} \tag{18}$$

where $v_{d,O3,KI}$ is the deposition velocity of O_3 on the potassium iodide coated concrete (m h^{-1}), $v_{t,O3}$ is the transport-limited deposition velocity of O_3 in the reactor (m h^{-1}), $\gamma_{O3,KI}$ is the reaction probability of O_3 with the potassium iodide coating (-).

The deposition velocity of O_3 on the KI-coated concrete was determined using a mass balance on the well-mixed reactor:

$$v_{t,O3} = v_{d,O3,KI} = \frac{\lambda V_{sample}}{A_{sample}} \left(\frac{c_{O3,inlet}}{c_{O3}} - 1 \right) - v_{d,O3,w} \frac{A_{w,sample}}{A_{sample}} \tag{19}$$

where λ is the reactor air exchange rate (h^{-1}) V_{sample} is the air volume of the reactor in the presence of a concrete sample (m^3), A_{sample} is the projected area of the concrete sample tested (m^2), $A_{w,sample}$ is the area of exposed reactor walls in the presence of a concrete sample (m^2), $c_{O3,inlet}$ is the O_3 concentration in the reactor inlet (ppb), c_{O3} is the O_3 concentration in the reactor outlet (ppb), $v_{d,O3,w}$ is the O_3 deposition velocity to the chamber walls (m h^{-1}), other parameters are as previously described.

The measured value for the transport-limited deposition velocity of O_3 in the reactor was used to estimate the transport-limited deposition velocities in the reactor for NO and NO_2, $v_{t,NO}$ and $v_{t,NO2}$, respectively. Mass transfer correlations for gas flow above a flat plate were used to determine the relationship between $v_{t,O3}$ and $v_{t,NO}$ and $v_{t,NO2}$ [86]:

$$v_{t,NO} = \left(\frac{D_{NO}}{D_{O3}}\right)^{2/3} \times v_{t,O3} \text{ and } v_{t,NO} = \left(\frac{D_{NO2}}{D_{O3}}\right)^{2/3} \times v_{t,O3} \quad (20)$$

where D_{NO}, D_{NO2}, and D_{O3} are the NO, NO_2 and O_3 diffusion coefficients ($m^2\ h^{-1}$), respectively and other parameters are as previously described.

The deposition velocity for each pollutant was then calculated using a steady-state mass balance on the well-mixed test reactor:

$$v_d = \frac{\lambda V_{sample}}{A_{sample}}\left(\frac{c_{inlet}}{c} - 1\right) - v_{d,w}\frac{A_{w,sample}}{A_{sample}} \quad (21)$$

where v_d is the pollutant deposition velocity on the coated concrete surface ($m\ h^{-1}$), c_{inlet} is the pollutant concentration in the reactor inlet (ppb), c is the pollutant concentration in the reactor outlet (ppb), $v_{d,w}$ is the pollutant deposition velocity to the reactor walls ($m\ h^{-1}$), and other parameters are as previously described.

Finally, the reaction probability was determined as:

$$\gamma = \frac{4}{< v >}\left(\frac{1}{v_d} - \frac{1}{v_t}\right)^{-1} \quad (22)$$

where parameters are as previously described.

3.2. TESTING OF INDOOR BUILDING MATERIALS

3.2.1. Materials

Four commercially available building materials were tested for their capacity to remove O_3 and the best performing materials were also tested for their ability to remove NO_x. The first material was an activated carbon (AC) mat made of a non-woven polyester fabric coated with activated carbon. The second material was a perlite-based green

ceiling tile. The third material was a carpet made with 70 % recycled material. The last material was a gypsum wallboard made of reclaimed gypsum and recycled paper onto which low-VOC primer and paint were applied. All materials were obtained new and kept in their original packaging until testing, except for the gypsum wallboard that was painted and left to air out in an unoccupied test house (described in section 5.1.1).

The samples used for testing in this study had dimensions of 20 × 25 cm. The sides and backside of the samples were covered with aluminum foil that was left on the samples during the experimental program. This avoided reaction of surfaces not usually in contact with indoor air during exposure and testing. More details on the materials tested are presented in Appendix C.

3.2.2. Experimental systems and analytical methods

3.2.2.1. O_3 removal and carbonyl emissions measurements

An experimental system was designed and constructed to test O_3 removal as well as pre and post-ozonation emissions of the indoor building materials selected (Figure 3.3).

Room air was dehumidified and cleaned by passing through a column containing Drierite™ and an activated carbon filter. The air stream was then split and a portion of the air was ozonated by passing through an ozone generator. Similarly, relative humidity was adjusted using an impinger. The air stream was then split and introduced through mass flow controllers into three parallel 48-L stainless-steel chambers, each containing a material sample or left empty for measurement of chamber walls effects. Ozone concentrations were measured in the inlet and outlet of the chambers using a UV absorbance ozone monitor. Carbonyl concentrations were measured using sorbent tubes. Light carbonyls (formaldehyde, acetaldehyde, acetone, propanal, butanal, and pentanal)

were sampled on pre-packed 2,4-Dinitrophenylhydrazine (DNPH) tubes. Heavy aldehydes (hexanal, heptanal, o-tolualdehyde, octanal, benzaldehyde, nonanal, and decanal) were sampled on large volume glass GC injection liners packed with Tenax-TA®. The 400 ± 3 mL min^{-1} and 50 ± 2 mL min^{-1} airflow through the DNPH and Tenax tubes, respectively, was provided by sampling pumps. Carbonyl concentrations were measured before and after O_3 had been introduced into the test chamber. The system followed ASTM D5116-10 standard recommendations except for temperature control of the reactor [87]. However, the reactor was operated in a laboratory where room temperature ranged from 21°C to 24°C [88]. More details on the experimental apparatus are provided in Appendix C.

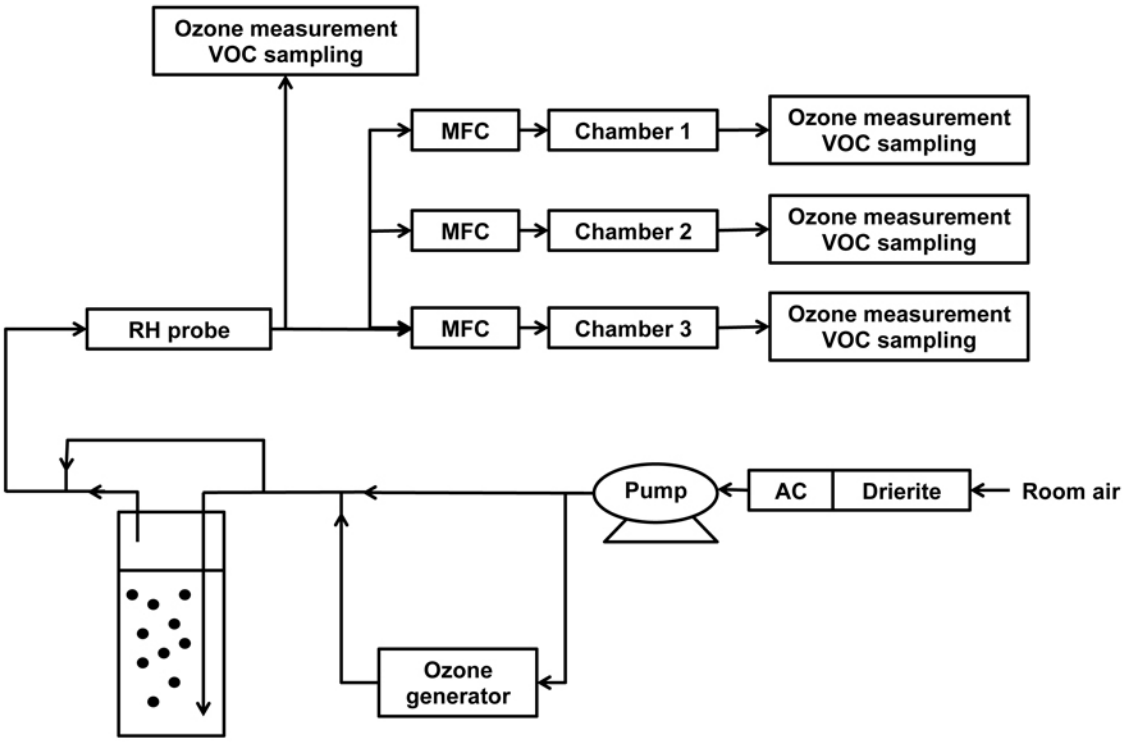

Figure 3.3. Experimental system for ozone removal and carbonyl emissions testing of indoor PRMs

DNPH tubes used to sample light carbonyls were wrapped in aluminum foil and placed in individual plastic bags after each experiment. The tubes were kept frozen until they were analyzed for C_1-C_5 carbonyls using high-performance liquid chromatography with UV detection (HPLC/UV). Tenax-TA tubes were analyzed by zero-path thermal desorption followed by gas chromatography with flame ionization detection (TD/GC/FID). More details on analytical methods are available in Appendix C.

3.2.2.2. NO and NO_2 removal measurements

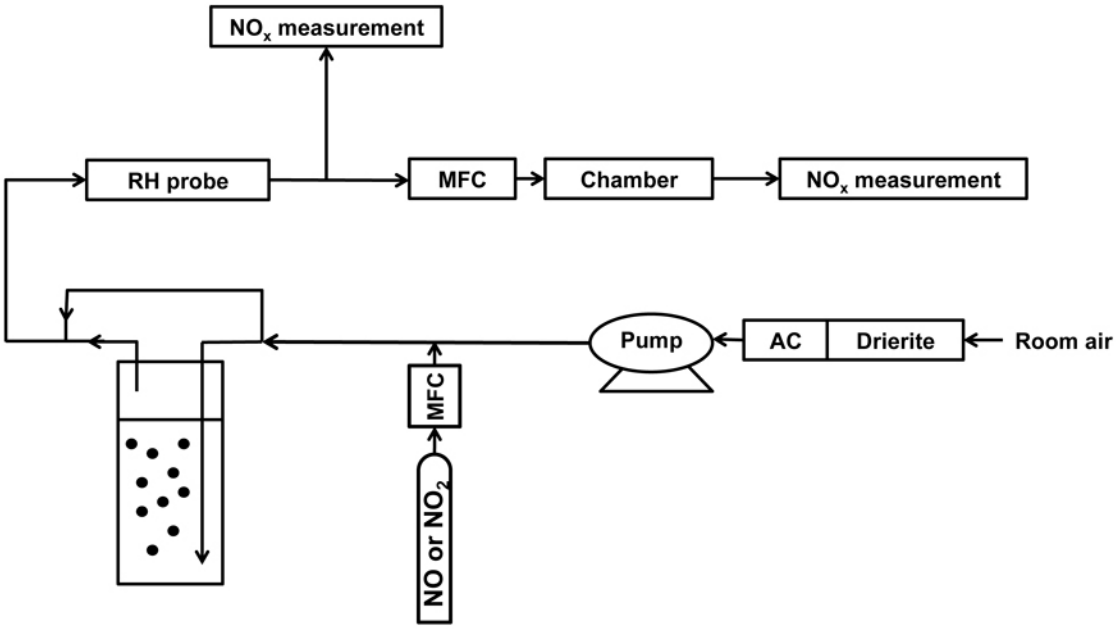

Figure 3.4. Experimental system for NO and NO_2 removal testing of indoor PRMs

A simplified version of the system used for ozone and carbonyl emissions testing was used to test NO and NO_2 removal by new indoor materials, as presented in Figure 3.4. A single 48-L stainless-steel chamber was used. Gas cylinders of NO and NO_2 (Praxair, Danbury, CT, USA) were obtained and gases were injected in the air stream

through mass flow controllers (Series FMA 5500; Omega Engineering Inc., Stamford, CT, USA). Concentrations of NO and NO_2 in the inlet and outlet of the test chamber were measured using a chemiluminescence NO_x analyzer (model 200E; Teledyne, San Diego, CA, USA).

3.2.3. Field exposure

3.2.3.1. Exposure sites

Samples were placed in real homes and institutional buildings around Austin for a six-month period. The field sites covered a wide range of indoor environments as described in Table 3.2. Material samples were placed vertically on metal stands on shelves or furniture, about 1.8 m from the floor, except for the carpet samples that were laid on the floor, in relatively protected areas to avoid occupants repeatedly stepping on the samples.

Indoor environmental conditions at each field site were monitored through continuous recording of relative humidity and temperature using data loggers, passive sampling of total VOC using sorbent tubes and sampling of indoor dust using tape sampling. More details on the field sites and environmental conditions monitoring are presented in Appendix C.

Table 3.2. Indoor PRMs field locations

Building type	Room type	Age (years)	Monthly average range		Number of samples			
			Temperature	Relative humidity	Activated carbon	Carpet	Ceiling tile	Painted gypsum wallboard
Office building	Office	24	23-25°C	32 – 59 %	1	2	1	1
Occupied by up to three students during regular business hours								
House 1	Kitchen	5	19-25°C	51 – 57 %	1	1	2	1
Used by five residents daily								
House 2	Home Office	44	16-29°C	47 – 63 %	1	1	1	2
Occupied by one resident and a pet daily								
House 1	Bedroom	5	19-27°C	44 – 60 %	2	1	1	1
Occupied by one resident daily								
Unoccupied Test House	Kitchen/ Dining	4	16-29°C	34 – 54 %	2	1	1	1
Occupancy and operation of the Test House varied greatly depending on experiments carried out								

3.2.3.2. Testing of exposed samples for ozone removal and carbonyl emissions

Exposed samples were tested before being installed in field sites for their O_3 removal capacity as well as pre and post-ozonation emissions. Following placement on the field, samples were returned on a monthly basis to the laboratory for testing and brought back to their original field location after testing. Each month, the O_3 removal capacity of the material samples was tested while pre- and post-ozonation carbonyl emissions were also measured after three months and at the end of the six-month exposure period. Measurements included determination of the deposition velocity of O_3 on each material sample as well as determination of emission rates of carbonyls including C_1 through C_{10} saturated n-aldehydes, acetone, o-tolualdehyde and benzaldehyde. Tests were run under the conditions described in Table 3.3.

Table 3.3. Experimental conditions for testing of indoor PRMs for ozone removal and carbonyl emissions

Parameter	**Value**
Temperature	21-24°C
Relative humidity	50 ± 2 %
Air exchange rate	2 h^{-1}
Inlet O_3 concentration	147 ± 10 ppb

3.2.4. Testing of building materials for NO and NO_2 removal

Deposition velocities of NO and NO_2 on the best performing materials during the field study (activated carbon mat and perlite-based ceiling tile) were measured on new samples of these materials that had been kept in their original packaging. The samples used were prepared identically to the ones used in the field study. Testing conditions were identical to those used for measurement of ozone deposition velocities on the indoor materials (Table 3.3), except for inlet pollutant concentrations. Inlet concentrations of NO

and NO_2 were 153 ± 5 ppb and 155 ± 5 ppb, respectively. Two empty chamber experiments were run, first with NO and then with NO_2, to measure NO and NO_2 deposition to the chamber walls. Then duplicate experiments were run for NO and NO_2 separately, with a material sample placed in the chamber, to measure NO and NO_2 deposition to the material samples.

3.2.5. Data analysis

3.2.5.1. O_3 deposition velocity

Chamber tests were run for sufficient time that a steady-state condition with respect to O_3 concentration was reached in the chamber. For every other set of experiments (three chambers operated in parallel), one of the chambers was left empty to allow calculation of the deposition velocity of O_3 to the chamber walls. The empty chamber was switched between experiments.

The deposition velocity for the material tested, v_d (m h^{-1}), is based on a steady-state mass balance on a well-mixed chamber, including reaction at chamber walls:

$$v_d = \frac{\lambda V}{A_s}\left(\frac{c_{in}}{c} - 1\right) - v_{d,w}\left(\frac{A_w}{A_s} - 1\right) \quad (23)$$

where λ is the air exchange rate of the chamber (h^{-1}), V is the volume of the chamber (m^3), A_w is the total area of the chamber walls (m^2), A_s is the horizontal projected area of the material sample (m^2), c_{in} is the inlet pollutant concentration (ppb), c is the pollutant concentration in a chamber containing a material sample (ppb), and $v_{d,w}$ is the pollutant deposition velocity for the chamber walls (m h^{-1}).

Mean values are expressed with a corresponding standard deviation around the mean. For all other analyses, uncertainties in the measured deposition velocities were calculated with an error propagation analysis using the maximum of instrument error,

± 2 % for the O_3 analyzer, ± 1 % for the bubble flow meter and an error on horizontally-projected area measurements that was estimated to be less than 10 %.

3.2.5.2. Carbonyl emission rates

One chamber in the system was left empty every other set of experiments to evaluate the carbonyl emission rates of chamber walls. The difference in carbonyl concentrations between empty chambers was on average less than 2 μg m^{-3}. Emission rates of each compound from test specimens were calculated based on a mass balance on a well-mixed flow-through chamber at steady-state, accounting for emissions from chamber walls:

$$e_{k,s} = \frac{\lambda V\left(c_k - c_{k,in}\right) - \lambda V\left(c_{k,e} - c_{k,in}\right)\left(1 - \frac{A_s}{A_w}\right)}{A_s} \tag{24}$$

where $c_{k,in}$ is the inlet concentration of carbonyl k (μg m^{-3}), $c_{k,e}$ is the concentration of carbonyl k in an empty chamber (μg m^{-3}), c_k is the concentration of carbonyl k in a chamber containing a material sample (μg m^{-3}), $e_{k,s}$ is the emission rate of carbonyl k for the material sample (μg m^{-2} h^{-1}), and all other variables are as previously described.

3.2.5.3. NO and NO_2 deposition velocity

Chamber tests were run for sufficient time that a steady-state condition with respect to NO or NO_2 concentration was reached in the chamber. Separate empty chamber experiments were run to determine deposition of NO and NO_2 to the chamber walls.

The deposition velocity for the material tested, v_d (m h^{-1}), is based on a steady-state mass balance on a well-mixed chamber, including reaction at chamber walls:

$$v_d = \frac{\lambda V}{A_s}\left(\frac{c_{in}}{c} - 1\right) - v_{d,w}\left(\frac{A_w}{A_s} - 1\right) \quad (25)$$

where all parameters are as previously described.

4. Summary of research findings

4.1. OUTDOOR PRMS

4.1.1. Preliminary test results

Tests results for preliminary tests conducted on three commercially-available photocatalytic coatings are presented in Figure 4.1. Results show that the stucco was the most effective coating for removal of NO_x and O_3. On the contrary, the white paint tested removed little NO_x relative to the uncoated concrete. The white paint contained the rutile crystalline form of TiO_2, which is not the most photoactive form, while the stucco and the clear paint each contained anatase, which is the most photoactive form of TiO_2. This might explain the poor performance observed in terms of pollution removal by the white paint. In light of these results, the stucco and the clear paint were chosen for further testing.

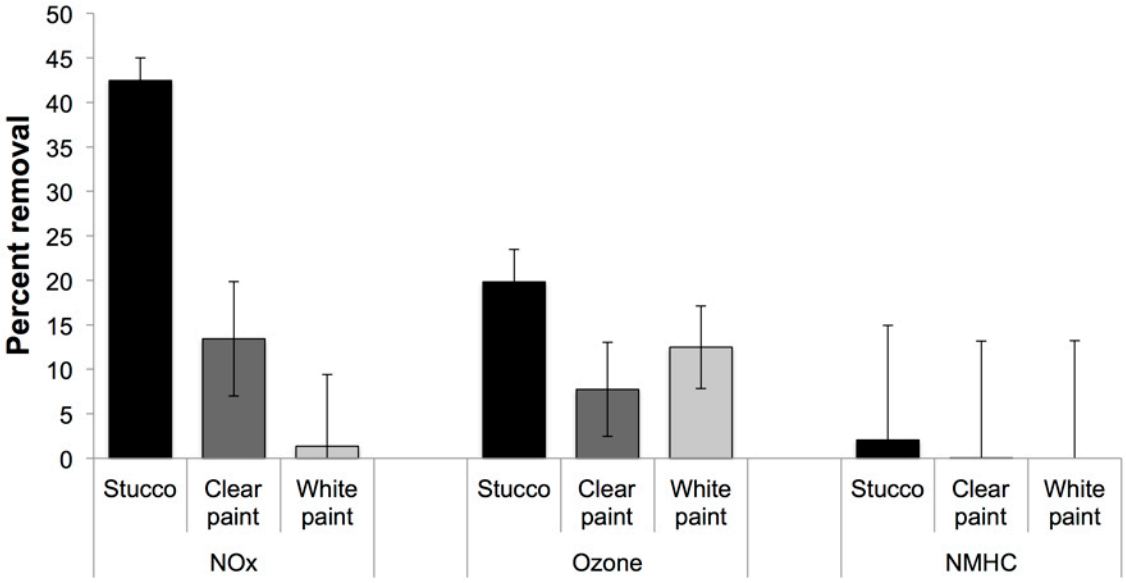

Figure 4.1. Results of preliminary testing of outdoor PRMs

4.1.2. Full factorial test results

Removals of NO_x obtained during full factorial testing are presented in Figure 4.2. The results confirmed that the photocatalytic stucco was the most effective for removal of NO_x, with removals ranging from 16 % to 85 %. For that reason, its NO_x removal effectiveness was further tested after outdoor exposure (section 4.1.3). Similar removals were observed by Dylla et al. [37] for concrete containing TiO_2 at contact times up to 7.1 minutes; they did not include other air pollutants such as O_3 and VOCs in their study. Ballari et al. [39] and Husken et al. [36] also observed similar levels of NO_x degradation by photocatalytic paving stones with removals in the range of 3 % to 63 % for similar contact times, light intensities, relative humidity and inorganic pollutant concentrations. A more detailed analysis of NO_x removal by the photocatalytic stucco is presented in Appendix A.

Removals of NO_x observed for the clear paint ranged from 0 % to 32 % and decreased over time. The first eight experiments presented on the top left of Figure 4.2 (long contact time, low RH, morning inorganics) were the first experiments run during the experimental program. It was during these experiments that the best performance of the clear paint was recorded, with all removals between 12 % and 32 %. It appears that after the first water rinse, the performance of the clear paint degraded: all other removals observed were below 15 % with only one experiment yielding a removal over 12 %. Such changes were not observed with the stucco. These results might be explained by wear of the coating leading to loss of the photocatalyst, TiO_2, as observed by Terpeluk [89]. The extent of the degradation of the clear paint coating during full factorial testing was not known, and experiments were analyzed assuming that some TiO_2 was still present on the clear paint sample. As such, this assumption should be considered when interpreting

results of the ANOVA analysis for the clear paint. Coating degradation might have affected the relevance of the statistical analysis.

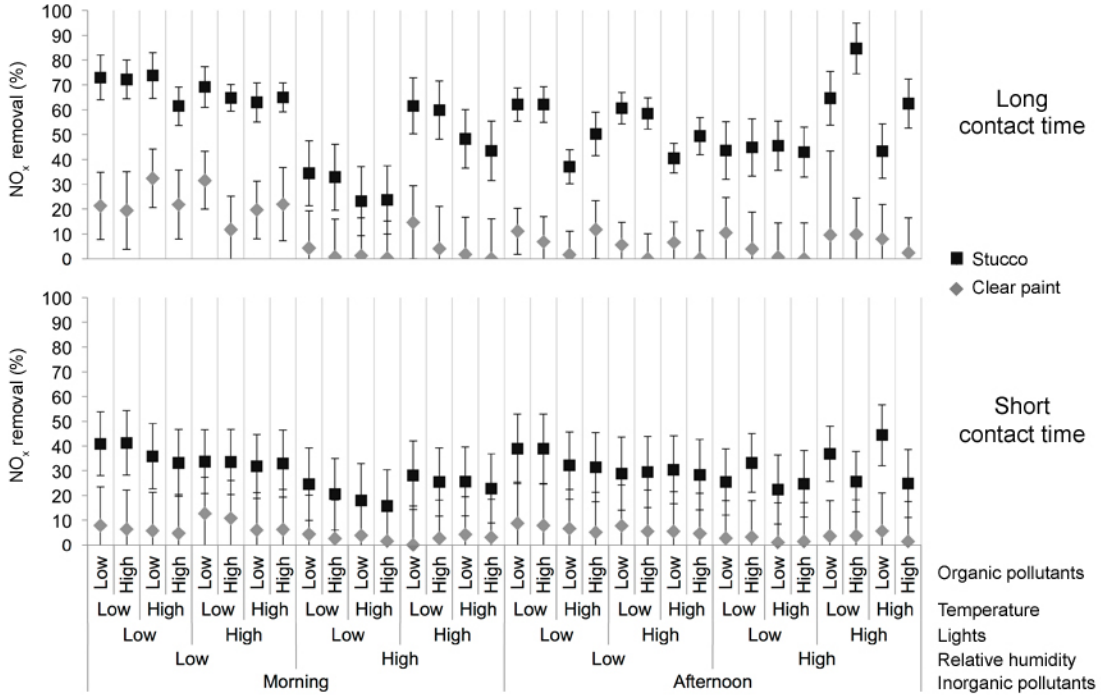

Figure 4.2. NO_x removals obtained during full factorial testing of outdoor PRMs

In the morning condition for inorganic pollutants (NO = 150 ppb, NO_2 = 20 ppb), formation of NO_2 was observed in some cases as a result of NO removal. It is possible that during the photocatalytic reaction process described in reactions 11 through 13, some of the NO_2 formed by photocatalytic oxidation of NO (reactions 11 and 12) could not be oxidized further and desorbed from the material surface. Molar yields were calculated as moles of NO_2 formed divided by moles of NO reacted. Molar yields, in the morning condition, for the stucco ranged from 0 to 0.32 moles NO_2 formed/moles NO reacted (average 0.08, standard deviation 0.10) with absolute increases in NO_2 concentrations

ranging from 0 to 17.5 ppb (average 5.0 ppb, standard deviation 5.4 ppb). Molar yields, in the morning condition, for the clear paint ranged from 0 to 0.58 moles NO_2 formed/moles NO reacted (average 0.38, standard deviation 0.13) with absolute increases in NO_2 concentrations ranging from 0 to 39.1 ppb (average 17.2 ppb, standard deviation 10.4 ppb).

Results from the ANOVA analysis of full factorial experiments are presented in Figure 4.3. The results show that both coatings were significantly affected in a similar fashion by three environmental factors: an increase in contact time led to increased NO_x removal while increases in RH and temperature led to decreases in NO_x removal by both coatings. Other environmental factors affected each coating differently.

While NO_x removal by the stucco was not significantly affected by levels of organic of inorganic pollutants in air, the clear paint was affected by these parameters. It is possible that differences in the surface morphologies of each coating were responsible for this difference: the stucco had a much rougher surface than the clear paint, hence more actual surface area exposed for the same projected area. With a larger surface area, the stucco offered more active sites, which might be why competition by non-NO_x molecules did not affect removal of NO_x molecules. Similarly, differences in coating surface morphologies might explain why the stucco was significantly affected by a change in UV light intensity while the clear paint was not. It is possible that some active sites at the stucco surface only received enough UV light to be activated when the UV light was set at its high level because of physical blinding (e.g. active sites in pores or shaded). A more detailed discussion of ANOVA results, including two-factor interactions, is presented in Appendix B.

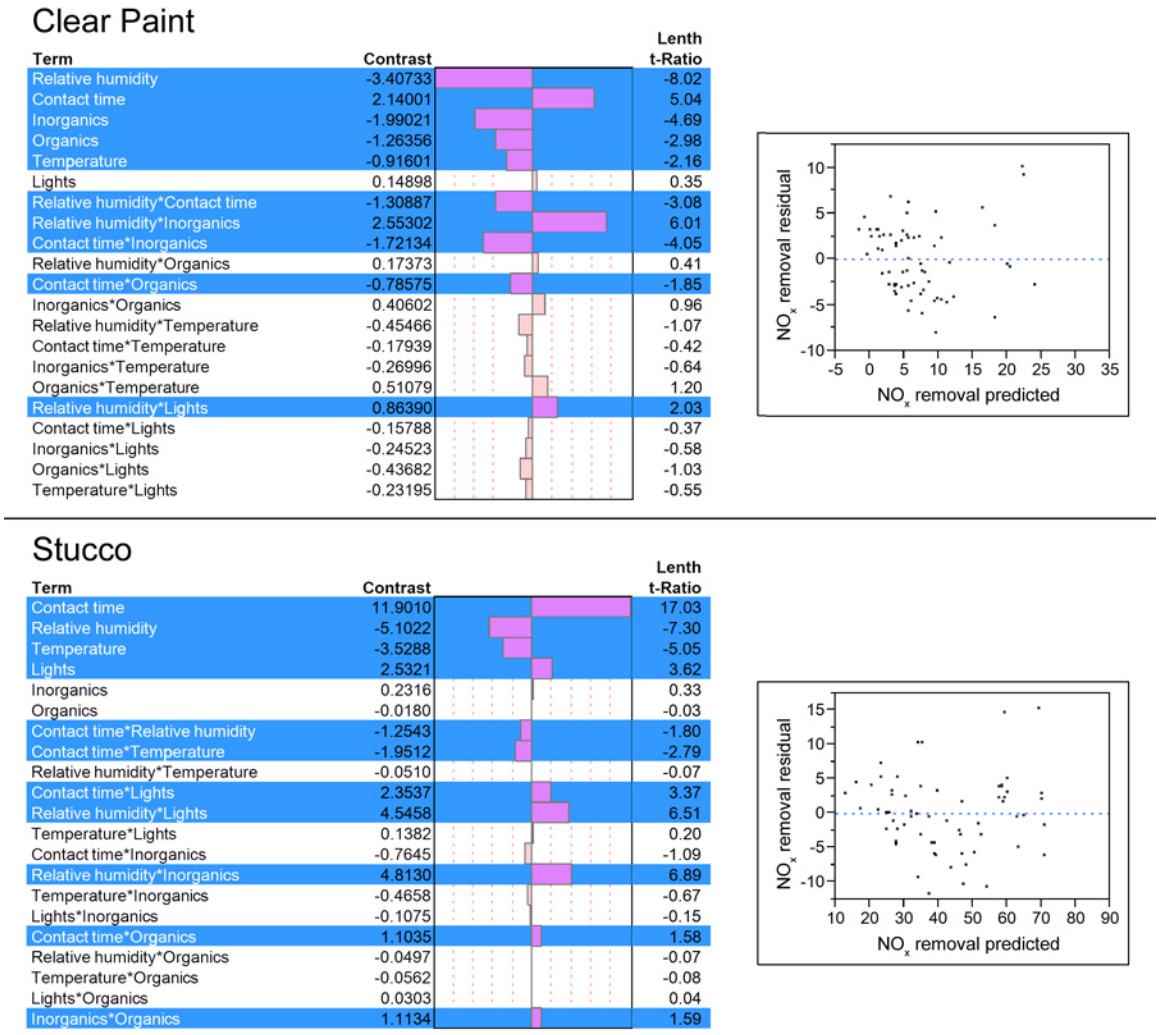

Figure 4.3. Results of ANOVA analysis of full factorial testing of outdoor PRMs

4.1.3. Exposed samples test results

Results from tests run on coated samples that had spent 1 year at field sites, and exposed to real near-roadway environmental conditions, are presented in Figure 4.4. Results indicate that exposed samples were not as effective at removing NO_x after a year of exposure, and prior to washing. Their removal efficiency before washing was up to 75 % lower than what it was for a new sample. The rinse with water did not have much of

an effect on the NO_x removal effectiveness but the soap and water wash did increase removal to over 60 % and 90 % of the removal by a new coating for the morning and afternoon conditions, respectively. Results for the uncoated concrete indicate that soap residues were not responsible for this increased removal. It is possible that compounds that are not water soluble and not readily oxidized by the photocatalyst, such as long chain hydrocarbons, occupied reaction sites and the soap surfactant helped to remove them from those sites. More details on tests run on exposed samples are presented in Appendix B.

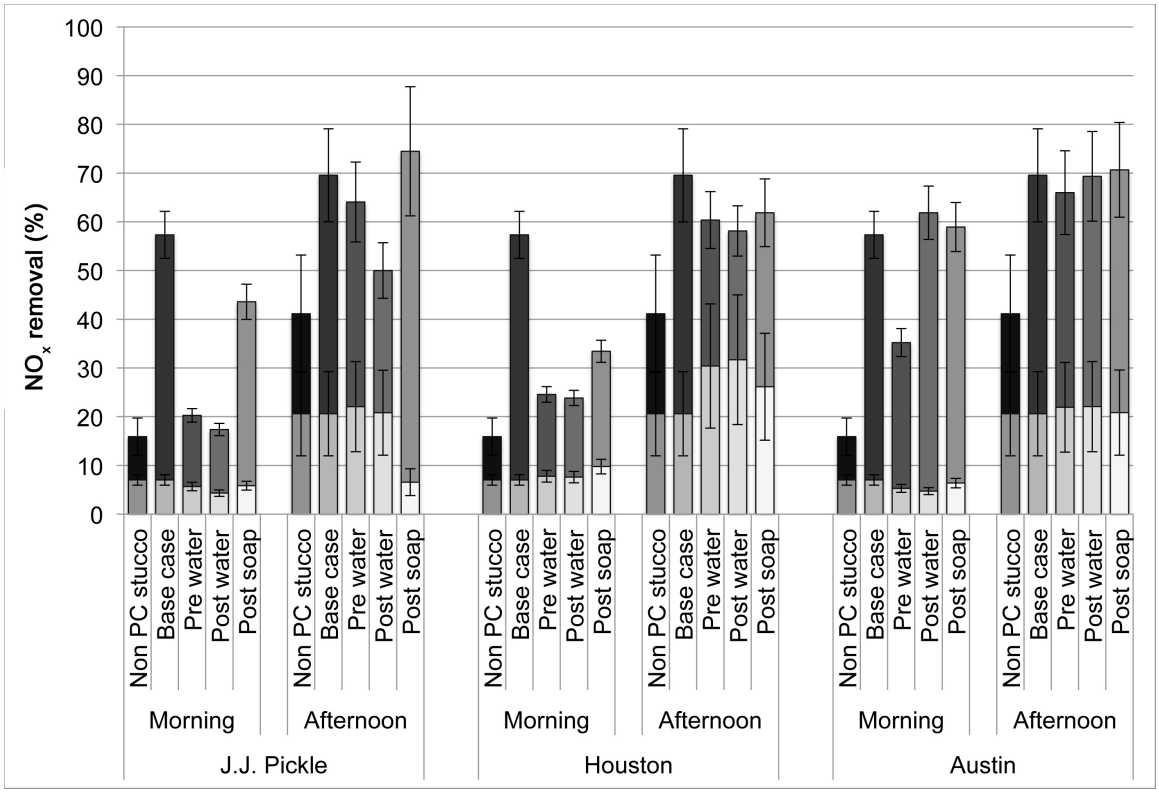

Figure 4.4. NO_x removals by stucco-coated samples after one year of outdoor exposure

4.1.4. Reaction probability of O_3, NO and NO_2 on stucco-coated concrete

To model deposition of NO, NO_2 and O_3 on the façade of the model building in Research Phase 3, the reaction probabilities between each pollutant and the stucco coating were determined. Concentrations measured during full factorial testing were used for these calculations. Reaction probabilities were determined for two conditions:

- a morning condition: morning inorganic pollutant levels, low organic pollutant levels, low temperature, high RH, low UV light intensity,
- an afternoon condition: afternoon inorganic pollutant levels, low organic pollutant levels, high temperature, low RH, high UV light intensity.

The method described in 3.1.6.3 was used to determine the pollutant transport-limited deposition velocities in the test reactor. Transport-limited deposition velocity of O_3 in the reactor was determined to be 19.4 m h^{-1}. Diffusion coefficients for NO and NO_2 were determined following the method described by Poling et al. [90] and were used to determine the transport-limited deposition velocities for NO and NO_2 based on that of O_3. The transport-limited deposition velocities for NO and NO_2 were 22.4 m h^{-1} and 18.1 m h^{-1}, respectively.

Calculated reaction probabilities are presented in Table 4.1. The reaction probability of ozone with the photocatalytic stucco was within the range of reaction probabilities reported in the literature for ozone reaction with cementitious materials that vary from 2.7×10^{-6} [91] to 7.9×10^{-5} [92]. Grøntoft and Raychaudhuri [66] also reported reaction probability with concrete made with fine aggregates (similar to the way the stucco was prepared) in the range of 1.9×10^{-6} to 4.8×10^{-6}. Judeikis and Wren [93] reported deposition of NO and NO_2 to concrete with reaction probabilities of 1.8×10^{-5} and 3.5×10^{-5}, respectively, two to five times higher than observed in this study.

However, experiments were run under sub-ambient pressures (0.1 atm), which makes direct comparison with results obtained here difficult. Reaction probabilities of NO_2 with concrete made with fine aggregates were reported by Grøntoft and Raychaudhuri [66] for similar RH levels as used in this study and ranged from 1.1×10^{-6} to 3.2×10^{-6}, approximately two to seven times lower than those calculated in this study.

Table 4.1. O_3, NO and NO_2 reaction probabilities with photocatalytic stucco

	Morning condition			Afternoon condition		
	O_3	NO	NO_2	O_3	NO	NO_2
Reaction probability	N/A	8.31×10^{-6}	N/A	8.59×10^{-6}	N/A	7.28×10^{-6}

4.2. INDOOR PRMS

4.2.1. O_3 removal results

Ozone removal capacity, measured in terms of deposition velocity, was evaluated on a monthly basis for indoor building materials placed in various indoor environments around Austin, TX. Materials were returned to the laboratory monthly for analysis before being returned to the field. Since test conditions were kept constant for all experiments involving indoor building materials, changes in observed deposition velocities were only due to changes in reactivity of the materials.

The effect of specific environments on O_3 removal by indoor building materials was studied. Deposition velocities for each material averaged over time are presented in Figure 4.5. Ozone deposition velocities measured for O_3 are in the 2.5 m h^{-1} to 3.8 m h^{-1} range, slightly lower than observed by other researchers [29, 55]. This might be due to low air velocities in the test chambers (measured < 5 cm s^{-1}), leading to higher transport resistance. The results observed for activated carbon, which is a highly reactive material,

confirm that deposition velocities measured in the chamber can realistically be applied to indoor environments. In effect, since activated carbon mat is highly reactive with O_3 [29], the surface reaction resistance is small, so the deposition velocity of O_3 on activated carbon mat should approximate the transport-limited O_3 deposition velocity in the test chambers. Transport-limited O_3 deposition velocities in indoor environments were measured by Morrison et al. [94] in the range of 1.2 m h^{-1} to 3.6 m h^{-1}, corresponding to the range of O_3 deposition velocities measured here.

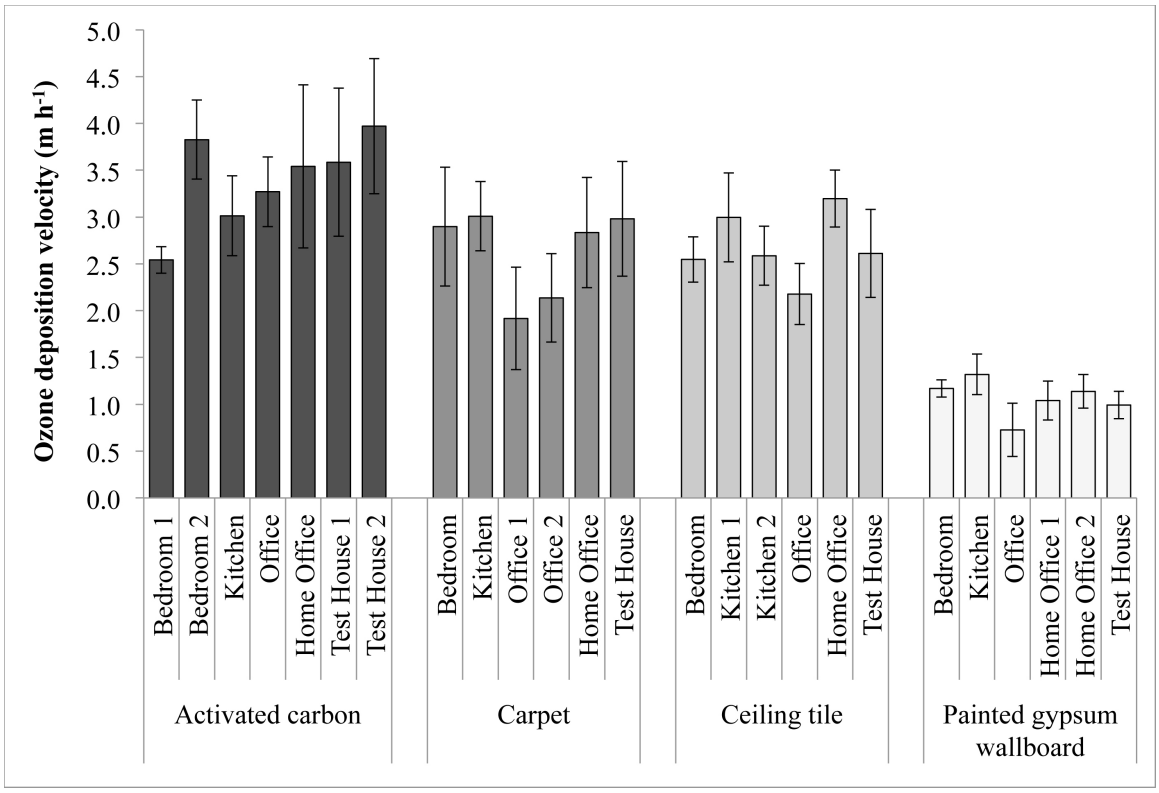

Figure 4.5. O_3 deposition velocity on indoor PRMs averaged over time

Deposition velocities for carpet and ceiling tile were slightly lower than for activated carbon, ranging from 2.0 m h^{-1} to 3.0 m h^{-1} and 2.2 m h^{-1} to 3.2 m h^{-1}, respectively, in the same range as previously reported [56, 59, 61, 91]. Finally, the

painted gypsum wallboard was the least reactive material with deposition velocities ranging from 0.7 m h^{-1} to 1.3 m h^{-1}, again in agreement with previous research [57, 59].

Green building materials in the office location exhibited reduced O_3 deposition velocity. It is possible that O_3 concentrations in that environment were higher relative to residential locations due to higher air exchange rate, outdoor air intake from the HVAC system or surfaces with lower reactivities in the environment. The influences of indoor environmental parameters on O_3 removal by each material are discussed in greater detail in Appendix C.

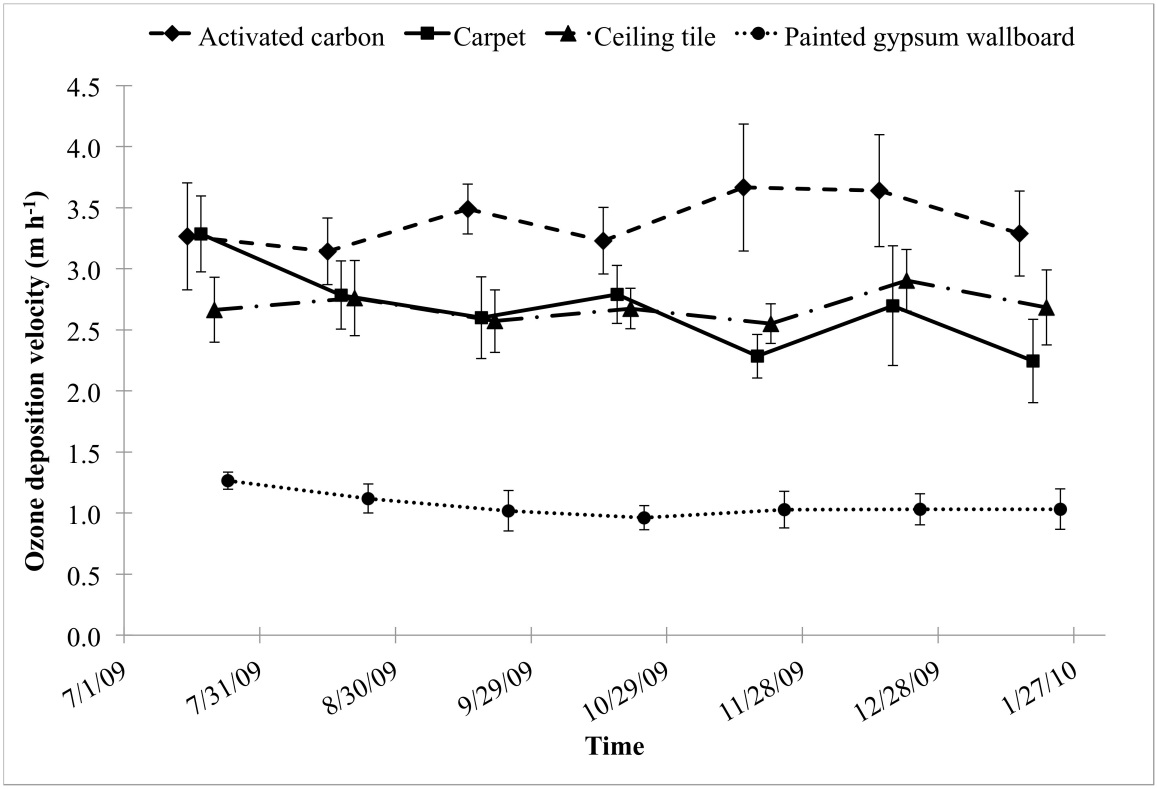

Figure 4.6. O_3 deposition velocity on indoor PRMs averaged over all field sites

Ozone deposition velocities averaged over all field locations are presented in Figure 4.6. This figure allows assessment of the durability of the material to remove O_3.

Deposition velocities for the carpet and gypsum wallboard presented a downward trend, with removals at the end of the experimental program about 30 % lower than at the beginning. Morrison et al. [58] and Wang et al. [59] also observed reduced O_3 removal by carpet with cumulative exposure or age. On the contrary, O_3 deposition velocities on the activated carbon mat and perlite-based ceiling tile remained consistent during the entire program. The activated carbon mat was the most effective material for O_3 removal. While the perlite-based ceiling tile was only the third best material for O_3 removal during initial testing, its consistency over time makes it more attractive than the carpet for long-term use.

4.2.2. Pre- and post-ozonation carbonyl emissions results

Pre-ozonation emissions refer to emissions that occurred before ozonated air was introduced into the test chambers. Post-ozonation emission rates were measured after ozonated air was introduced into the chambers. Emission rates averaged over all locations are presented in Figure 4.7. Carbonyl emissions from the activated carbon mat were lower than any other material, both before and after ozonation. Emissions were however dominated by formaldehyde (22 % to 58 % by mass) and acetaldehyde (5 % to 35 % by mass).

For all three green building materials, post-ozonation emissions were higher than pre-ozonation, and dominated by nonanal as previously observed for aged materials in homes [59].

Carpet exhibited the highest emission rates, both pre and post-ozonation. These emission rates were especially high initially, compared to the other materials, but decreased dramatically between the initial and three-month measurements. Post-ozonation emissions for carpet were consistent with results from Morrison et al. [60] and

Waring et al. [21]. However, Morrison et al. [60] observed higher pre-ozonation emissions for aged samples compared to new samples, unlike this study.

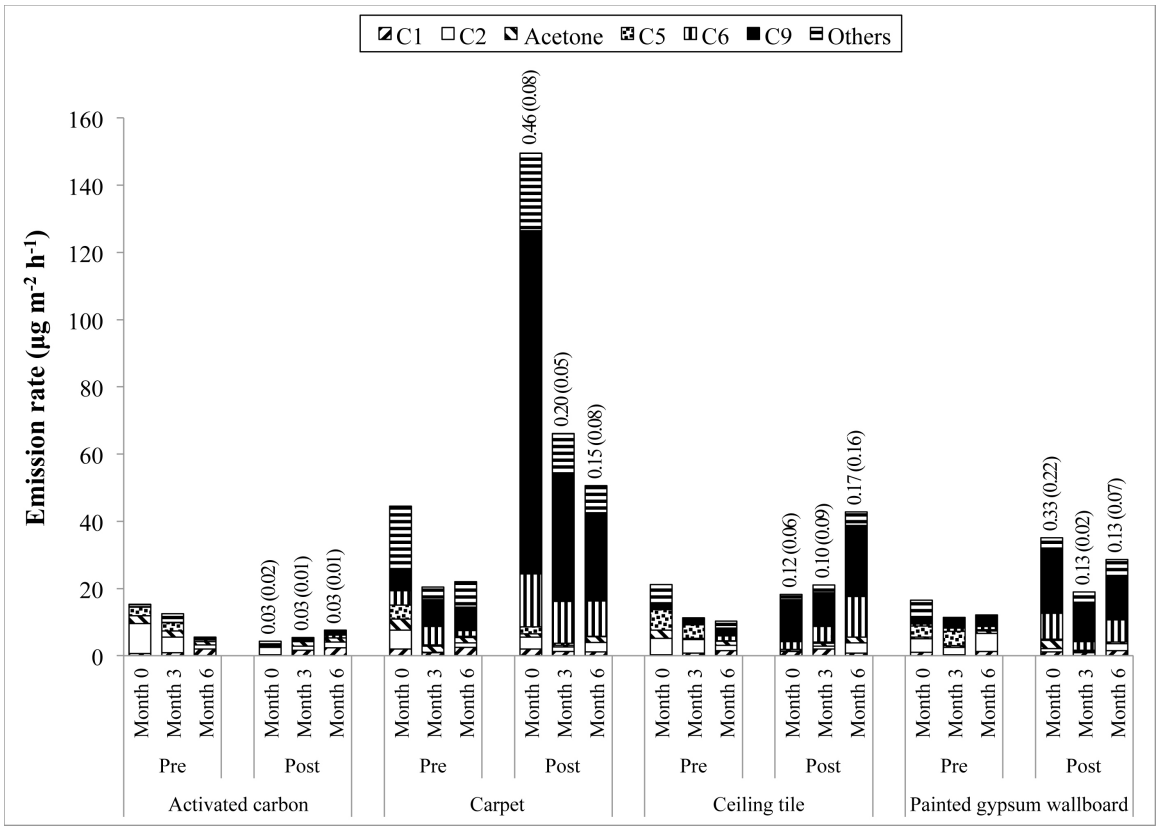

Figure 4.7. Emissions of carbonyls from indoor materials (Pre = pre-ozonation; Post = post-ozonation). Mean carbonyl mass yields are presented on top of each bar with standard deviation in parenthesis.

Results for the ceiling tile display a different trend, with pre-ozonation emissions decreasing over time but post-ozonation emissions increasing, when averaged over all field sites. In reality, the kitchen location greatly influenced the averaged results for this material and was the only location where post-ozonation emissions increased over time. It is possible that, because the ceiling tile was made of a porous material, it adsorbed gases or particles from cooking events that later reacted with O_3 during testing [95].

Finally, the painted gypsum wallboard presented a different emissions pattern, with both pre- and post-ozonation emissions decreasing between the initial and three-month measurements but increasing between the three- and six-month measurements. It is difficult to evaluate how emissions would have evolved further. More details on the influence of indoor environmental conditions on emissions are presented in Appendix C.

4.2.3. NO and NO_2 removal results

Nitric oxide and nitrogen dioxide deposition velocities on the two best performing indoor PRMs (activated carbon mat and perlite-based ceiling tiles) were measured for inclusion in the modeling of Research Phase 3. Deposition velocities of NO and NO_2 on the chamber walls were measured and the results obtained are as follows: 5.7×10^{-4} m h^{-1} and 8.9×10^{-3} m h^{-1}, respectively. Deposition velocities of NO and NO_2 on the selected indoor materials are presented in Table 4.2.

Table 4.2. Deposition velocities of NO and NO_2 on indoor PRMs

	$v_{d,NO}$ (m h^{-1})	$v_{d,NO2}$ (m h^{-1})
Ceiling tile	0.12 ± 0.02	0.48 ± 0.05
Activated carbon mat	0.92 ± 0.17	3.2 ± 0.25

Deposition velocities of NO and NO_2 to a variety of indoor materials were reported in the literature. Deposition velocity of NO on the perlite-based ceiling tile was at the upper end of the range of NO deposition velocities to ceiling materials, 0.00-0.12 m h^{-1}, reported in the literature [67]. Deposition velocity of NO_2 on the perlite-based ceiling tile tested in this study was also in the range of NO_2 deposition velocities, 0.36-0.7 m h^{-1}, reported by Grøntoft and Raychaudhuri [66] for porous stone materials.

Deposition velocity of NO to activated carbon for realistic indoor conditions could not be found in the literature. A deposition velocity of 5.0 m h^{-1} for NO_2 on an activated carbon cloth was reported by Grøntoft and Raychaudhuri [66]. It is higher than the value measured in this study. However, as explained in the case of O_3, transport limitations in the test chamber might explain the lower deposition velocities observed for very reactive materials in this study compared to other studies. This is confirmed by the fact that Grøntoft and Raychaudhuri [66] tested both O_3 and NO_2 deposition on activated carbon cloth using the same test conditions and found similar deposition velocities for both gases, as was observed in this study (average O_3 deposition velocity in this study = 3.4 m h^{-1}).

5. Modeling

5.1. METHODS

5.1.1. Model building and PRMs included

The UTest House, a 120 m^2, three bedroom/two bath manufactured home located on the J.J. Pickle Research campus of the University of Texas at Austin, was used as a model building for this study. It is equipped with pressure sensors on its façade and wind velocity sensors in its vicinity as shown in Figure 5.1. Monitoring data from a previous experimental program by Lo et al. [96] was used to validate computational fluid dynamics (CFD) simulation of airflow around the house.

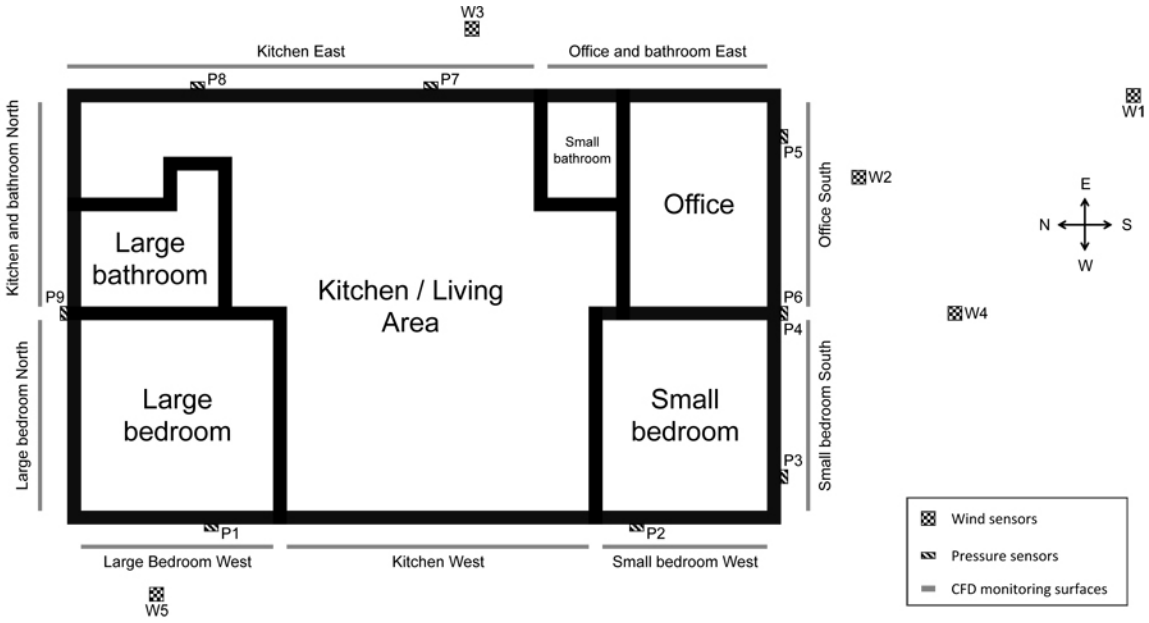

Figure 5.1. UTest House floorplan and pressure and wind sensors

In light of results from indoor and outdoor PRMs testing, activated carbon mat and perlite-based ceiling tiles were selected for inclusion in the model as indoor PRMs while the photocatalytic stucco was selected for inclusion on the model building façade.

Deposition velocities, for indoor PRMs, and reaction probabilities, for the outdoor PRM, obtained during the experimental program were used to simulate pollutant removal by the building materials.

5.1.2. Modeling conditions and scenarios

A subset of data from Lo et al. [96] was used as a basis for outdoor wind conditions of the model. The wind conditions were assumed to be constant for the duration of the model and are as follows: approach wind velocity of 7.9 m s^{-1} measured at 4 m above the ground, and azimuth angle of 163°. The wind power law (α = 0.125 [96]) was used to estimate wind velocities at various heights. Turbulence intensity was determined using data recorded by wind sensor W1 (Figure 5.1).

Three scenarios were considered and compared for the modeling effort as indicated in Table 5.1. Relative reductions in concentration between scenarios were calculated as:

$$R_{i,j} = 1 - \frac{c_i}{c_j} \tag{26}$$

where $R_{i,j}$ is the relative concentration reduction in scenario i relative to scenario j (-), c_i and c_j are the average concentrations in scenario i and j, respectively (ppb).

A scenario including the photocatalytic stucco applied on roadway barriers to reduce NO_x concentrations downwind of a roadway was also considered. A screening model was run and results suggested that the solution was not appropriate. For a best case scenario where transport resistance to the reactive surface was assumed to be negligible and for wind speeds as low as 1 m s^{-1}, only a 6 % reduction was estimated downwind of

the road when wind was perpendicular to the road, and 9 % when it was parallel to the road. The screening model is described in Appendix E.

Table 5.1. Modeling scenarios

<table>
<tr><th></th><th>Activated carbon mat</th><th>Perlite-based ceiling tile</th><th>Photocatalytic stucco</th></tr>
<tr><td>Scenario 0</td><td>None</td><td>None</td><td rowspan="2">None</td></tr>
<tr><td>Scenario 1</td><td rowspan="2">Covers half of the kitchen/living area ceiling for a total area of 23 m^2</td><td rowspan="2">Covers the ceiling of both bedrooms and the office for a total area of 36 m^2</td></tr>
<tr><td>Scenario 2</td><td>Covers entire façade of the house for a total area of 164 m^2</td></tr>
</table>

5.1.3. Determination of outdoor concentrations at the building façade

5.1.3.1. CFD model of the test house

Airflow in the vicinity of the exterior façade of the house was simulated using CFD solving the Reynolds Averaged Navier-Stokes (RANS) equations with the two-layer Realizable k-ε model. The commercially available ANSYS Fluent 12.1 code was used.

The model mesh included 500,000 computational cells. The first layer of cells adjacent to the house walls was 5 mm deep with a growth factor of 1.2 for the first 5 layers. The study domain was a rectangular prism of dimensions 45 m × 30 m × 15 m. South and East faces of the domain were set with velocity inlet boundary conditions. West and North faces were set with pressure outlet boundary conditions. The top face of the computational domain (Sky) was set with a symmetry boundary condition and the bottom face (Ground) was set with a wall boundary condition. Grid and domain

independence were verified by running the model with a coarser grid and a larger domain. More details of the model set-up are presented in Appendix D.

5.1.3.2. Outdoor conditions

Environmental conditions affecting pollutant removal by the outdoor PRM were defined using parameters and levels defined in section 3.1.4 (Table 3.1). At night, the photocatalytic coating was assumed to be non reactive since UV light was absent. Inorganic pollutant levels for the nighttime condition were determined by averaging nighttime ambient concentration data for NO, NO_2 and O_3 measured in Houston for August and September 2009 [97].

Table 5.2. Morning, afternoon and nighttime modeling conditions

	Morning	Afternoon	Night
Inorganic pollutants	NO: 150 ppb NO_2: 20 ppb	NO_2: 50 ppb O_3 : 150 ppb	NO: 5 ppb NO_2: 15 ppb O_3 : 15 ppb
Temperature	Low: 30°C	High: 40°C	N/A
Light intensity	Low: 1 mW/cm^2	High: 2 mW/cm^2	
Relative humidity	High: 65 %	Low: 20 %	
Organic pollutants	Low: 0.3 ppm	Low: 0.3 ppm	

5.1.3.3. Inclusion of outdoor PRM in CFD model

A two-step process was used to describe the effect of the outdoor PRM. First, it was assumed that the UTest House façade was a perfect sink for the pollutants considered. In that case, only the effects of transport resistance are modeled. Through the

CFD model, average air speeds above various sections of the house façade (Figure 5.1) were determined. Using correlations described by Morrison et al. [94], the transport-limited deposition velocity v_t, was calculated for each pollutant on each section of the façade. Average pollutant concentrations in the vicinity of the façade for the case where it is considered to be a perfect sink were also determined through the CFD model.

The second step consisted in adjusting pollutant concentrations in the vicinity of the UTest House façade for the case in which it is coated with the actual photocatalytic coating, which is not a perfect sink for NO, NO_2 and O_3. The method described by Rim et al. [98] was applied. The actual concentration in the vicinity of the façade was calculated as:

$$c_{actual} = \left(\frac{4v_t}{4v_t + \langle v_b \rangle \gamma}\right) c_{bulk} + \left(\frac{\langle v_b \rangle \gamma}{4v_t + \langle v_b \rangle \gamma}\right) c_{perfect} \quad (27)$$

where c_{actual} is the pollutant concentration in the vicinity of the façade with the outdoor PRM present (ppb), c_{bulk} is the pollutant concentration in the bulk air (ppb), $c_{perfect}$ is the pollutant concentration in the vicinity of the façade when it is considered to be a perfect sink for the pollutant (ppb), $<v_b>$ is the pollutant Boltzmann velocity (m h^{-1}), γ is the pollutant reaction probability with the reactive surface (-), v_t is the pollutant transport-limited deposition velocity on the façade (m h^{-1}).

For the morning condition (NO = 150 ppb, NO_2 = 20 ppb, no O_3), the concentration of NO_2 had to be adjusted differently because of a small amount of NO_2 formation as a result of NO photocatalytic oxidation observed during full factorial testing (section 4.1.2). The molar yield of NO_2 during NO photocatalytic oxidation calculated in the morning environmental conditions used for the model was y_{NO2} = 0.24 mole of NO_2

formed per mole of NO reacted. More details about the inclusion of the effect of the outdoor PRM in the CFD model are presented in Appendix D.

5.1.4. Determination of indoor concentrations

Concentrations of pollutants indoors were determined for the UTest House using the multi-zone modeling software CONTAM. Air circulation and leakage between rooms and the outside were modeled through flow paths with flow characteristics for a manufactured home obtained from Persily and Martin [99]. Pressures at the openings to the outside were determined through the CFD model and used as inputs to the CONTAM model. Pollutant concentrations at each opening were also used as inputs to the CONTAM model. For scenarios 0 and 1, ambient pollutant concentrations were used at all openings. For scenario 2, the average outdoor concentration on the outside of each wall section (Figure 5.1) was determined as described in section 5.1.3 and used for all openings on that wall. More details are presented in Appendix D.

Pollutant deposition to indoor surfaces was modeled through sink elements in CONTAM that were characterized by a deposition velocity. Deposition of the pollutants to the background (existing materials, present before introduction of PRMs) was modeled using literature values reported by Lee et al. [100] and Nazaroff and Cass [64]. Deposition to the PRMs was modeled using experimentally obtained deposition velocities (section 4.2).

A simple occupancy scenario was used in order to include the effect of the operation of the HVAC system on recirculation of air between the rooms of the house and changes in indoor/outdoor air exchange rate. It was assumed that no removal of the pollutants took place in the HVAC system, a reasonable assumption for ozone and likely

NO_x in residential environments [101, 102]. More details on the CONTAM model are presented in Appendix D.

5.2. RESULTS

5.2.1. Validation of CFD model

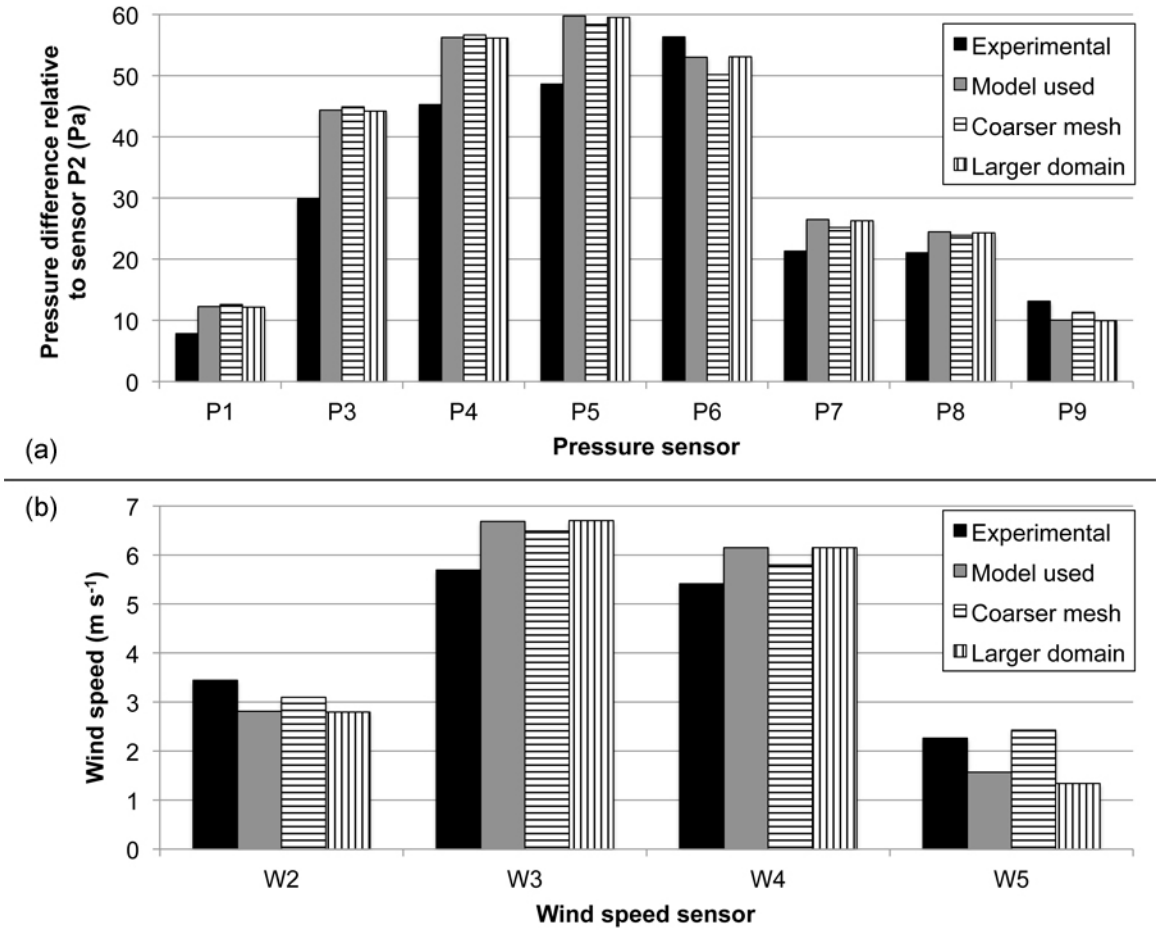

Figure 5.2. Pressure (a) and wind speed (b) simulation results compared to experimental data

Results of the CFD simulation were compared to experimentally measured pressure and wind velocity data for the approach wind condition used in this study.

Results obtained with a coarser mesh and larger computational domain were also compared to results obtained with the model used to verify mesh and domain independence of the results. Results are presented in Figure 5.2. The model appears to properly capture the important features of the airflow around the house. Moreover, grid and domain independence of the model are verified.

5.2.2. Outdoor wall concentration estimates with photocatalytic stucco

Transport limited deposition velocities calculated for each section of the UTest House façade are presented in Table 5.3. Free stream velocity above each wall section was obtained from the CFD model and used to calculate v_t using mass transfer correlations as described in section 5.1.3.3.

Table 5.3. Transport-limited deposition velocities for the sections of the UTest House façade

	$v_{t,O3}$ (m h^{-1})	$v_{t,NO}$ (m h^{-1})	$v_{t,NO2}$ (m h^{-1})
Office South	12.4	14.5	11.5
Small bedroom South	21.8	25.4	20.2
Small bedroom West	14.9	17.4	13.8
Kitchen West	13.4	15.6	12.4
Large bedroom West	11.5	13.4	10.7
Large bedroom North	7.1	8.3	6.6
Kitchen North	9.4	11.0	8.7
Kitchen East	28.9	33.8	26.8
Office and bathroom East	28.7	33.6	26.7

Estimated concentrations of pollutants in the vicinity of the UTest House façade, assuming a perfect sink and adjusted for the presence of the photocatalytic stucco, are

presented in Figure 5.3. Surface resistance represented 71% or more of the overall resistance to deposition, which explains the large differences observed between the perfect sink and non-perfect-sink cases modeled here.

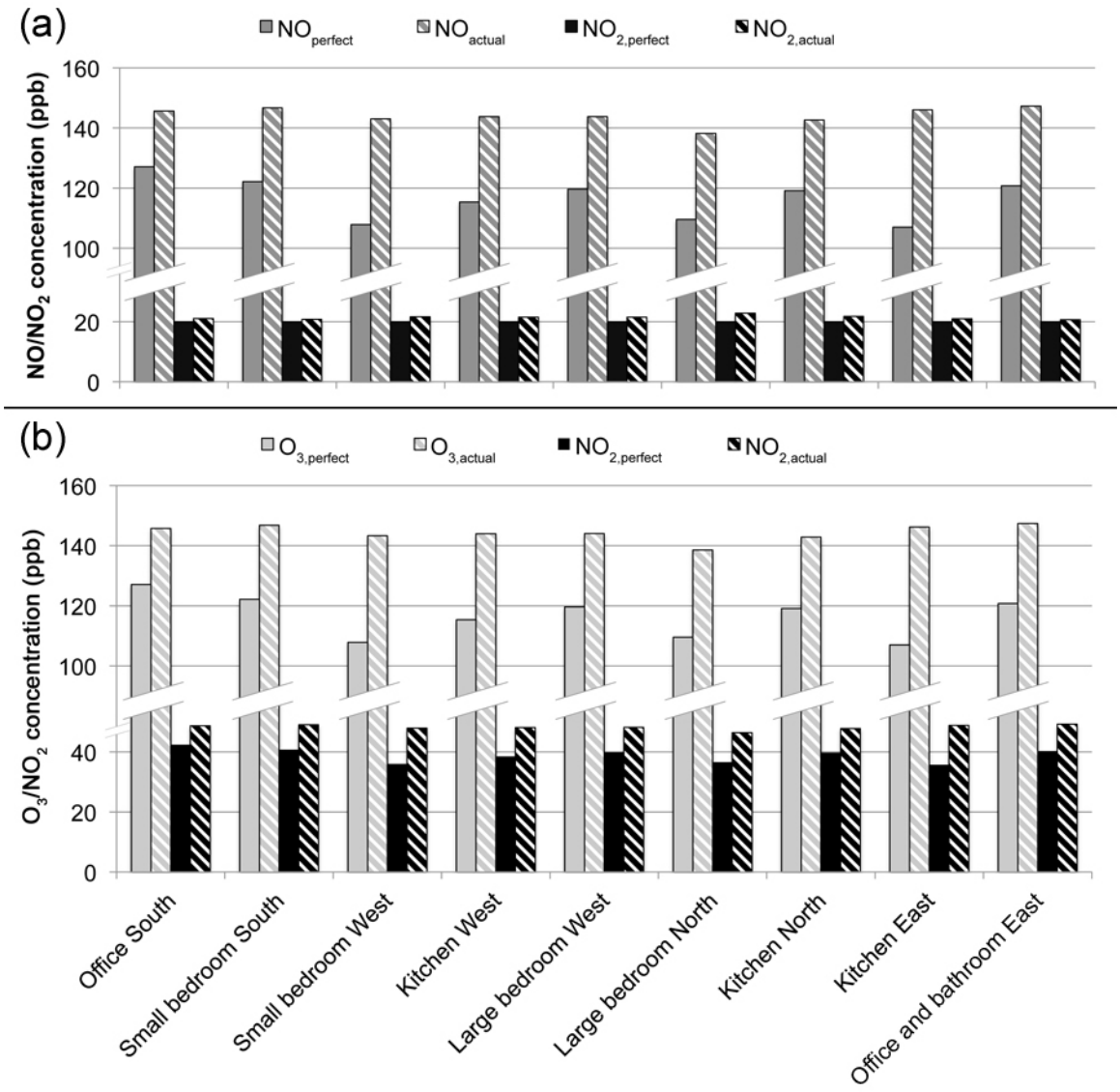

Figure 5.3. Pollutant concentrations in the vicinity of the UTest House façade in (a) the morning condition, (b) the afternoon condition

In the case where the UTest House façade was considered to be a perfect sink, pollutant concentrations in the vicinity of the façade were 15 % to 29 % lower than ambient pollutant concentrations. Taking into account the surface resistance to deposition of the photocatalytic stucco, actual pollutant concentrations in the vicinity of the façade were 7 % to 15 % lower than ambient concentrations.

Formation of NO_2 during the photocatalytic oxidation of NO in the morning condition led to small increases in NO_2 concentrations in the vicinity of the façade in the morning. Absolute NO_2 increases ranged from 0.7 to 2.8 ppb. Despite some NO_2 being formed in the morning, overall NO_x concentrations in the vicinity of the façade were lower than ambient concentrations.

Reductions observed on the windward side of the house (South and East walls) were generally lower than reductions obtained on the leeward side (North and West walls). It is possible that lower air speeds on the leeward side of the house allowed more time for reaction between pollutant molecules and the reactive surface to take place. Moreover, a fraction of the air on the leeward side of the house might have come in contact with the reactive surface while traveling along the building façade.

Moussiopoulos et al. [103] reported NO_x concentration reductions of up to 60 % in the vicinity of walls covered with a photocatalytic material in an experimental street canyon, much higher than reductions estimated in this study. The street canyon configuration offers a much higher surface-to-volume ratio for reaction and lower air speeds that might explain the higher reductions observed. More details on the CFD simulation results are presented in Appendix D.

5.2.3. Comparison of scenario results

Relative concentration reductions for O_3, NO and NO_2 obtained with the addition of indoor PRMs relative to the base case are presented in Figure 5.4. Ozone and NO_2 concentrations were reduced by up to 18 % and 23 %, respectively, with implementation of indoor PRMs. The largest concentration reduction was observed in the kitchen/living area for NO_2, where the activated carbon mat was placed. Deposition velocity of NO_2 is three times higher on the activated carbon mat than the ceiling tile, which explains why the highest reduction was observed in this room for NO_2 concentration. The largest reduction in O_3 concentration was observed in the master bedroom, equipped with perlite-based ceiling tile. Deposition velocity of O_3 on activated carbon is only 25 % higher than on the perlite-based ceiling tile, which explains the different pattern in concentration reductions between O_3 and NO_2. These reductions are in the lower range of O_3 reductions estimated by Gall et al. [30] who studied possible O_3 reductions that could be obtained for a subset of homes in Houston, TX, if they were outfitted with indoor PRMs. For the rooms equipped with ceiling tile, the leeward rooms saw larger concentration reductions than the windward rooms. It is possible that, since elevated pressures were present on the windward side of the house, the overall airflow inside the house followed the same direction as outdoors. In that case, the air present in leeward rooms had traveled through other rooms containing PRMs and pollutants had more opportunities to react away.

Incremental reductions in O_3, NO and NO_2 concentrations obtained with the addition of outdoor PRMs are presented in Figure 5.5. As expected, given the small concentration reductions simulated in the vicinity of the UTest House façade, the indoor concentration reductions observed in scenario 2 relative to scenario 1 were small, with maximum reductions of 1.7 % for O_3, 0.2 % for NO_2 and 2.0 % for NO. These reductions are negligible compared to the effect of the indoor PRMs. Installing outdoor PRMs on

house façades does not appear to be an attractive solution to reduce pollutant levels indoors. It is possible that certain urban configurations, such as street canyons, might offer more favorable conditions for passive removal [103].

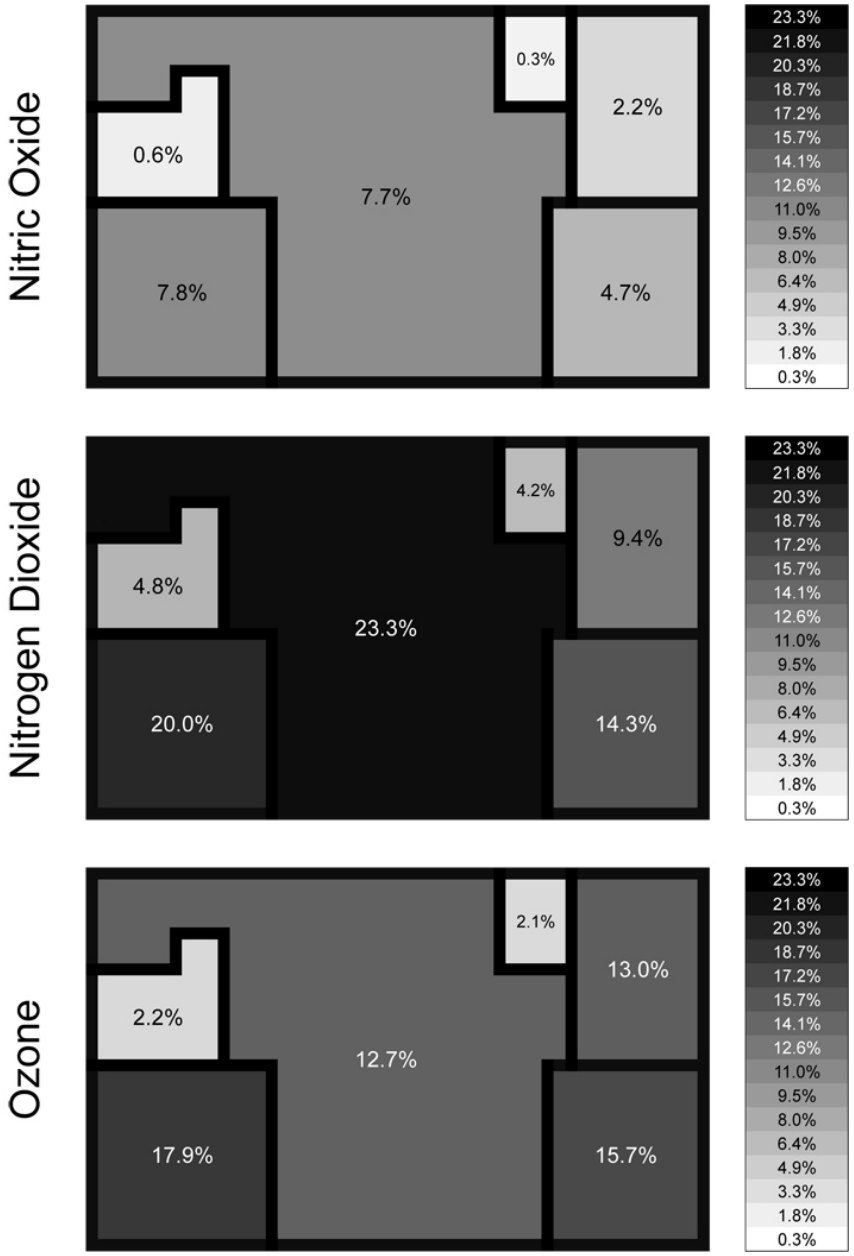

Figure 5.4. Relative concentration reductions obtained with scenario 1 (indoor PRMs only) relative to scenario 0 (no PRMs)

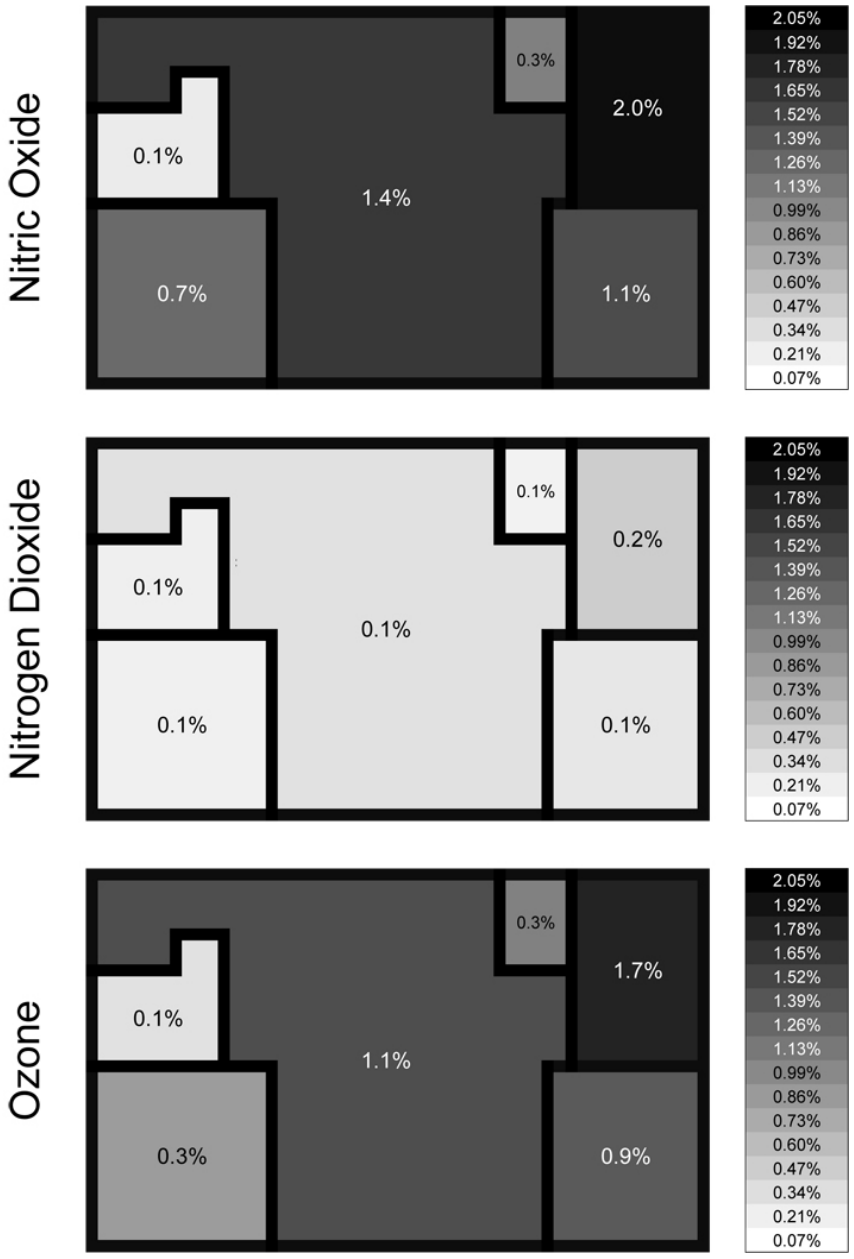

Figure 5.5. Relative concentration reductions obtained with scenario 2 (indoor and outdoor PRMs) relative to scenario 1 (indoor PRMs only)

6. Conclusions

The primary objective of this study was to evaluate the long-term feasibility of using building materials, both indoors and outdoors, to reduce concentrations of NO_x and O_3 in the indoor environment. The study involved an evaluation of removal capabilities of O_3 and NO_x by four indoor materials and three photocatalytic coatings for use outdoors.

Photocatalytic materials were tested in the laboratory and effects of environmental parameters were evaluated through full factorial testing. These coatings were also exposed to real outdoor conditions for evaluation of long-term performance. Conclusions related to the performance of outdoor PRMs are:

- Coatings containing the anatase crystalline form of TiO_2 perform better at removing NO_x.
- Contact time, relative humidity and temperature significantly affect coatings that contain anatase in the same way: increased contact time leads to increased removal of NO_x while increased relative humidity or temperature lead to reduced removal.
- Wear of a coating can lead to a rapid decline of its NO_x removal capacity.
- Long-term exposure of a photocatalytic coating to real outdoor conditions reduces its NO_x removal capacity.
- Removal capacity of NO_x cannot be restored by a simple water rinse, but can be largely restored by rinsing with a soap solution.

Samples of four indoor materials were placed in a wide range of real indoor environments and were tested monthly for a six-month period, for their capacity to remove O_3 as well as pre- and post-ozonation emissions of carbonyls. Removal of NO_x to

select new indoor building materials was also tested. Conclusions related to the performance of indoor PRMs include:

- Carpet and painted gypsum wallboard are not good choices for removal of indoor ozone. Their O_3 removal effectiveness decreased by 30 % between the initial and six-month tests.
- Activated carbon mat and perlite-based ceiling tiles can provide consistent and relatively high O_3 removal capability over six months, and possibly longer periods.
- Activated carbon mat can provide relatively high NO and NO_2 removal capability as well.
- Specific indoor environments and occupant behavior can affect O_3 removal performance of building materials.
- Both pre- and post-ozonation carbonyl emissions by activated carbon mats are low compared to conventional green building materials.
- Post-ozonation carbonyl emissions of green building materials are higher than pre-ozonation carbonyl emissions, and dominated by nonanal.

Material characteristics pertaining to pollutant removals and measured during laboratory experiments were included in a multi-zone/CFD model in order to estimate possible O_3 and NO_x concentration reductions through the use of indoor and a combination of indoor and outdoor PRMs. A model building, the UTest House, and previously measured outdoor wind conditions were utilized. Conclusions stemming from the modeling exercise include:

- Indoor PRMs could help reduce occupants' inhalation exposure to O_3 and NO_x. Concentration reductions estimated with the implementation of

indoor PRMs were as high as 18 % for O_3 and 23 % for NO_2 in rooms outfitted with activated carbon mat or perlite-based ceiling tiles.

- Outdoor PRMs can reduce pollutant concentrations in air infiltrating into a building. Concentrations in the vicinity of the model building equipped with a photocatalytic stucco were 7 % to 15 % lower than ambient concentrations.
- Incremental indoor O_3 and NO_x concentration reductions obtained by addition of outdoor PRMs to a detached house already equipped with indoor PRMs are negligible.

The results of this study show that properly selected indoor materials are a viable solution to reduce the inhalation-exposure of building occupants to O_3 and NO_x. Future research is needed to identify more indoor building materials suitable for PRM use through exhaustive testing or by identifying physico-chemical characteristics that make them efficient for pollutant removal. Extension to other pollutants would also be beneficial.

Despite promising results in laboratory experiments, simulation of the application of an outdoor PRM on the façade of a detached house led to negligible pollutant reductions indoors. Future research should focus on other urban building configurations, such as street-canyons, that might make better use of outdoor PRMs.

Appendix A

Paper 1: Clement J. Cros, Alexandra L. Terpeluk, Neil E. Crain, Maria G. Juenger, Richard L. Corsi. Influence of environmental factors on removal of oxides of nitrogen by a photocatalytic coating. Submitted to *Atmospheric Environment* on March 20th 2013.

ABSTRACT

Nitrogen oxides (NO_x) emitted from combustion processes have elevated concentrations in large urban areas. They cause a range of adverse health effects, acid rain, and are precursors to formation of other atmospheric pollutants, such as ozone, peroxyacetyl nitrate, and inorganic aerosols. Photocatalytic materials containing a semi-conductor that can be activated by sunlight, such as titanium dioxide, have been studied for their ability to remove NO_x. The study presented herein aims to elucidate the environmental parameters that most influence the NO_x removal efficiency of photocatalytic coatings in hot and humid climate conditions. Concrete samples coated with a commercially available photocatalytic coating (a stucco) and an uncoated sample have been tested in a reactor simulating reasonable summertime outdoor sunlight, relative humidity and temperature conditions in southeast Texas. Two-level full factorial experiments were completed on each sample for five parameters. It was found that contact time, relative humidity and temperature significantly influenced both NO and NO_2 removal. Elevated concentrations of organic pollutants reduced NO removal by the coating. Ultra-violet light intensity did not significantly influence removal of NO or NO_2, however, ultra-violet light intensity was involved in a two-factor interaction that significantly influenced removal of both NO and NO_2.

Keywords: Photocatalysis, oxides of nitrogen, coating, full-factorial

1. INTRODUCTION

Nitrogen oxides are ubiquitous in urban environments. They are produced by various fossil fuel combustion processes found in industries, power generation facilities, and vehicles. In the United States, emissions from highway vehicles represent 31 % of

NO_x emissions (EPA, 2011). Oxides of nitrogen are responsible for acid rain, which damages structures and vegetation. They are also precursors to the formation of ozone and other pollutants through photochemical processes (Seinfeld and Pandis, 2006). Exposure to NO_x has been associated with adverse health effects including increased airway reactivity, decreased pulmonary function (Bauer et al., 1986; Mohsenin, 1987; Frampton et al., 1991), onset of asthma (Gauderman et al., 2005; Clark et al., 2009), arrhythmia (Peters et al., 2000), and lung cancer (Nafstad et al., 2004; Raaschou-Nielsen and Reynolds, 2006). Populations living near roadways are routinely exposed to elevated levels of NO_x and are subject to greater adverse health effects than the general population (Brunekreef et al., 1997; Krämer et al., 2000; Janssen et al., 2003; Thoma et al., 2008; EPA, 2010).

Finding new ways to remove NO_x originating on roadways from urban atmospheres could be very beneficial for both the environment and the health of populations in these areas. Photocatalytic materials have been studied for years because of their capacity to remove NO_x through oxidation reactions (Fujishima and Honda, 1972; Allen et al., 2005; Ballari et al., 2010a; Laufs et al., 2010). Built structures near roadways are candidates for the application of this technology. They are in close proximity to a NO_x emission source, and enhanced dispersion of pollutants from roadways due to mechanical shear of air caused by motor vehicles increases opportunity for contact. In contrast to other stationary sources such as industries or power plants, the pollutant source is close to the ground, so it is possible to take advantage of surrounding structures for passive removal. It is also possible to implement new structures for the purpose of pollution reduction, with other added benefits (e.g. noise reduction and enhanced roadway safety). Application of photocatalytic material is attractive because, once it is applied it could potentially remove NO_x without necessitating energy input. Moreover,

because the material acts as a catalyst, it could theoretically be used indefinitely without replacement as long as it can be regenerated.

Photocatalysis is a process that occurs at the surface of a semi-conductor exposed to light (Fujishima and Honda, 1972). When a photon with energy equal or larger than the band gap of the semiconductor is absorbed, an electron (e^-) from the valence band is promoted to the conduction band. The result is the generation of a "hole" in the valence band (h^+). Both h^+ and e^- are strong oxidizing and reducing agents, respectively. The electron-hole pair may react with electron donors or acceptors adsorbed to the semi-conductor surface (Fujishima and Honda, 1972; Hoffmann et al., 1995; Chen and Poon, 2009). Oxygen and water adsorbed at the semi-conductor surface are catalyzed to form reactive species, superoxide anions (O_2^-) and hydroxyl radicals ($OH^\bullet$). Hydroxyl radicals and superoxide anions are strong oxidizing and reducing agents, respectively. They can react with pollutant molecules adsorbed to the photocatalytic surface, such as NO_x or hydrocarbons (Dalton et al., 2002; Allen et al., 2005; Ohko et al., 2009; Laufs et al., 2010; Ballari et al., 2010a). In the case of NO_x, the product of the reactions involving NO, NO_2 and hydroxyl radicals is nitric acid, which remains adsorbed on the photocatalytic surface until it is washed off by water (Devahasdin et al., 2003; Hunger et al., 2010; Ballari et al., 2010a).

Titanium dioxide (TiO_2) is the most widely used semi-conductor for photocatalysis applications. It is inexpensive, chemically and biologically inert and stable with respect to photo and chemical corrosion (Hoffmann et al., 1995). Of its three crystalline forms (anatase, rutile and brookite), anatase is the preferred photocatalyst because it has the highest photoactivity (Chen and Poon, 2009).

Researchers have previously studied environmental parameters that can affect the photocatalytic removal of NO_x. Removal increases non-linearly with light intensity (Ollis

et al., 1991; Lim et al., 2000; Bengtsson and Castellote, 2010), but decreases with increasing relative humidity (Hüsken et al., 2009; Dylla et al., 2010; Laufs et al., 2010; Ballari et al., 2011). Relative humidity might also influence NO_x removal through reactions taking place in water films at the material surface (Svensson et al., 1987; Jenkin et al., 1988; Saliba et al., 2001; Finlayson-Pitts et al., 2002). Some researchers have also observed that for NO and NO_2 concentrations less than 1 ppm the conversion rate does not depend on the initial concentration injected, even when both chemicals are introduced at the same time (Bengtsson and Castellote, 2010; Laufs et al., 2010). But others have observed removal to increase with decreasing concentration in air (Hüsken et al., 2009). However, most researchers have not investigated NO_x removals with realistic outdoor air mixtures that contain other pollutants such as ozone or VOCs. Of those who have, none have studied the simultaneous effect of environmental conditions such as light intensity, temperature and relative humidity.

This study aimed to elucidate the environmental parameters that have a significant effect on the NO_x removal efficiency of a photocatalytic coating when tested under realistic conditions. In the past, researchers have studied a wide range of photocatalytic materials, from TiO_2 slurries (Lim et al., 2000; Devahasdin et al., 2003; Ohko et al., 2009; Bengtsson and Castellote, 2010), to paints (Maggos et al., 2007b; Laufs et al., 2010), paving stones (Hüsken et al., 2009; Ballari et al., 2010b; 2011) or concrete containing TiO_2 in its cement matrix (Beeldens, 2006; Chen and Poon, 2009; Dylla et al., 2010; 2011). In this study, we focused on a TiO_2-containing stucco coating applied to concrete. The application of a stucco coating provides advantages over concrete that includes TiO_2 in the cement. Since stucco is applied in a thin surface layer, a smaller amount of semi-conductor material is needed for the same active surface area as concrete that contains TiO_2 through the full depth. Since TiO_2-containing cement is expensive, the

stucco coating is a more cost-effective solution for new structures. Moreover, stucco coatings can also be applied on existing concrete structures, reducing the cost of implementation of this technology on existing near-roadway structures.

2. EXPERIMENTAL METHODS

2.1. Materials

The stucco tested in this study is a commercially available product. It was applied on concrete slabs manufactured following mixture proportions provided by a commercial concrete precast company in Texas for use in highway barriers: 25 % fly ash/75 % Type III cement, water to cementitious materials ratio by mass of 0.34, limestone coarse and fine aggregate, and Plastiment and Sika 2110 admixtures (Sika Corporation U.S., Lyndhurst, NJ, USA). The photocatalytic coating was applied to the concrete samples after one week of curing in a 100 % relative humidity (RH) room and two weeks of drying in a 50 % RH room, both at 23°C. The concrete samples were 7.5 cm thick and 33 cm wide. Two different lengths were fabricated to vary the contact time during chamber testing. Full size samples were 90 cm in length and half-size samples were 45 cm in length. The stucco (TX Active; ESSROC, Nazareth, PA, USA) is composed of portland cement, admixtures and 4.98 % by mass of solids of TiO_2. It was mixed with sand and water to achieve the desired consistency (by weight: 67 % sand, 13 % water, 20 % stucco cement) and applied in a 5 mm thick layer. Uncoated concrete samples were also manufactured and tested for comparison.

2.2. Laboratory system

The experimental set-up used for testing of the photocatalytic coating is presented in Figure 1. There are few standards related to testing of photocatalytic materials (ISO, 2007; JIS, 2010; UNI, 2010), which were developed to test different materials under a

single, uniform condition. In this study, the goal was to examine the effect of varying environmental conditions on NO_x removal by a coating. For that reason, a custom reactor was designed to recreate outdoor conditions and to provide a consistent airflow pattern above the material surface for various airflow rates. A 150-L stainless steel electro-polished chamber was used to test coated concrete samples, with dimensions 33 cm × 137 cm × 35 cm. Well-mixed conditions were confirmed by a tracer test using carbon dioxide and ASTM standard D5116-10 (ASTM, 2006). Airflow in the test chamber was simulated through computational fluid dynamics using Airpak (Airpak 3; Ansys, Canonsburg, PA, USA). It was determined that the most homogeneous air speeds over the material sample surface were obtained when the entire bottom of the test chamber was flat. Stainless steel blocks were made to fit at each end of the samples in order to create a flat surface extending the length of the chamber. Once a sample and the stainless steel blocks were placed in the chamber, the air volume was 115 L.

Eight UV lamps (40 W, 280-400 nm, λ_{max} = 310 nm, model QFS-40; Q-Lab Corp., Cleveland, OH, USA) were installed in the chamber. The inlet and outlet of the chamber were equipped with relative humidity probes (model HD2XVSX; Veries Industries, Portland, OR, USA) and thermistors (model 44203; YSI, Yellow Springs, OH, USA). A third thermistor was placed in the middle of the reactor, above the concrete sample.

An air stream provided by two zero air generators (model 701; Teledyne, San Diego, CA, USA) was split, and a portion of the air was passed through an impinger in order to adjust the relative humidity. Pollutant species mixed with nitrogen were obtained in gas cylinders (Praxair, Danbury, CT, USA): nitrogen oxide, nitrogen dioxide, propane (as a surrogate for volatile organic compounds) and propylene (as a surrogate for highly reactive volatile organic compounds). Ozone was produced by passing pure oxygen

through a UV-based ozone generator (Model 97-0067-01; UVP, LLC, Upland, CA, USA). Pollutant species were introduced at a known rate through mass flow controllers (Series FMA 5500; Omega Engineering, Inc., Stamford, CT, USA; Series GFC 1700; Aalborg, Orangeburg, NY, USA). The influent air stream then passed through a mixing zone before being introduced in the chamber. The mixing zone consisted of a succession of sections of tubing of two different diameters and a 12 L inlet mixing chamber separated from the main chamber volume by a baffle.

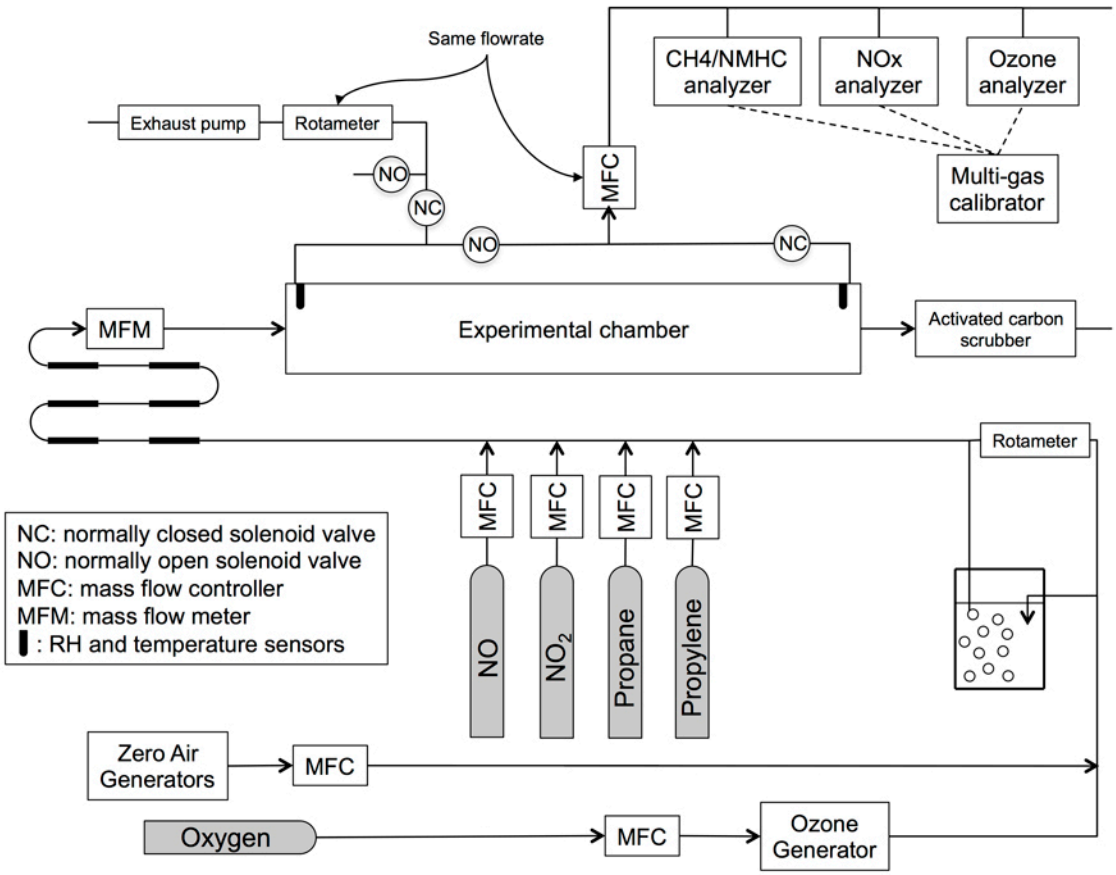

Figure 1. Schematic of experimental system

Chamber air was sampled at both the inlet and outlet of the chamber. A system of solenoid valves (models SV123/133; Omega Engineering Inc.) automatically switched sampling between the inlet and outlet. When sampling the outlet, an exhaust pump removed a flow rate of gas equal to the flow rate going to the instruments to maintain a constant gas flow rate through the chamber. Measurements for NO and NO_2 concentrations were made by a chemiluminescence analyzer (model 200E; Teledyne). Ozone concentrations were measured by a UV absorbance ozone analyzer (model 1008-AH; Dasibi, Glendale, CA, USA). Volatile organic compound (VOC) concentrations were measured by a methane/non-methane hydrocarbons analyzer (model 55i; Thermo Fisher Scientific, Waltham, MA, USA). These instruments were calibrated daily using a multi-gas calibrator (model 700E; Teledyne) and concentration certified gas standards (Praxair).

Testing conditions deviate from some aspects from the ISO 22197 standard for testing of photocatalytic materials. UV lamps were placed inside the reactor enclosure. This produced well-mixed conditions in the reactor and heated the air and concrete to temperatures typically encountered during summer months in Southeast Texas. NO_x concentrations used for testing are also lower than concentrations prescribed in the ISO 22197-1 standard (1 ppm NO). The goal was to study NO_x pollution levels under realistic outdoor conditions.

2.3. Full factorial experiments

To determine which environmental parameters influence NO_x removal, the stucco-coated concrete and uncoated concrete underwent two-level factorial testing. Five parameters were varied between a low and a high level, as listed in Table 1. Low and high levels represented the bounds of ranges of values commonly observed for the

different variables during the ozone season in Southeast Texas. Some limitations of the experimental system also influenced the range of variables that could be recreated in the test chamber. Nitric oxide and nitrogen dioxide removals were tested in the presence of other inorganic pollutants to simulate outdoor air conditions. Nitric oxide concentrations are usually highest in the morning, with lower NO_2 and ozone concentrations at that time. The situation is reversed in the afternoon, when NO_2 and ozone concentrations are highest and NO concentrations are low. However ozone and NO could not be injected simultaneously in the reactor because of immediate titration of NO by ozone. Hence, NO removal was tested in a "morning" condition with a high level of NO (150 ppb) and a low level of NO_2 (20 ppb). Nitrogen dioxide removal was tested in an afternoon condition with a high level of NO_2 (50 ppb) and ozone (150 ppb) and no NO. These concentrations were determined by analyzing Houston air quality data from 2009 (TCEQ, 2009). Maximum concentrations of NO, NO_2 and ozone for the period between August 15th and September 15th 2009 were analyzed. The maximum concentrations were used to establish experimental values of NO concentration in the morning and NO_2 and ozone concentrations in the afternoon. The NO_2 concentration used in the morning condition corresponds to twice the value usually observed in morning hours, in order to obtain better detection by the NO_x analyzer (lower detection limit: 0.4 ppb). These conditions correspond to a worst-case scenario.

Eight experiments were consecutively run on one test coupon before it was removed from the chamber and the next sample was tested. Before the first experiment and between rounds of experiments, each sample was rinsed with distilled water. The goal was to regenerate the catalyst by washing off nitric acid, the product of the photocatalytic conversion of NO and NO_2, that might have remained at the catalyst surface. For rinsing, full size samples were placed horizontally first and 4 liters of

distilled water were poured on the sample in increments of 1 liter. Between each rinse with 1 liter, the sample was left to drip for 30 seconds. Finally, the sample was tilted at a 30° angle and 4 liters of distilled water were poured on the sample, running off quickly. The sample was then set out to dry in the laboratory for 24 hours. Half-size samples were rinsed following the same methodology, but using half the amount of water.

Table 1. Full factorial experimental parameters and their magnitudes

	Low level	**High level**
Contact time	1.5 minutes	15 minutes
Relative humidity	20%	65%
Temperature	30°C	40°C
Organic pollutants		
- propane (VOC)	0.25 ppm	2.5 ppm
- propylene (HRVOC)	0.05 ppm	0.5 ppm
Lights	1 mW cm^{-2}	2 mW cm^{-2}

2.4. Data analysis

Oxides of nitrogen removals were calculated using steady-state concentration data obtained during full factorial tests. First, removal by the uncoated concrete was calculated using:

$$R_b = 100 \times (1 - c_{out,b}/c_{in,b}) \quad (1)$$

where $c_{in,b}$ is the pollutant concentration measured in the chamber inlet for the test run with uncoated concrete (ppb), $c_{out,b}$ is the pollutant concentration measured in the chamber outlet for the test run with uncoated concrete (ppb), R_b is the pollutant removal by the uncoated concrete (%).

The removals for the photocatalytic coating were calculated in a similar fashion. For each test, the removal by the uncoated concrete was subtracted from that of the coated concrete to determine the removal by the photocatalytic coating over the existing structures made of uncoated concrete. This process allowed an evaluation of the incremental NO_x removal that would be obtained by coating existing concrete structures with a photocatalytic coating:

$$R = 100 \times (1 - c_{out}/c_{in}) - R_b \quad (2)$$

where c_{in} is the pollutant concentration measured in the inlet of the chamber (ppb), c_{out} is the pollutant concentration measured in the outlet of the chamber (ppb), R is the pollutant removal by the coated concrete (%).

The uncertainty associated with calculated removals was determined using standard error propagation techniques. The uncertainty on the concentration measurements was taken as two standard deviations of measured values for all calibrations run during the experimental program. Relative uncertainties were determined to be 8.0 % for NO measurements and 9.8 % for NO_2 measurements.

The results from the full factorial experiments were analyzed using JMP software (JMP 9; SAS, Cary, NC, USA) to determine the most important factors affecting NO_x removal, using analysis of variance (ANOVA) techniques. ANOVA determines whether the means of different groups are statistically different. Main factors as well as two-factor interactions were taken into account. Higher-level interactions were not considered. Ten percent of the experiments were replicated. The Lenth method was used to provide approximate tests of significance (Tamhane, 2009). The Lenth method provides an

estimate of the standard error, called the Lenth pseudo standard error (PSE), where PSE = $1.5 \times \text{Median}(|\theta_i|: \theta_i < 2.5 \times \tau 0)$ and $\tau 0 = 1.5 \times \text{Median}(|\theta_i|)$ with θ_i the ith contrast.

The Lenth t-ratio was calculated as the ratio of the contrast for a factor over the PSE (Mee, 2009). The t-statistic for each factor was compared to critical values provided by Mee (2009). Factors with a Lenth t-ratio larger than the critical value were deemed significant. A significance level $\alpha = 0.15$ was used to determine the critical value. Outliers were determined by using the studentized residuals test described by Mee (2009).

3. RESULTS

Results for NO and NO_2 removals observed during full factorial testing are presented in Figure 2. Nitric oxide removals averaged 46 % (standard deviation: 13 %) while NO_2 removals averaged 41 % (standard deviation: 14 %). The pattern of the removal data was different for NO and NO_2 removals, suggesting that different factors or two-factor interactions affected the removal of each gas.

Results from the analysis of data using JMP software are presented in Figure 3. The PSE were 0.896 and 1.609 for NO and NO_2 removal, respectively. The critical value to which Lenth t-ratios were compared is 1.446 according to Mee (2009) for a significance level $\alpha = 0.15$. Four main factors (contact time, organic pollutants concentrations, RH, temperature) and three two-factor interactions (contact time × organic pollutants concentrations, RH × organic pollutants concentrations, RH × UV light intensity) were deemed significant for NO removal and three main factors (contact time, temperature, RH) and two two-factor interactions (temperature × RH, RH × UV light intensity) were deemed significant for NO_2 removal.

The linear models associated with NO and NO_2 removals and determined using JMP havd R^2 of 0.89 and 0.79, respectively. Residuals calculated with respect to the linear model determined using JMP were fairly consistent across the range of predicted values suggesting that the hypothesis of equal variance was met. Residuals were also normally distributed as verified using a Shapiro-Wilk test with W = 0.97, p = 0.41 for NO removal residuals and W = 0.94 and p = 0.08 for NO_2 removal residuals.

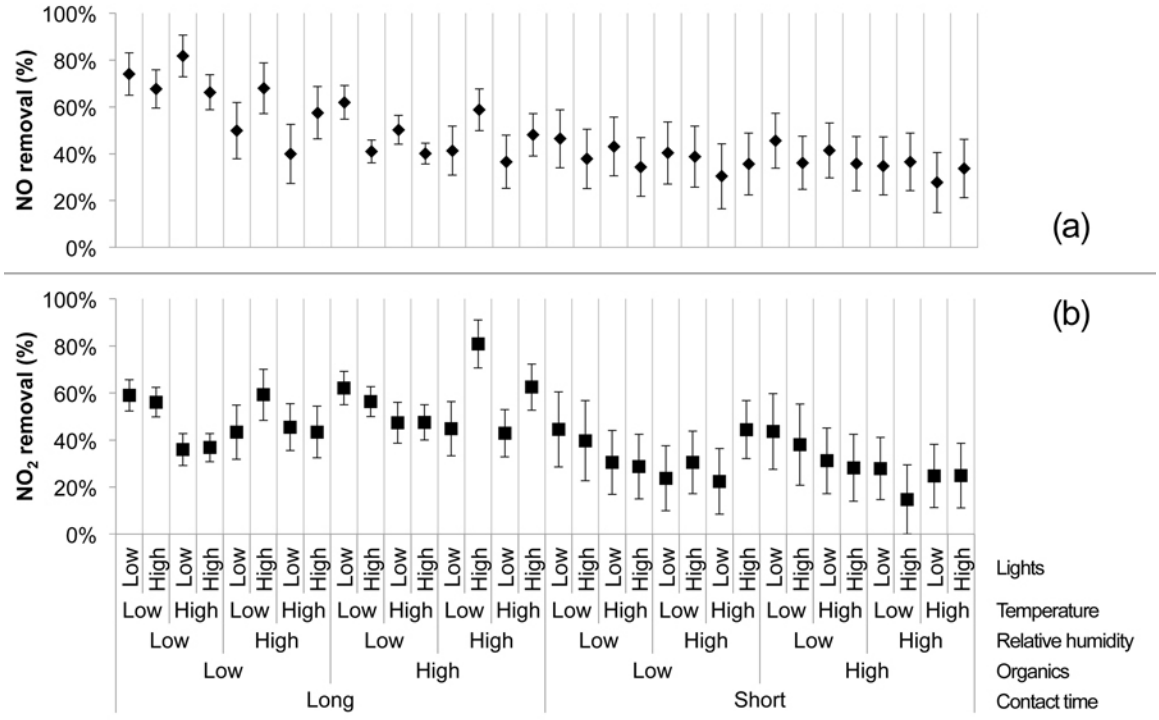

Figure 2. (a) NO and (b) NO_2 removals by TxActive stucco observed during full factorial testing

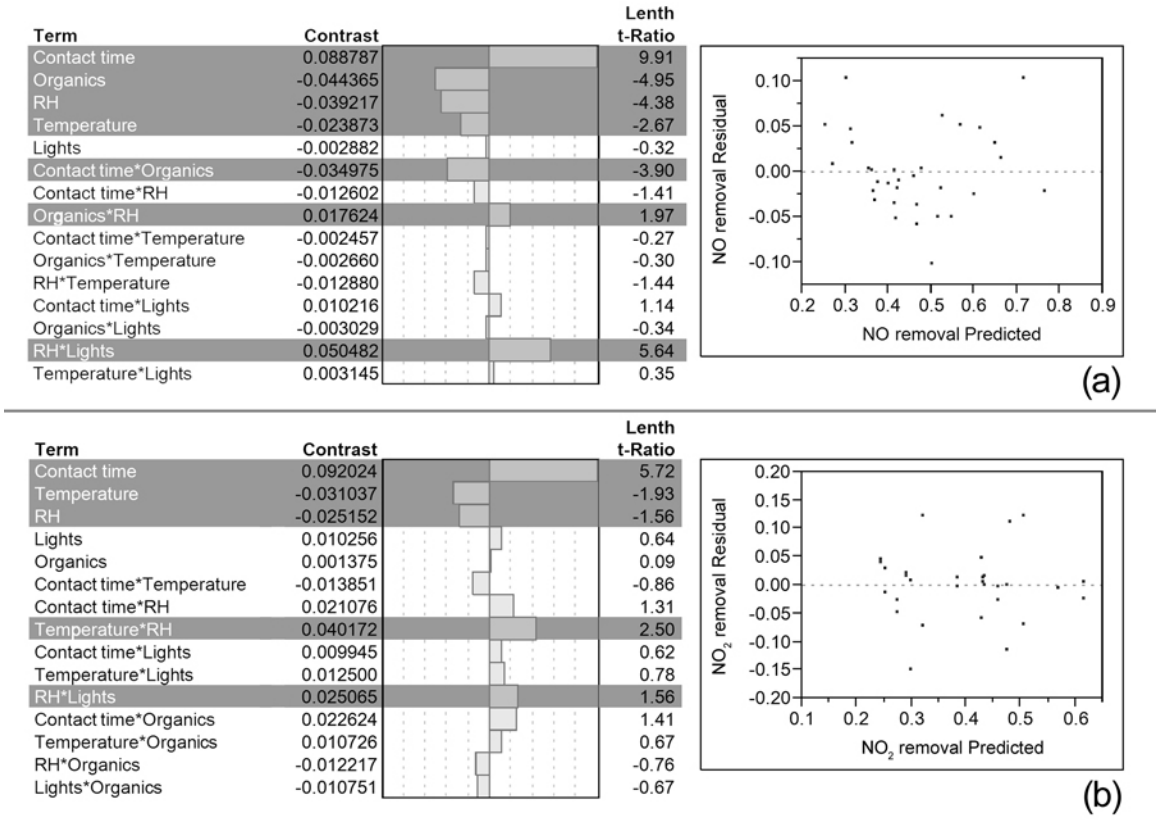

Figure 3. Significant effects and residual plots for the removal of (a) NO and (b) NO_2

Interaction plots for the three two-factor interactions for NO and the two two-factor interactions for NO_2 removal are presented in Figure 4. It is interesting that for both gases the interaction plots exhibit crossing lines for the plots involving interactions between relative humidity and light intensity. This suggests that when RH was at its high level, an increase in light intensity also increased removal, but when RH was at its low level, removal decreased with increasing light intensity. Other interactions had different effects on each NO_x species.

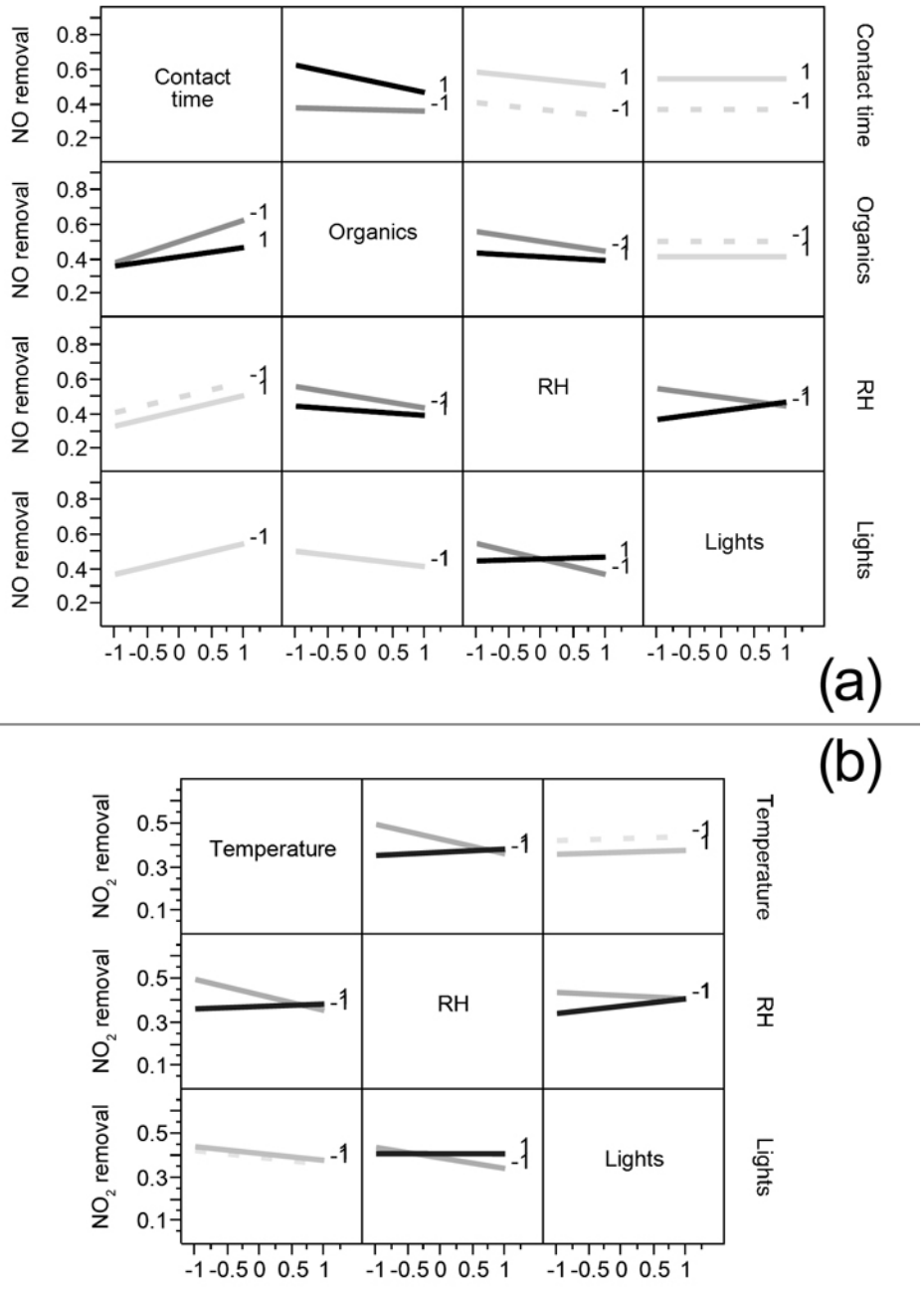

Figure 4. Interaction plots for (a) NO removals and (b) NO_2 removals

4. DISCUSSION

The NO removals observed in this study (46 % on average; Figure 2a) were in the same range as removals previously observed by researchers testing photocatalytic concrete specimens or pavers. It should be noted, however, that the other studies used higher inlet concentrations (300 ppb and over) than this study (150 ppb). For example, Dylla et al. (2010) observed NO removals in the 20 % to 60 % range for contact time varying from 2.4 to 7.1 minutes. Similarly, Ballari et al. (2011) observed NO removals in the 43 % to 83 % range for UV light intensity, temperature and RH conditions similar to the ones used here and contact times less than 1 minute. Both researchers also noted a decrease in removal with increasing relative humidity as observed in this study (Figure 3a). It has been assumed that at higher relative humidity water molecules compete with pollutant molecules for adsorption sites at the material surface, which would explain the decrease in pollutant removal (Ao et al., 2003; Maggos et al., 2007a; Hüsken et al., 2009; Laufs et al., 2010). Dylla et al. also observed an increase in removal with higher contact times as observed in this study (Figure 3a). Increasing contact time increases the probability of pollutants coming in contact with the material surface and being adsorbed and reacted, hence the positive contrast for that factor.

Other researchers have studied the effect of the presence of VOCs on photocatalytic removal of NO_x. Ao et al. (2003) studied the degradation of NO at realistic outdoor levels (200 ppb) in the presence of BTEX (0 to 70 ppb) and observed a reduction in NO removal when BTEX was present versus when it was absent. However, for BTEX concentrations between 3 and 70 ppb, NO conversion was almost constant. In this study, we found NO removal to decrease with increasing VOC concentration (Figure 3a). However the change in concentration spanned an order of magnitude (0.3 to 3 ppm). It is possible that VOC molecules competed with NO molecules for adsorption sites at the

surface of the photocatalytic material, which would explain the decrease in removal with increased VOC concentration.

Finally, Bengtsson et al. (2010) also observed a reduction in NO removal with increasing temperature as observed in this study (Figure 3a). Changes in adsorption kinetics with temperature could explain the decrease observed.

Nitrogen dioxide removals observed in this study under multi-gas conditions (41 % average; Figure 2b) are similar to removals observed by Ballari et al. (2011) when studying removal of NO_2 alone on photocatalytic paving stones. Ballari et al. observed removals between 20 % and 75 % for UV light intensity, temperature and RH conditions similar to the ones used here and contact times less than 1 minute. Similar to NO removal, an increase in contact time led to an increase in NO_2 removal while increases in relative humidity or temperature led to decreases in removal. It is interesting to note that, unlike NO removal, levels of VOCs did not influence NO_2 removal. Nitrogen dioxide is an oxidant and it is possible that it reacted with organics in the gas phase or at the material surface, hence counteracting the reduced availability of photocatalytic reaction sites at the material surface.

Interaction plots presented in Figure 4 give more insight into how different environmental parameters interact to affect pollutant removal by the photocatalytic coating. These plots exhibit how one parameter might have a different effect depending on the level of one of the other parameters. For example, for both NO and NO_2 removal, the effect of light intensity was different when the relative humidity wass at its high level (coded 1 on the plots) or at its low level (coded -1). When UV light intensity was at its high level, an increase in RH led to no or very small increase in removal, but when UV light intensity was at its low level, increasing RH decreased removal. It is possible that, when UV light was at its low level, some photocatalytic sites did not receive enough

energy to be activated and increasing RH only led to more water molecules competing with pollutants for adsorption sites. Without enough sites activated, these water molecules were not oxidized to form hydroxyl radicals. When the UV light intensity was at its high level, more photocatalytic sites were active, and by increasing the RH, more water molecules were made available to form hydroxyl radicals that could then react with pollutant molecules, balancing the reduced availability of reaction sites.

For NO removal, organic pollutant concentrations were involved in two significant interactions, with RH and contact time (Figure 4a). When RH increased from its low level to its high level, NO removal decreased. But the decrease was larger when the organic pollutant concentrations were low versus high. Competition between water, organic pollutant and NO molecules for adsorption sites might explain this interaction. At the low organic pollutant concentrations condition, few adsorption sites were occupied by VOC molecules, but the change in RH made a large difference in how many sites were available for NO adsorption. On the other hand, under the high organic concentrations condition, a large number of sites were already occupied by VOC molecules, and the addition of water did not change dramatically the number of sites available for NO adsorption, which might explain the interaction observed.

The increase in NO removal from a short to a long contact time condition was larger when organic pollutant concentrations were at the low level. This might be related to the adsorption rate of organic pollutants to the material surface. If the time scale for adsorption of organics to the material surface was longer than the 1.5 minute contact time, few organics adsorbed and the change between low and high concentrations of organics did not significantly affect removal. But if the time scale for adsorption was shorter than the 15 minute contact time tested, a larger portion of adsorption sites may have been occupied when the level of organics was high versus low. This might explain

why the NO removal did not increase as much with increasing contact time when the concentration of VOCs was high versus low.

An interaction between RH and temperature was also determined to be significant for NO_2 removal (Figure 4b). An increase from the low to the high temperature condition led to a decrease in NO_2 removal when RH was at its low level, but not when it was at its high level. It is possible that this was again related to adsorption kinetics. At low RH, there was little competition from water for adsorption of NO_2 molecules to the surface. An increase in temperature may have changed adsorption kinetics for NO_2, leading to reduced removal at the stucco surface. However, at high RH, a large portion of adsorption sites may have been occupied by water molecules, reducing the effect of the change in temperature on NO_2 adsorption and removal.

Overall, NO_x removal increased with increased contact time but was negatively impacted by high relative humidity and, to a lesser extent, temperature. Organic pollutants negatively affected removal of NO but did not affect removal of NO_2. While NO_x emissions from motor vehicles are mostly in the form of NO, the NO is rapidly transformed to NO_2 in the presence of ozone (Yao et al., 2005). Moreover, new diesel technologies have led to increased emissions of primary NO_2 from road vehicles. As such, NO_2 accounts for about 20 % of NO_x emitted on roadways in European cities (Carslaw, 2005; Hueglin et al., 2006; Kessler et al., 2006; Grice et al., 2009). This makes photocatalytic coatings particularly attractive for removal of NO_2 near roadways, where it is present at elevated levels in mixed pollutant gases. The case for NO removal near roadways is more complex. Removals observed in this study indicate that on average NO is removed more efficiently than NO_2 (average removals of 46 and 41 % respectively). However, peak NO concentrations occur in the morning when temperatures are low and RH high. While low temperature is beneficial to NO removal, high RH and VOC levels

are detrimental making it difficult to evaluate what the overall impact on removal might be. Finally, NO removal was affected by more two-factor interactions than NO_2 removal. It is possible that, because NO_2 is more reactive than NO with cementitious materials (Judeikis and Wren, 1978), some removal occured through deposition and reaction to non-photocatalytic sites on the material surface. This might explain why its removal was less affected by environmental parameters. Nitric oxide dry deposition on the other hand has been found to be low compared to NO_2 dry deposition (Judeikis and Wren, 1978). The overall higher removals observed for NO than NO_2 in this study suggest that the photocatalytic process removes NO particularly efficiently.

5. CONCLUSIONS

Results of this study suggest that stucco photocatalytic coatings may be appropriate for removing NO_x in some realistic outdoor conditions. Placement of the photocatalytic materials will matter as locations with longer contact time will lead to greater removals. Areas experiencing lower relative humidity will also be more suitable for use of photocatalytic materials similar to the one tested here. The results also suggest that the presence of organic pollutants does not affect NO_2 removal by the material, which could make it suitable as a control strategy for NO_2 near roadways, where elevated NO_2 levels in combination with VOCs are observed.

6. ACKNOWLEDGEMENTS

This work was funded by the Texas Department of Transportation (TxDOT) under project 0-6636. The findings are part of an ongoing research project and the final results of the study will be considered by TxDOT before full release of the project final report.

7. REFERENCES

Allen, N.S., Edge, M., Sandoval, G., Verran, J., Stratton, J., Maltby, J., 2005. Photocatalytic coatings for environmental applications. Photochemistry and Photobiology 81, 279–290.

Ao, C.H., Lee, S.C., Mak, C.L., Chan, L., 2003. Photodegradation of volatile organic compounds (VOCs) and NO for indoor air purification using TiO_2: promotion versus inhibition effect of NO. Applied Catalysis B: Environmental 42, 119–129.

ASTM, 2006. Standard Guide for Small-Scale Environmental Chamber Determinations of Organic Emissions From Indoor Materials/Products (No. D5116-10).

Ballari, M.M., Hunger, M., Hüsken, G., Brouwers, H.J.H., 2010a. Modeling and experimental study of the NO_x photocatalytic degradation employing concrete pavement with titanium dioxide. Catalysis Today 151, 71–76.

Ballari, M.M., Hunger, M., Hüsken, G., Brouwers, H.J.H., 2010b. NO_x photocatalytic degradation employing concrete pavement containing titanium dioxide. Applied Catalysis B: Environmental 95, 245–254.

Ballari, M.M., Yu, Q.L., Brouwers, H.J.H., 2011. Experimental study of the NO and NO_2 degradation by photocatalytically active concrete. Catalysis Today 161, 175–180.

Bauer, M.A., Utell, M.J., Morrow, P.E., Speers, D.M., Gibb, F.R., 1986. Inhalation of 0.30 ppm nitrogen dioxide potentiates exercise-induced bronchospasm in asthmatics. American Review of Respiratory Disease 134, 1203–1208.

Beeldens, A., 2006. An environmental friendly solution for air purification and self-cleaning effect: the application of TIO_2 as photocatalyst in concrete, in: Proceedings of Transport Research Arena Europe, Göteborg, Sweden.

Bengtsson, N., Castellote, M., 2010. Photocatalytic Activity for NO Degradation by Construction Materials: Parametric Study and Multivariable Correlations. Journal Of Advanced Oxidation Technologies 13, 341–349.

Brunekreef, B., Janssen, N.A.H., de Hartog, J., Harssema, H., Knape, M., van Vliet, P., 1997. Pollution from Truck Traffic and Lung Function in Children Living near Motorways. Epidemiology 8, 298–303.

Carslaw, D.C., 2005. Evidence of an increasing NO_2/NO_x emissions ratio from road traffic emissions. Atmospheric Environment 39, 4793–4802.

Chen, J., Poon, C.-S., 2009. Photocatalytic construction and building materials: From fundamentals to applications. Building And Environment 44, 1899–1906.

Clark, N.A., Demers, P.A., Karr, C.J., Koehoorn, M., Lencar, C., Tamburic, L., Brauer, M., 2009. Effect of Early Life Exposure to Air Pollution on Development of Childhood Asthma. Environmental Health Perspectives 118, 284–290.

Dalton, J., Janes, P., Jones, N., Nicholson, J., Hallam, K., Allen, G., 2002. Photocatalytic oxidation of NO_x gases using TiO_2: a surface spectroscopic approach. Environmental Pollution 120, 415–422.

Devahasdin, S., Fan, C., Li, K., Chen, D.H., 2003. TiO_2 photocatalytic oxidation of nitric oxide: transient behavior and reaction kinetics. Journal Of Photochemistry And Photobiology A-Chemistry 156, 161–170.

Dylla, H., Hassan, M.M., Mohammad, L.N., Rupnow, T., Wright, E., 2010. Evaluation of environmental effectiveness of titanium dioxide photocatalyst coating for concrete pavement. Transportation Research Record: Journal of the Transportation Research Board 2164, 46–51.

Dylla, H., Hassan, M.M., Schmitt, M., Rupnow, T.S., Mohammad, L.N., 2011. Laboratory investigation of the effect of mixed nitrogen dioxide and nitrogen

oxide gases on titanium dioxide photocatalytic efficiency in concrete pavements. Journal of materials in civil engineering 23, 1087–1093.

EPA, 2010. Final Revisions to the Primary National Ambient Air Quality Standard for Nitrogen Dioxide (NO_2), in: Office of Air Quality Planning and Standards.

EPA, 2011. National Emissions Inventory (NEI) Air Pollutant Emissions Trends Data. Office of Air Quality Planning and US EPA Standards.

Finlayson-Pitts, B.J., Wingen, L.M., Sumner, A.L., Syomin, D., Ramazan, K.A., 2002. The heterogeneous hydrolysis of NO_2 in laboratory systems and in outdoor and indoor atmospheres: An integrated mechanism. Physical Chemistry Chemical Physics 5, 223–242.

Frampton, M.W., Morrow, P.E., Cox, C., Gibb, F.R., Speers, D.M., Utell, M.J., 1991. Effects of Nitrogen Dioxide Exposure on Pulmonary function and Airway Reactivity in Normal Humans. American Journal of Respiratory and Critical Care Medicine 143, 522.

Fujishima, A., Honda, K., 1972. Electrochemical photolysis of water at a semiconductor electrode. Nature 238, 37–38.

Gauderman, W.J., Avol, E., Lurmann, F.W., Kuenzli, N., Gilliland, F., Peters, J., McConnell, R., 2005. Childhood asthma and exposure to traffic and nitrogen dioxide. Epidemiology 16, 737–743.

Grice, S., Stedman, J., Kent, A., Hobson, M., Norris, J., Abbott, J., Cooke, S., 2009. Recent trends and projections of primary NO_2 emissions in Europe. Atmospheric Environment 43, 2154–2167.

Hoffmann, M.R., Martin, S.T., Choi, W., Bahnemann, D.W., 1995. Environmental applications of semiconductor photocatalysis. Chemical Reviews 95, 69–96.

Hueglin, C., Buchmann, B., Weber, R.O., 2006. Long-term observation of real-world road traffic emission factors on a motorway in Switzerland. Atmospheric Environment 40, 3696–3709.

Hunger, M., Hüsken, G., Brouwers, H.J.H., 2010. Photocatalytic degradation of air pollutants - From modeling to large scale application. Cement And Concrete Research 40, 313–320.

Hüsken, G., Hunger, M., Brouwers, H.J.H., 2009. Experimental study of photocatalytic concrete products for air purification. Building And Environment 44, 2463–2474.

ISO, 2007. Fine ceramics (advanced ceramics, adva,ced technical ceramics) - Test method for air-purification perforlance of semiconducting photocatalytic materials - Part 1: Removal of nitric oxide (No. 22197-1:2007). Geneva, Switzerland.

Janssen, N.A.H., Brunekreef, B., van Vliet, P., Aarts, F., Meliefste, K., Harssema, H., Fischer, P., 2003. The relationship between air pollution from heavy traffic and allergic sensitization, bronchial hyperresponsiveness, and respiratory symptoms in Dutch schoolchildren. Environmental Health Perspectives 11, 1512–1518.

Jenkin, M.E., Cox, R.A., Williams, D.J., 1988. Laboratory studies of the kinetics of formation of nitrous acid from the thermal reaction of nitrogen dioxide and water vapour. Atmospheric Environment 22, 487–498.

JIS, 2010. Fine ceramics (advanced ceramics, advanced technical ceramics) – Test method for air purification performance of photocatalytic materials – Part 1: Removal of nitric oxide (No. R1701-1:2010).

Judeikis, H.S., Wren, A.G., 1978. Laboratory Measurements of NO and NO_2 depositions onto soil and cement surfaces. Atmospheric Environment 12, 2315–2319.

Kessler, C., Niederau, A., Scholz, W., 2006. Estimation of NO_2/NO_x relations of traffic emissions in Baden-Württemberg from 1995 to 2005, in: 2nd conference Environment & Transport, Reims, France, pp. 101–105.

Krämer, U., Koch, T., Ranft, U., Ring, J., Behrendt, H., 2000. Traffic-related air pollution is associated with atopy in children living in urban areas. Epidemiology 11, 64–70.

Laufs, S., Burgeth, G., Duttlinger, W., Kurtenbach, R., Maban, M., Thomas, C.E.S., Thomas, C., Wiesen, P., Kleffman, J., 2010. Conversion of nitrogen oxides on commercial photocatalytic dispersion paints. Atmospheric Environment 44, 2341–2349.

Lim, T., Jeong, S., Kim, S., Gyenis, J., 2000. Photocatalytic decomposition of NO by TiO_2 particles. Journal Of Photochemistry And Photobiology A-Chemistry 134, 209–217.

Maggos, T., Bartzis, J.G., Leva, P., Kotzias, D., 2007a. Application of photocatalytic technology for NO_x removal. Applied Physics A - Materials Science & Processing 89, 81–84.

Maggos, T., Bartzis, J.G., Liakou, M., Gobin, C., 2007b. Photocatalytic degradation of NO_x gases using TiO_2-containing paint: A real scale study. Journal Of Hazardous Materials 146, 668–673.

Mee, R.W., 2009. A comprehensive guide to factorial two-level experimentation. Springer.

Mohsenin, V., 1987. Airway responses to nitrogen dioxide in asthmatic subjects. Journal of Toxicology and Environmental Health 22, 371–380.

Nafstad, P., Håheim, L.L., Wisløff, T., Gram, F., Oftedal, B., Holme, I., Hjermann, I., Leren, P., 2004. Urban air pollution and mortality in a cohort of Norwegian men. Environmental Health Perspectives 112, 610–615.

Ohko, Y., Nakamura, Y., Negishi, N., Matsuzawa, S., Takeuchi, K., 2009. Photocatalytic oxidation of nitrogen monoxide using TiO_2 thin films under continuous UV light illumination. Journal Of Photochemistry And Photobiology A-Chemistry 205, 28–33.

Ollis, D.F., Pelizzetti, E., Serpone, N., 1991. Photocatalyzed destruction of water contaminants. Environmental Science & Technology 25, 1522–1529.

Peters, A., Liu, E., Verrier, R.L., Schwartz, J., Gold, D.R., Mittleman, M.A., Baliff, J., Oh, J.A., Allen, G., Monahan, K., Dockery, D.W., 2000. Air pollution and incidence of cardiac arrhythmia. Epidemiology 11, 11–17.

Raaschou-Nielsen, O., Reynolds, P., 2006. Air pollution and childhood cancer: A review of the epidemiological literature. International Journal of Cancer 118, 2920–2929.

Saliba, N.A., Yang, H., Finlayson-Pitts, B.J., 2001. Reaction of Gaseous Nitric Oxide with Nitric Acid on Silica Surfaces in the Presence of Water at Room Temperature. The Journal of Physical Chemistry A 105, 10339–10346.

Seinfeld, J.H., Pandis, S.N., 2006. Atmospheric Chemistry and Physics, Second edition. ed. Wiley-Interscience.

Svensson, R., Ljungström, E., Lindqvist, O., 1987. Kinetics of the reaction between nitrogen dioxide and water vapour. Atmospheric Environment 21, 1529–1539.

Tamhane, A.C., 2009. Statistical analysis of designed experiments. A John Wiley & Sons, Inc., Publication.

TCEQ (Ed.), 2009. Hourly air pollution data. TCEQ. URL http://www.tceq.texas.gov/airquality/monops/hourly_data.html

Thoma, E.D., Shores, R.C., Isakov, V., Baldauf, R.W., 2008. Characterization of Near-Road Pollutant Gradients Using Path-Integrated Optical Remote Sensing. Journal of the Air & Waste Management Association 58, 879–890.

UNI, 2010. Determination of the degradation of nitrogen oxides in the air by inorganic photocatalytic materials: continuous flow test method. (No. 11247).

Yao, X., Lau, N.T., Khan, C.K., Fang, M., 2005. The use of tunnel concentration profile data to determine the ratio of NO_2/NO_x directly emitted from vehicles. Atmospheric Chemistry and Physics Discussion 5, 12723–12740.

Appendix B

Paper 2: Clement J. Cros, Alexandra L. Terpeluk, Neil E. Crain, Richard L. Corsi, Maria G. Juenger. Removal of oxides of nitrogen by photocatalytic coatings: influence of environmental parameters and material properties. Ready for submission to *Construction and Building Materials*.

ABSTRACT

Oxides of nitrogen are ubiquitous pollutants in most large urban areas of the world. Photocatalytic materials have been studied, primarily in the laboratory, for their ability to remove oxides of nitrogen (NO_x). The study described herein compared NO_x removal efficacies by two commercially available photocatalytic coatings and aimed to elucidate how environmental parameters and exposure to real roadside conditions affect their effectiveness. Relative humidity, temperature, and contact time were found to similarly affect removal effectiveness of both coatings. Exposure to roadside conditions decreased NO_x removal effectiveness, but appropriate washing methods led to almost complete recovery of the photocatalytic removal efficiency.

Keywords: photocatalysis, coatings, roadside exposure, nitrogen oxides, full-factorial

1. INTRODUCTION

Oxides of nitrogen (NO_x) are ubiquitous pollutants in most urban areas around the world. They are products of combustion processes taking place in motor vehicles, industries and power generation facilities. Exposure to nitrogen dioxide (NO_2) has been associated with a variety of adverse health effects ranging from decreased lung function and increased airway reactivity [1-3] to onset of asthma [4,5], arrhythmia [6] and lung cancer [7,8]. Oxides of nitrogen also have adverse environmental effects: they are precursors to the formation of ozone and other atmospheric pollutants through photochemical processes [9] and the presence of NO_x in ambient air can also cause acid rain that damages structures and vegetation.

Populations living near roadways, where a large fraction of NO_x emissions take place, e.g. 31 % of all NO_x emissions in the US [10], are exposed to elevated levels of

NO_x leading to greater adverse health effects than the general population [11-13]. Finding new ways to remove NO_x emitted on roadways could have health and environmental benefits. Photocatalytic materials have been studied for years for their capacity to remove NO_x [14-17]. Built structures in close proximity to roadways could be used to passively remove NO_x emitted by motor vehicles through the use of photocatalytic materials, whether by retrofitting existing structures or by implementing new structures with other added benefits (e.g., noise reduction and enhanced roadway safety). This is an opportunity for passive removal of pollutants that is not usually available for other major sources of NO_x such as industries or power facilities that emit NO_x through stacks, further away from the ground and the built environment. The built environment around roadways is close to the emission source while traffic increases dispersion of pollutants, hence the probability of pollutants coming into contact with surfaces for reaction. However, in contrast with the road surface itself, surrounding structures are not subject to intense fouling and wearing that might alter the pollutant removal performance of the reactive material. Use of photocatalytic materials is attractive because, once applied, they could potentially remove NO_x without necessitating additional energy input as long as the catalyst can be regenerated.

Photocatalysis is a process that occurs at the surface of a semi-conductor exposed to light [14]. Oxygen and water, adsorbed at the semi-conductor surface, are catalyzed to form reactive species, superoxide anion (O_2^-) and hydroxyl radical ($OH^\bullet$). Hydroxyl radicals and superoxide anions are strong oxidizing and reducing agents, respectively. They can react with pollutant molecules adsorbed to the photocatalytic surface, such as NO_x or hydrocarbons [15,17-20]. In the case of NO_x, the product of the reactions involving NO, NO_2 and hydroxyl radicals is nitric acid, which remains adsorbed on the photocatalytic surface until it is washed off by water [18,21,22]. Titanium dioxide (TiO_2)

is the most widely used semi-conductor for photocatalysis applications. It is inexpensive, chemically and biologically inert and stable with respect to photo and chemical corrosion [23]. Of its three crystalline forms (anatase, rutile and brookite), anatase is the preferred photocatalyst because it has the highest photoactivity [24].

The study presented in this paper focused on coatings such as paints and stuccos. Coatings have the advantage of requiring very small amounts of semi-conductor, compared to solutions where the semi-conductor is present through the full depth of a concrete structure, making them more cost-effective. Coatings can also be used to cover existing surfaces, allowing retrofit of structures already in place. While various types of photocatalytic materials have been studied in the past, little research has been conducted specifically on coatings for outdoor application. Maggos et al. [25] studied two photocatalytic paints for their capacity to remove NO_x during batch tests. They found that up to 91 % removal could be achieved after 6 hours. They also found that an increase in relative humidity (RH) from 20 % to 50 % led to reduced removal by the photocatalytic coating. Laufs et al. [17] tested two photocatalytic paints as well and studied how environmental parameters affected their NO_x removal. It was determined that the inlet concentration of NO or NO_2 did not affect removal. Laufs et al. [17] also observed a decrease in removal of NO for increasing RH. For NO_2, a decrease in removal efficiency was observed for RH > 10 %, but an increase in removal was observed for increasing RH between 0 % and 10 %.

Other researchers have studied different types of photocatalytic materials such as slurries [20,21,26,27], paving stones [16,28,29] or concrete containing TiO_2 in its cement matrix [24,30-32]. They found that photocatalytic removal of NO_x increased non-linearly with light intensity [26,27] but decreased with increasing relative humidity [17,28-30]. Similarly to what Laufs et al. [17] observed for photocatalytic paints, some researchers

have observed that for NO and NO_2 concentrations less than 1 ppm the conversion rate did not depend on the initial concentration injected, even when both chemicals were introduced at the same time [26]. But others observed removal to increase with decreasing air concentrations of NO and NO_2 [29]. However, most researchers did not investigate NO_x removals for realistic outdoor air mixtures that contain other pollutants such as ozone or volatile organic compounds (VOCs). Of the researchers who have, none studied the simultaneous effect of environmental conditions such as light intensity, temperature and relative humidity.

Long-term efficiency of photocatalytic materials in real environments is another concern that needs to be addressed, especially for coatings. Hassan et al. [33] studied the wear resistance of photocatalytic coatings through abrasion and loaded-wheel tests. They found that the NO_x removal performance of the coatings was not significantly affected by wear. The TiO_2 concentration at the material surface remained consistent after the wear tests and NO removal changed only slightly depending on the TiO_2 concentration in the original coating. Ramirez et al. [34] also studied the resistance of photocatalytic coatings applied on various cementitious materials to wear from simulated rain and wind of photocatalytic coatings applied on various cementitious materials. They found that the more porous/rough substrates (such as white cement plaster) retained the most TiO_2 after application but also lost more TiO_2 through wear. On the other hand, the more smooth substrates (such as concrete) had better resistance to wear.

Research performed under real outdoor conditions has also been conducted on photocatalytic materials directly applied on the road surface [35-37]. Generally, for these types of studies, road sections were made with concrete containing TiO_2 or photocatalytic concrete pavers and the concentration of NO_x was compared to NO_x concentrations measured on nearby untreated roadways. Concentrations of NO_x over the photocatalytic

section were initially between 40 % and 50 % lower compared to the regular road section during daytime. However, most researchers observed drastic reductions in removal efficiency after a few weeks/months of placement. The photocatalytic materials were placed on the road surface over which vehicles travel, leading to rapid fouling of the surface that is not encountered to the same degree for coatings placed on surfaces near roadways, as considered in the present study.

This study compared two different photocatalytic coatings through NO_x removal testing in a laboratory system and determined how various environmental factors affected their removal efficiency. In particular, the effect of other inorganic and organic pollutants was studied, in conjunction with environmental factors such as temperature and RH. The coatings were also exposed at field sites in Austin and Houston, TX, and tested again after a year to evaluate the effect of exposure to roadside conditions on their physical and chemical properties as well as on their NO_x removal effectiveness.

2. METHODS

2.1. Materials

2.1.1. Concrete specimens

Two types of concrete specimens were used throughout the experimental program. Highway barriers were obtained through a local manufacturer (Tricon Precast; New Braunfels, TX, USA) and placed at field sites. Each barrier was divided into four equal sections, one for each photocatalytic coating (including one not presented here), and one left uncoated. Concrete slabs were manufactured at the University of Texas, using the same materials and mixture proportions used for the fabrication of the highway barriers by Tricon Precast. Slabs were 7.5 cm thick and 33 cm wide. Two lengths were manufactured in order to vary contact time during laboratory testing. The full size

samples were 90 cm long, while the half size samples were 45 cm. The concrete materials were as follows: 25 % fly ash/75 % Type III cement, water to cementitious materials ratio by mass of 0.34, limestone coarse and fine aggregate, and Plastiment and Sika 2110 admixtures (Sika Corporation U.S., Lyndhurst, NJ, USA). The photocatalytic coating was applied following manufacturer recommendations to the concrete samples after one week of curing in a 100 % RH room at 23°C and two weeks of drying in a 50 % RH, 23°C room.

2.1.2. Photocatalytic coatings

Two commercially available photocatalytic coatings were tested during the experimental program. One coating was a clear paint, obtained as a water-based photocatalytic spray that can be applied to virtually any surface. It contained 1 % TiO_2 by weight, in the anatase crystalline form. It was applied by the manufacturer's representatives using a paint sprayer. The second coating was a stucco made from portland cement, a proprietary mix of admixtures and 5 % by weight of TiO_2, primarily in the anatase crystalline form. It was applied in a 5 mm thick layer, using a hand trowel. Some concrete samples were also left uncoated for comparison with the coated samples.

2.2. Field testing

Three field sites were set up to expose concrete samples coated with photocatalytic coatings to real environmental conditions. Two field sites were located within 30 m of major highways: one in Houston, TX, located next to I-10 and one in Austin, TX, located next to I-35. The third site was located further away from a major highway, about 400 m from Loop 1 in Austin, TX, at the J.J. Pickle Research campus of the University of Texas.

2.3. Laboratory testing

2.3.1. Material testing

X-ray diffraction (XRD) and Scanning Electron Microscopy (SEM) were used to characterize the material samples before and after field exposure. Samples were retrieved from the highway barriers described in section 2.1. The samples used for testing were small cores (75 mm diameter, 12.5 mm depth) removed using either a Hilti TE-C-BK-TW percussion core bit or a Hilti DD 120 coring rig (Hilti, Inc., Tulsa, OK, USA). X-ray diffraction was used to determine the presence of TiO_2 in the material and changes in the concrete phase assemblage that might have resulted from the interaction with the photocatalytic coating and/or outdoor degradation. The samples used for XRD were crushed using a grinder (Micro-Mill; Bel-Art, Wayne, NJ, USA) until they passed through a #325 sieve (45 μm). The samples were then stored under vacuum until testing. Samples were scanned from 10° to 70° 2θ (Cu-Kα radiation, D500; Siemens, Washington D.C., USA).

Scanning electron microscopy was used to determine the presence and distribution of TiO_2 at the material surface. The concrete core removed for testing was split into two sections. The first section was used for imaging the material surface using SEM. The second section was used to view a cross-section of the concrete and coating. The sample was prepared by slicing the concrete core to approximately 6 mm thickness with a precision saw (Isomet 1000; Buehler, Lake Bluff, IL, USA). The sawed sample was put under vacuum for at least 24 hours before being placed in a two-part epoxy resin (Epoxy Technology, Billerica, Mass., USA) under vacuum and allowed to cure for 24 hours at 23°C. Epoxy impregnated samples were finished by hand grinding with #180, 400, 800, and 1200 grit sandpaper then polishing with 3, 1, and ¼ μm diamond pastes using an automated Automet 2000 powerhead (Buehler, Lake Bluff, Ill. USA). A variable

pressure SEM (Quanta 650 FEG; FEI, Hillsboro, OR, USA) with an automated backscattered electron detector was used for imaging samples after sputter coating with gold-palladium for conductivity. The accelerating voltage used was 30 kV. Energy dispersive spectroscopy (EDS) was used for compositional analysis (XFlash® Detector 5010; Bruker, Ewing, NJ, USA) using a 5.0 μm spot size with a 3 μs dwell time.

2.3.2. Air quality testing system

The experimental system used for testing of the photocatalytic coatings applied on the concrete slabs is presented in detail in [38]. A 150-L stainless steel electro-polished chamber was used to test coated concrete samples under well-mixed conditions. Eight UV lamps (40 W, 280-400 nm, λ_{max} = 310 nm, model QFS-40; Q-Lab Corp., Cleveland, OH, USA) were installed in the chamber to provide UV radiation necessary to the activation of the photocatalyst.

Two zero air generators (701; Teledyne, San Diego, CA, USA) provided air flow to the test reactor. Humidity was adjusted by passing a portion of the air through an impinger. Pollutant species were introduced at a known rate through mass flow controllers (FMA 5500; Omega Engineering, Inc., Stamford, CT, USA). Pollutant species included ozone, obtained by passing pure oxygen through a UV-based ozone generator (97-0067-01; UVP, LLC, Upland, CA, USA) as well as NO, NO_2, propane (VOC surrogate) and propylene (highly reactive VOC surrogate) obtained in gas cylinders, mixed with nitrogen (Praxair, Danbury, CT, USA).

Chamber air was sampled at both the inlet and outlet of the chamber with one set of instruments, by automatically switching sampling between inlet and outlet through solenoid valves (SV123/133; Omega Engineering Inc.) Ozone concentrations were measured by a UV absorbance ozone analyzer (1008-AH; Dasibi, Glendale, CA, USA),

NO and NO_2 concentrations were measured by a chemiluminescence analyzer (200E; Teledyne) and VOC concentrations were measured by a methane/non-methane hydrocarbon analyzer (55i; Thermo Fisher Scientific, Waltham, MA, USA). These instruments were calibrated daily using a multi-gas calibrator (700E; Teledyne) and concentration certified gas standards (Praxair).

2.3.3. Full factorial testing

To determine which environmental parameters influenced NO_x removal, the two coatings as well as an uncoated concrete sample underwent full factorial testing. Six parameters were varied, as listed in Table 1.

Table 1. Full factorial experimental parameters and their magnitudes

	Low level	**High level**
Contact time	1.5 minutes	15 minutes
Relative humidity	20 %	65 %
Temperature	30°C	40°C
Organic pollutants		
propane (VOC)	0.25 ppm	2.5 ppm
propylene (HRVOC)	0.05 ppm	0.5 ppm
Inorganic pollutants[a]	"morning"	"afternoon"
- NO	150 ppb	
- NO_2	20 ppb	50 ppb
- Ozone		150 ppb
Lights	1 mW cm^{-2}	2 mW cm^{-2}

[a]: selection of inorganic pollutant levels described in [38].

Eight experiments were consecutively run on one sample before it was removed from the chamber and the next sample was tested. Before the first experiment and between rounds of experiments, each sample was rinsed with distilled water, as described Cros et al. [38]. The goal was to regenerate the catalyst by washing off the product of the photocatalytic conversion of NO and NO_2, nitric acid, that might have remained adsorbed

to the material surface, as well as oxidized VOCs that may be present at the material surface.

2.3.4. Exposed samples testing

Field samples of the best performing coating as determined by the full factorial tests were collected and returned to the laboratory for additional tests to assess the effects of the near roadway environment on NO_x removal effectiveness. Three tests were consecutively run on each sample. For the first test, the sample was tested without any treatment after transport from the field site. For the second test, the sample was rinsed with distilled water before testing, as described by Cros et al. [38]. For the third test, the sample was rinsed with soap and water before testing. The soap and water solution was made with 30 mL of Greenworks free & clear dishwashing soap (Clorox, Oakland, CA, USA) mixed in 4 L of distilled water and was poured on the sample while layed flat, followed by a rinse with distilled water as described by Cros et al. [38] to remove soap residues. Samples freshly coated with the photocatalytic stucco, as well as samples coated with the same stucco formulation but without TiO_2 were also tested for comparison.

The three consecutive tests were run under the following conditions: 50 % RH, 35°C, 1.5 minute contact time, low organic pollutant (0.25 ppm propane, 0.05 ppm propylene), and high UV light intensity (2 mW cm^{-2}). The tests were run for both "morning" and "afternoon" conditions (Table 1) in terms of inorganic pollutant levels.

2.3.5. Data analysis

Oxides of nitrogen removals were calculated using steady-state concentrations obtained during full factorial tests. Oxides of nitrogen removal by the uncoated concrete was subtracted from the NO_x removal for the photocatalytic coating to determine the removal of the photocatalytic coating over the existing structures made of uncoated

concrete. This process allowed an evaluation of the incremental NO_x removal that would be obtained by coating existing concrete structures with a photocatalytic coating:

$$R = 100 \times (1 - c_{out}/c_{in}) - 100 \times (1 - c_{out,b}/c_{in,b}) \quad (1)$$

where $c_{in,b}$ is the pollutant concentration measured in the chamber inlet for the test run with uncoated concrete (ppb), $c_{out,b}$ is the pollutant concentration measured in the chamber outlet for the test run with uncoated concrete (ppb), c_{in} is the pollutant concentration measured in the inlet of the chamber for the test run with a coated sample (ppb), c_{out} is the pollutant concentration measured in the outlet of the chamber for the test run with a coated sample (ppb), R is the pollutant removal by the coated concrete (%).

The uncertainty associated with NO_x removals was determined using standard error propagation techniques. The uncertainty on the concentration measurements was taken as two standard deviations of measured concentrations for all calibrations run during the experimental program. Relative uncertainties were determined to be 8.0 % for NO measurements and 9.8 % for NO_2 measurements.

Results from the full factorial experiments were analyzed using JMP software (JMP 9; SAS, Cary, NC, USA) and analysis of variance (ANOVA) techniques following the method described by Cros et al. [38].

3. RESULTS

3.1. Nitrogen oxides removal from laboratory specimens

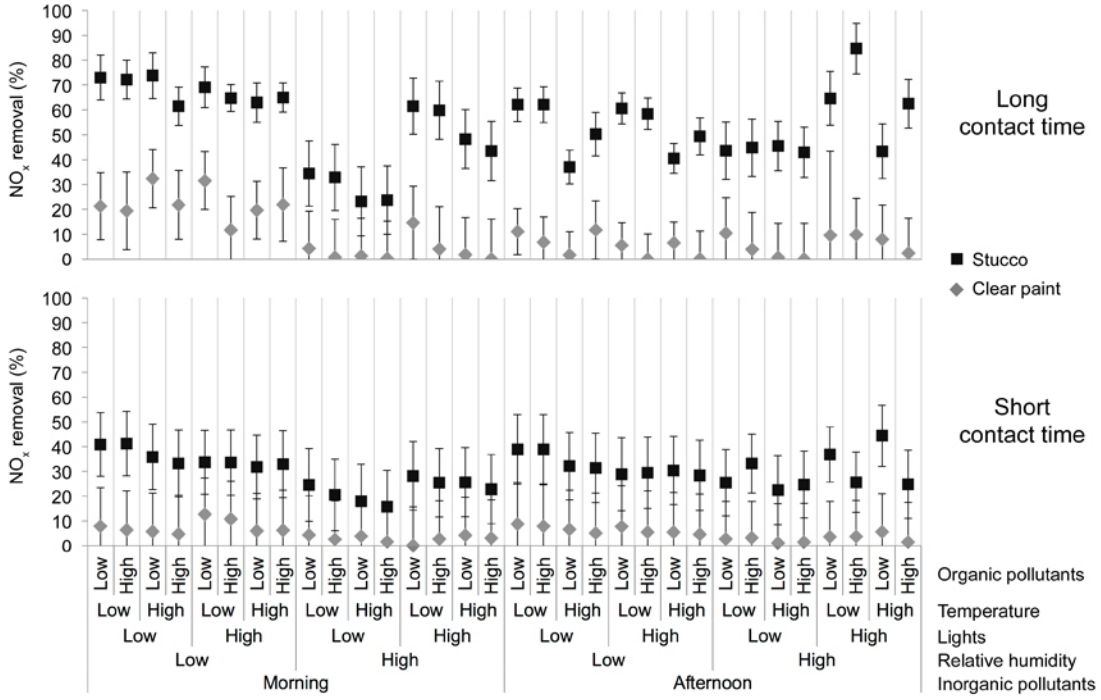

Figure 1. Nitrogen oxides removals obtained during full factorial testing

Removals of NO_x obtained during full factorial testing are presented in Figure 1. Removals of NO and NO_2 by the stucco coating were studied in more details by Cros et al. [38] by distinguishing factors influencing removal of NO and NO_2 separately. Here, overall removal of NO_x by the stucco was studied and compared to NO_x removal by the clear paint to evaluate how physical and chemical properties of a coating might influence its NO_x removal effectiveness. Removals by the clear paint averaged 7.1 % (standard deviation = 7.1 %), while removals by the stucco averaged 41.9 % (standard deviation = 16.7 %). These removals are above and beyond what an uncoated concrete specimen removed, as shown in equation 1. For the clear paint, a degradation of the coating over

time might explain the results observed. In effect, the first eight experiments presented in Figure 1 (long contact time, low RH) were the first experiments run on the coating. During these experiments, the coating performed fairly well, with NO_x removals averaging 20 %. After the first water rinse, the coating did not perform as well and all subsequent tests run at long contact time averaged only 5 % removal. The stucco did not exhibit such a change over the experimental program period.

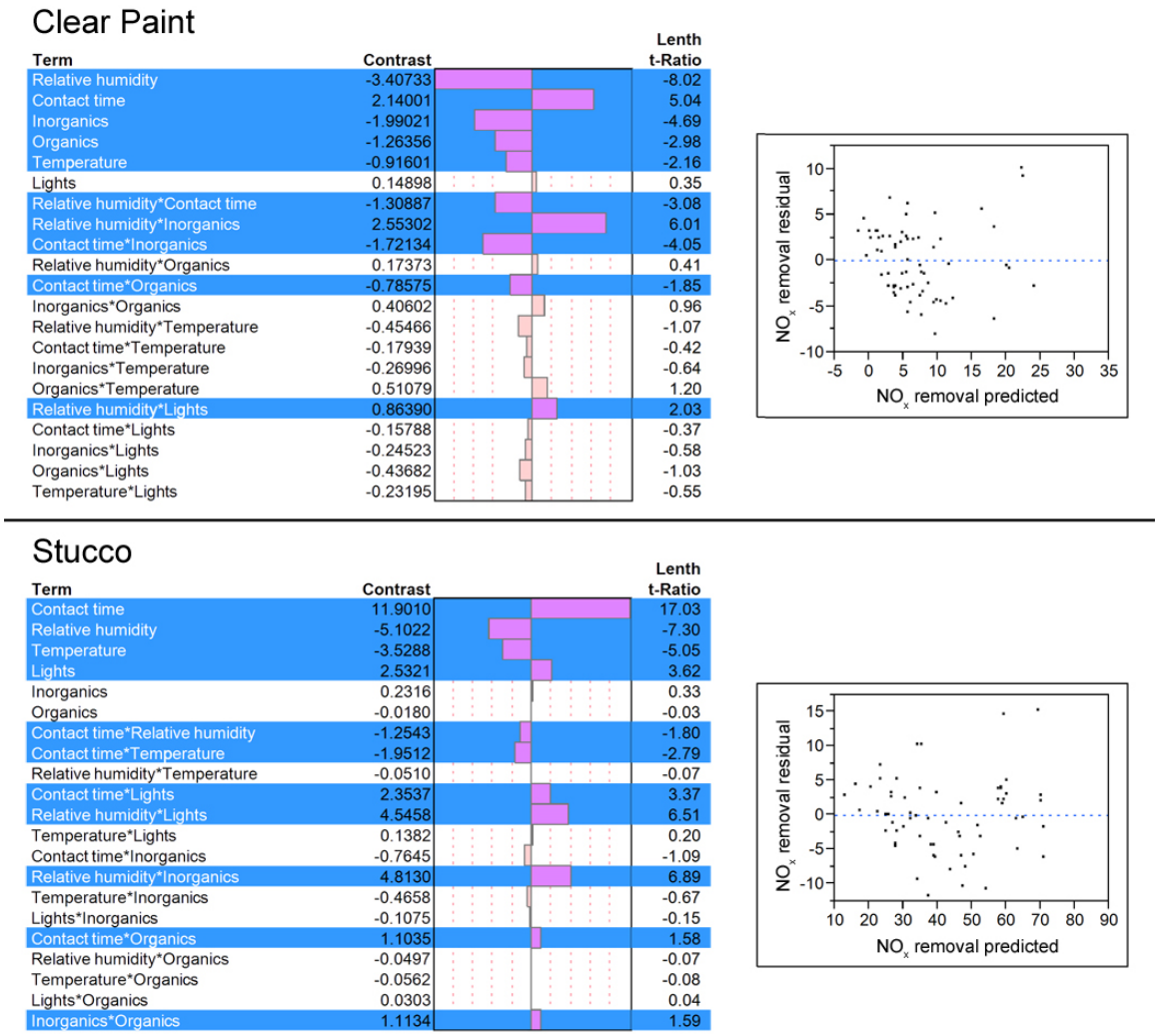

Figure 2. Results of the ANOVA analysis

Results from the ANOVA are presented in Figure 2. The PSE are 0.42471 and 0.6987 for NO_x removal by the clear paint and stucco, respectively. The critical value to which Lenth t-ratios are compared is 1.445 according to Mee (2009) for a significance level $\alpha = 0.15$. For the clear paint, five main factors and five two-way interactions were deemed significant for NO_x removal. For the stucco, four main factors and seven two-way interactions significantly affected removal of NO_x by the coating. Three common main factors affected NO_x removal by both coatings in the same fashion: an increase in contact time led to increased NO_x removal, while increases in temperature or relative humidity led to decreases in removal. The linear models associated with NO_x removals by the clear paint and stucco and determined in JMP had R^2 of 0.70 and 0.89, respectively. Residuals calculated with respect to the linear model determined in JMP were fairly consistent across the range of predicted values suggesting that the ANOVA hypothesis of equal variance was met. Residuals were also normally distributed as verified using a Shapiro-Wilk test with $W = 0.98$, $p = 0.28$ for residuals of NO_x removal by the clear paint and $W = 0.98$ and $p = 0.24$ for residuals of NO_x removal by the stucco.

Plots for the two-factor interactions that influence NO_x removal by each coating are presented in Figure 3. For both coatings, three two-factor interactions involving relative humidity significantly influence NO_x removal: interactions between RH on one hand and contact time, inorganic pollutant concentrations and light intensity on the other.

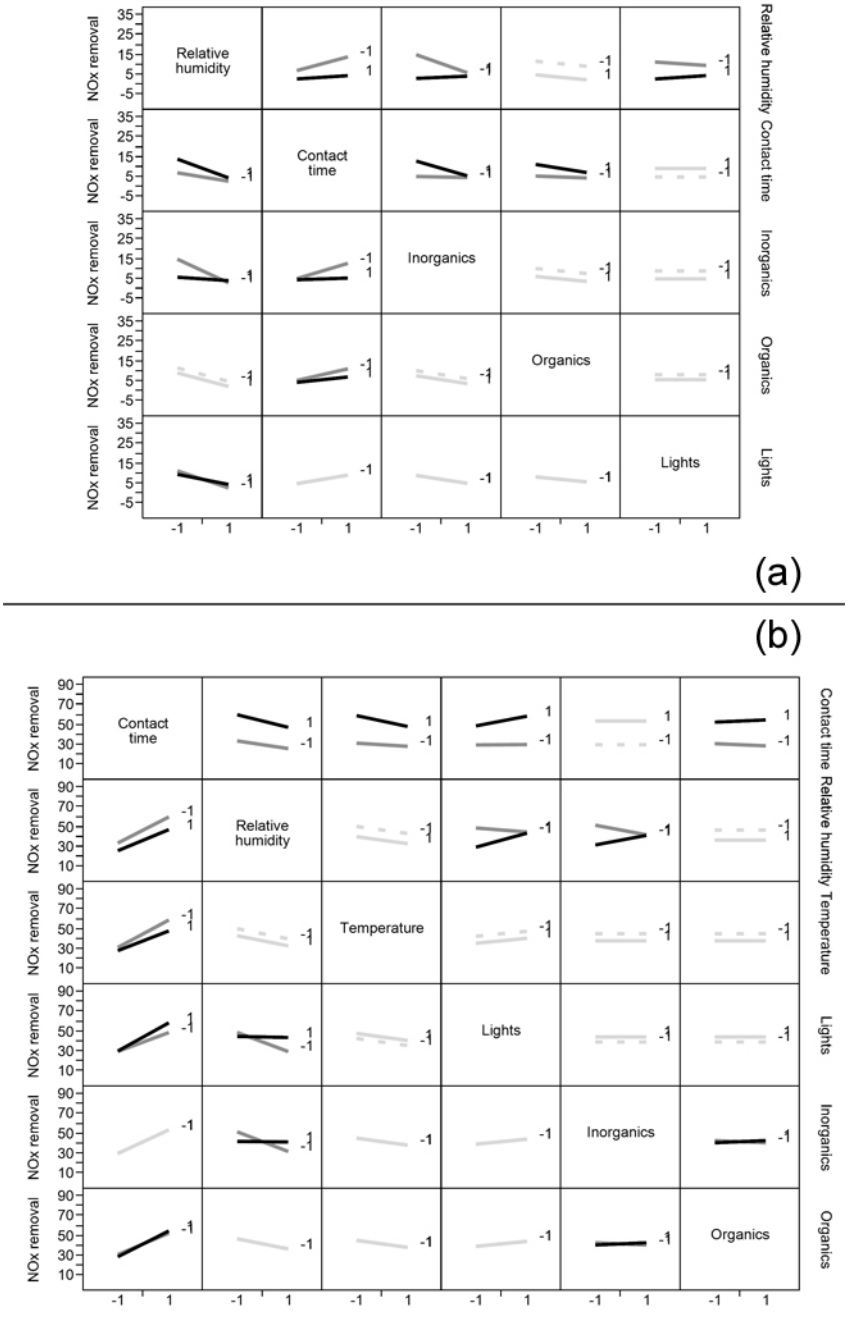

Figure 3. Interaction plots for (a) the clear paint (b) the stucco

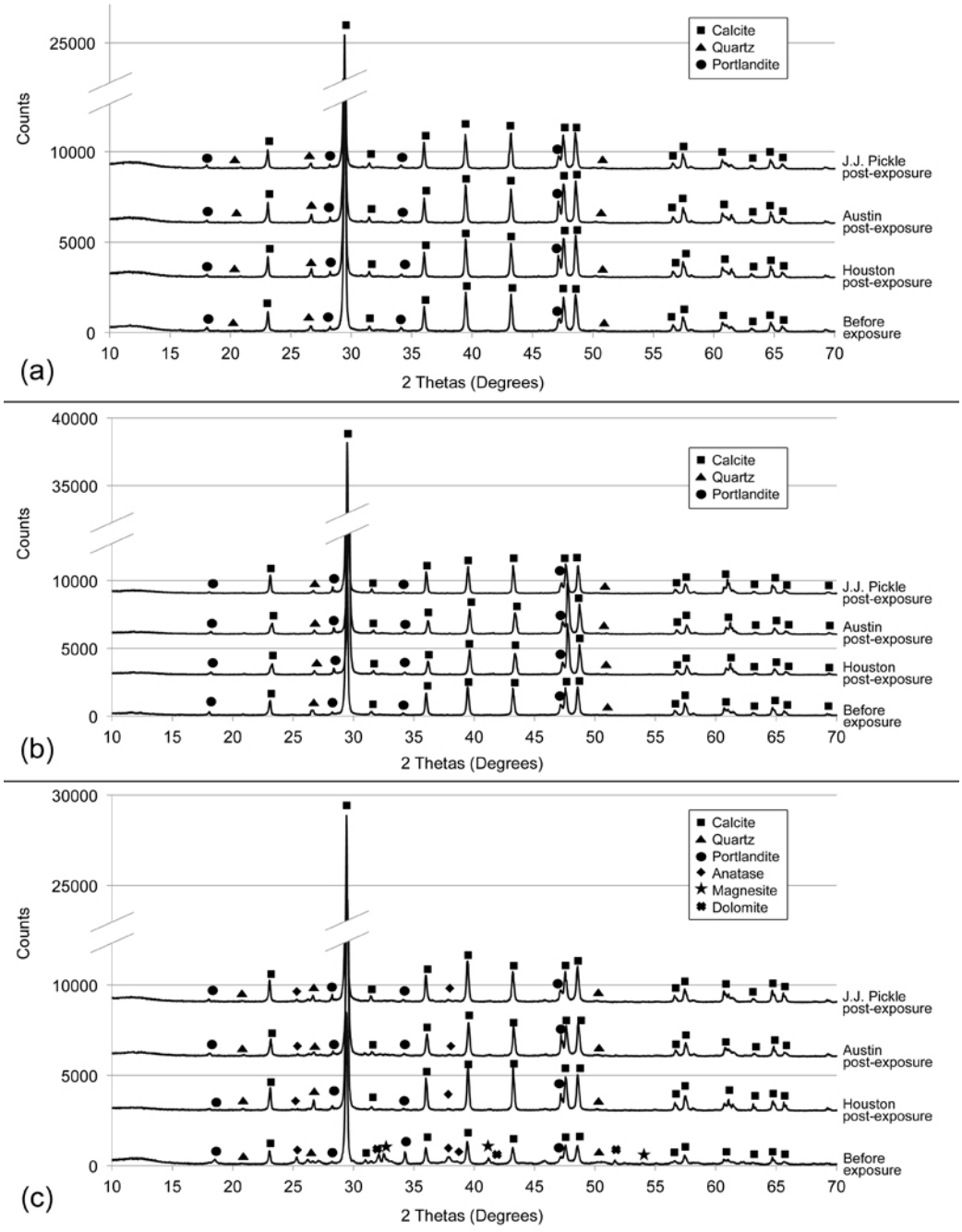

Figure 4. X-Ray diffraction results for (a) the uncoated concrete, (b) the clear paint, (c) the stucco

3.2. Field exposure results

Results from the XRD analysis of field samples are presented in Figure 4. The stucco retained the TiO_2 anatase phase after field exposure and exhibited no significant changes to the composition of the concrete or coating. For the clear paint, no TiO_2 was detected through XRD either before or after exposure. This may be due to the very small amount of TiO_2 in the coating (only 1 % by weight) compared to other phases present in the analyzed sample, specifically the phases from the concrete. Hence, it is not possible to determine from the XRD analysis whether or not the TiO_2 in the clear paint was retained after exposure.

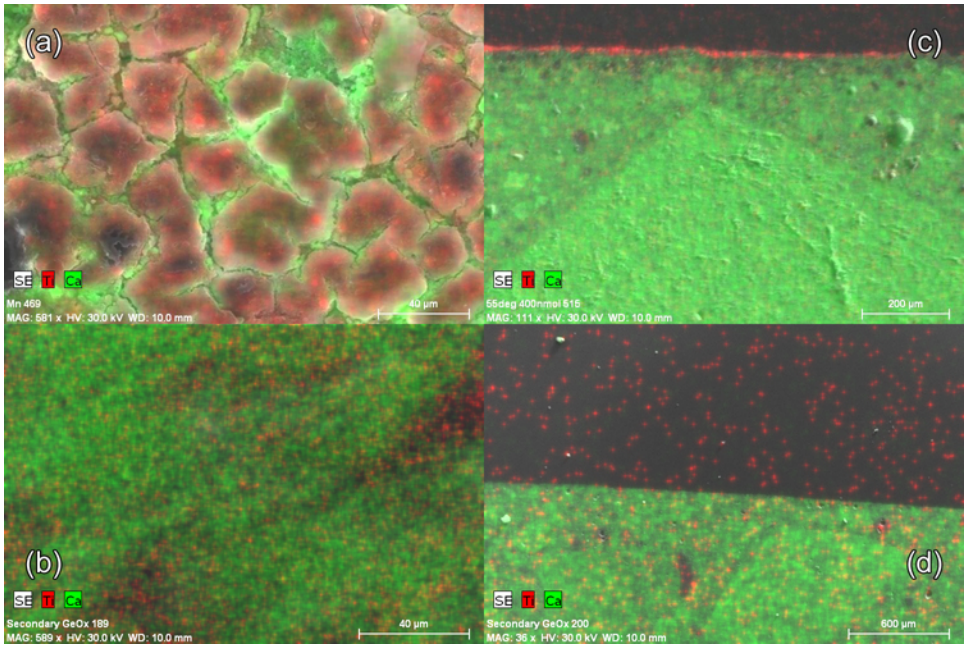

Figure 5. Scanning electron microscopy results for the clear paint

Results from the SEM analysis of the samples placed in the Houston field site are presented here and are representative of results obtained at other sites. Images obtained for the clear paint show significant degradation of the coating after one year of exposure.

Before exposure (Figure 5a), TiO_2 covered most of the surface of the test coupon. The pattern observed at the surface (Figure 5a) may be explained by the drying of the coating during desiccation prior to imaging. After exposure, little or no TiO_2 was observed on the surface of the sample (Figure 5c). Titanium dioxide was also absent in the post-exposure cross-section picture (Figure 5d), where a thin layer of TiO_2 was observed before exposure (Figure 5b). The degradation of the coating over time might explain the reduction in NO_x removals observed for the clear paint after the first few experiments.

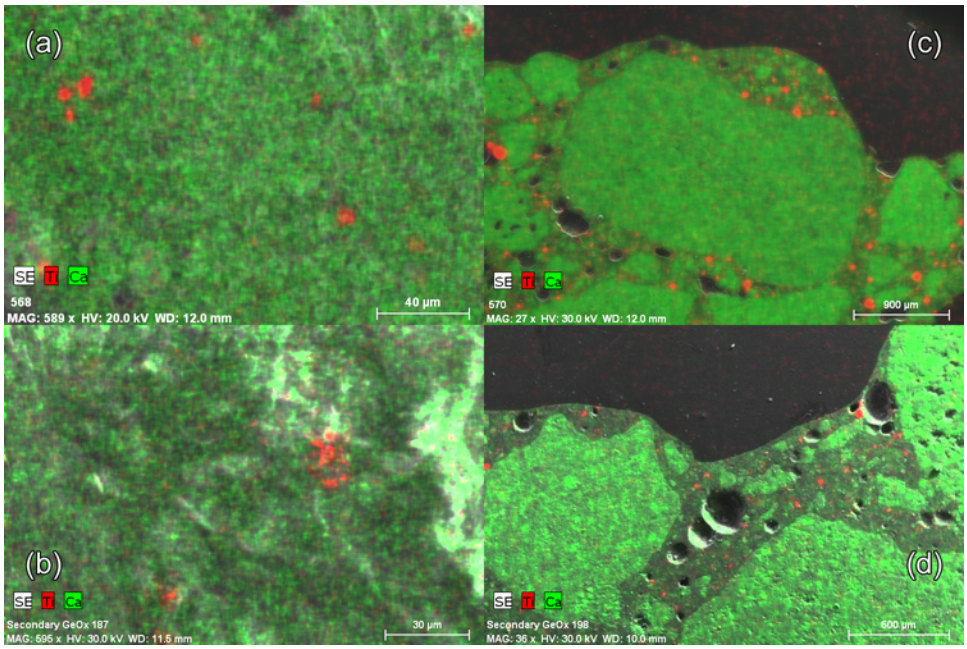

Figure 6. Scanning electron microscopy results for the stucco

Images obtained for the stucco coating are presented in Figure 6. Titanium dioxide is interspersed in the stucco cement matrix, forming small pockets visible as dots in the pictures. The images look similar before and after exposure suggesting that there is no appreciable degradation of the coating.

Results from the NO_x removal testing of the stucco after roadside exposure are presented in Figure 7 and compared to removals by a newly applied photocatalytic stucco as well as a newly applied stucco of the same composition, but without TiO_2. For all field sites, the NO_x removal after exposure decreased, by up to 75 % compared to the newly applied photocatalytic stucco, when the sample was tested without prior washing. The water wash had little effect on the samples from all field sites except the Austin field site, where NO_x removal remained comparatively high. It is difficult to explain the differences in results, especially between the Austin and Houston sites, which had similar conditions (very close to roadway). The samples from Houston were returned first for testing and the Austin ones last, with about a month lag. It is possible that conditions at the Austin field site in that period were more favorable to regeneration of the catalyst: average solar insolation in Austin during the week prior to retrieval of the Austin field site samples was 55 % higher than average insolation in Houston in the week prior to the retrieval of those samples. Higher insolation might have promoted the oxidation of pollutants adsorbed on the surface of the stucco samples in Austin. Finally, the soap wash led to improved removal effectiveness with removals 60 % and above of the initial level for the "morning" inorganic pollutants condition and 90 % and above the initial level for the "afternoon" inorganic pollutants condition. Results for the non-photocatalytic stucco show that it removes NO_x more efficiently than uncoated concrete, probably because of its larger surface area. However, the photocatalytic stucco was more efficient at removing NO_x compared to the stucco that does not contain TiO_2. This result indicates that differences in material surface morphologies alone cannot explain the differences in NO_x removal of the photocatalytic stucco over the uncoated concrete. All exposed photocatalytic stucco samples, even before any type of washing, removed NO_x more efficiently compared to the newly applied non-photocatalytic stucco.

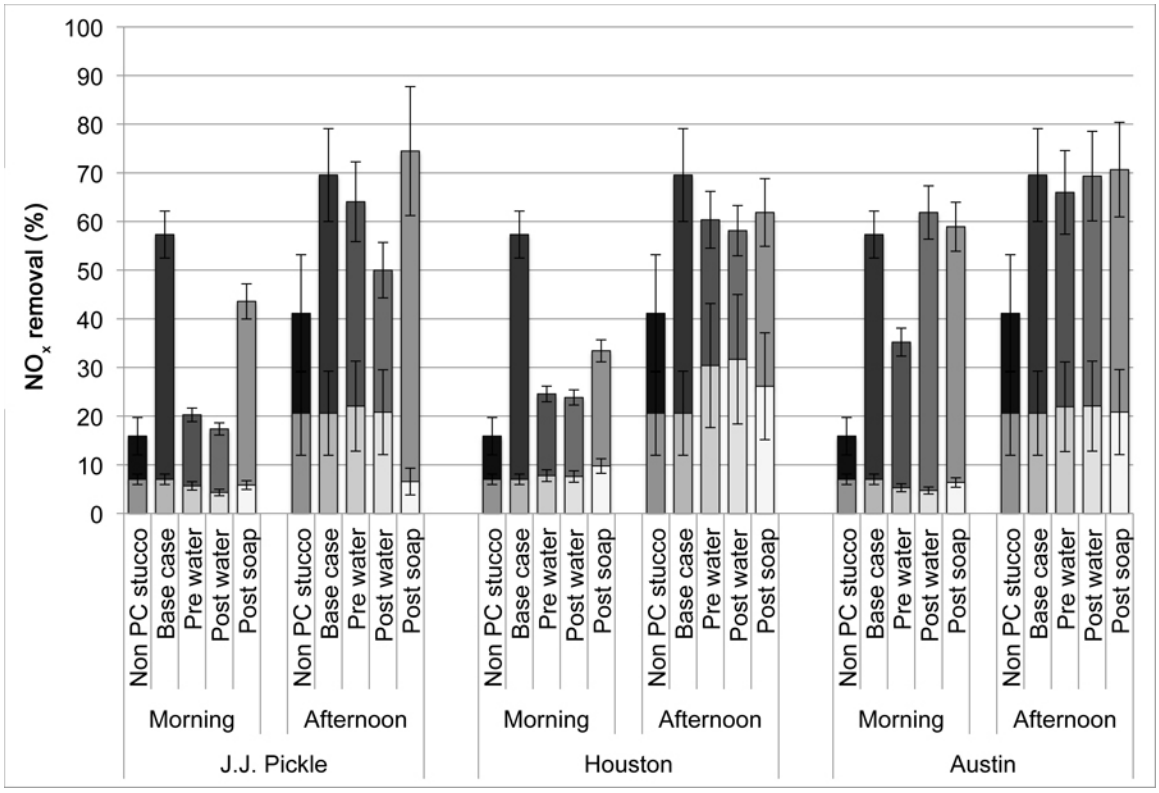

Figure 7. NO_x removal after roadside exposure for a year. The lighter and darker shades on each bar represent the fraction of the total removal due to the uncoated concrete and the stucco, respectively. Non PC stucco = stucco that does not contain TiO_2. Base case = test run on a newly applied photocatalytic stucco.

4. DISCUSSION

The clear paint performed fairly well during the first experiments of the testing program. However, removals were at the lower end of removals observed by other researchers. The removal efficiency of the clear paint continued to decrease and fell below most results previously reported in the literature. Results for the stucco coating were similar to removals reported by other researchers testing cementitious materials. For example, Dylla et al. [30] observed NO removals in the 20 – 60 % range for photocatalytic concrete tested at a contact time of 7 minutes and with an inlet

concentration of NO of 410 ppb. Ballari et al. [28] tested photocatalytic pavers and observed removals in the 43 – 83 % range. Their tests were run for contact times under 1 minute and an inlet NO concentration of 300 ppb while UV light intensity, temperature and RH conditions were similar to the ones used here. Dylla et al. [30] and Ballari et al. [28], observed a decrease in NO_x removal with increasing relative humidity, as observed in this study (Figure 2). This observation has been confirmed by other researchers [17,25,29]. It has been hypothesized that water molecules compete with pollutant molecules for reactive sites at the photocatalytic material surface [17,29].

Removal of NO_x by both coatings was also significantly affected by two common factors. An increase in contact time led to an increase in NO_x removal due to the longer time available for pollutant molecules to come in contact with the reactive surface. On the other hand, an increase in temperature led to a decrease in NO_x removal. Bengtsson et al. [26] observed a similar behavior when testing a colloidal suspension of TiO_2 in deionized water applied on white mortar for temperatures ranging from 21 to 31°C. It was hypothesized that a change in temperature affected the adsorption kinetics of the pollutant species on the material surface, hence affecting removal. It should be noted that these three factors also significantly affected NO and NO_2 removal by the stucco, independently [38].

Other environmental parameters affected NO_x removal by the two coatings differently (Figure 2). Increases in concentrations of inorganic or organic pollutants negatively affected removal by the clear paint while these two environmental factors did not significantly affect removal by the stucco. It is possible that the inorganic or organic pollutant molecules competed with NO_x for reaction sites at the surface of the concrete coated with clear paint. On the other hand, the stucco had a much rougher surface and more surface area for the same projected area. It is possible that the larger surface area

provided enough reaction sites so that there was no significant competition with NO_x molecules from the other pollutants present on the stucco surface. On the contrary, UV light intensity significantly affected removal by the stucco coating while it did not affect removal by the clear paint. Again, the surface morphology of the coating might explain this difference as it is possible that when UV light intensity was at the low level some reaction sites at the stucco surface did not receive enough light to be activated (e.g., inside pores, shaded sites). When the UV light intensity increased, more pores on the stucco surface might have been activated, explaining the associated increase in removal.

Three two-factor interactions involving RH influenced NO_x removal by both coatings (Figure 3). An increase from short contact time to long contact time was more beneficial for NO_x removal when the RH was at its low level (coded -1 in Figure 3) compared to its high level (coded 1). It is possible that when RH was low, only a limited amount of hydroxyl radicals were created at the photocatalytic surface. The longer contact time allowed greater chance for pollutant molecules to come in contact with the radicals available. When the RH was at its high level, more hydroxyl radicals were available for reaction, making the change in contact time less important. The two-factor interaction between RH and inorganic pollutant levels influenced NO_x removal by both coatings similarly (Figure 3). A change from a "morning" to an "afternoon" condition for inorganic pollutants led to a decrease in removal when the RH was low but an increase when the RH was high. It is interesting to note that the total NO_x concentration in the chamber inlet was higher in the morning condition (170 ppb NO_x, as 150 ppb NO and 20 ppb NO_2) compared to the afternoon condition (50 ppb NO_x as NO_2). It is possible again that under the low RH condition there were limited amounts of hydroxyl radicals formed at the coating surface. When the total NO_x concentration increased, a smaller fraction of it could be removed. However, when RH was high and hydroxyl radicals were

abundant, the removal increased. Finally, the effect of the two-factor interaction between RH and UV light intensity also held across both coatings. When the RH changed from its low level to its high level, the decrease in removal was larger at the low UV light condition versus the high UV light condition. It is possible that when the UV light intensity was low, a limited number of sites were activated at the material surface. Increasing the RH led to more competition with water molecules hence a reduced removal of NO_x. When the lights were high, more sites were activated making the competition for active sites less important. This might explain why the decrease in NO_x removal with increasing RH was smaller at high UV light intensity versus low.

Results from the SEM analysis of samples placed at field sites for a year and presented in Figures 5 and 6 help evaluate long term use of such coatings. In the case of the clear paint, TiO_2 almost completely covered the surface of the concrete during the initial test, but after one year of exposure most of the photocatalyst had disappeared. This explains the degradation of the coating performance observed during testing for pollutant removal. A paint matrix with a formulation offering more resistance to weathering may allow sustained NO_x removal performance of the coating. The stucco showed no sign of physical degradation over time. However, it is possible that other factors, not visible through SEM analysis, may affect the coating after months spent on a roadside field site. The results of NO_x removal tests conducted on stucco-coated samples after a year of exposure to roadside conditions (Figure 7) show that some deactivation of the catalyst occurs over time. A simple water wash had little effect on the removal efficiency of the coating, suggesting that the pollutants responsible for the deactivation of the catalyst were not water-soluble. However, a wash with a water and soap solution restored more than 60 % and 90 % of the catalytic activity in the morning and afternoon inorganic pollutant conditions, respectively. The same was not true for the soap-washed uncoated

concrete (Figure 7), indicating that the increased removal was not due to soap residues left on the material surface. This is an encouraging result compared to other studies that have considered photocatalytic materials for road applications. De Melo et al. [37] applied photocatalytic pavement blocks on the surface of a road and a sidewalk in Brazil. They found that heavy fouling and wearing of the surface, especially on the road, led to a significant decrease in removal efficiency after one year of exposure (87 % decrease in removal compared to initial test for road samples and 79 % for sidewalk samples). A water jet wash restored some efficiency but removals were still down 61 % and 45 % for the road and sidewalk samples, respectively, compared to initial tests. Similar results were observed by Petit and Guerrini [35,36] for studies conducted in Italy and France. This suggests that surfaces not directly in contact with vehicles may be better options for application of such pollution controls.

5. CONCLUSION

Some photocatalytic coatings have potential for NO_x removal. The tests conducted in this study showed that the ability of the coating to retain TiO_2 is an important factor for long term use of photocatalytic coatings for NO_x removal. Both coatings that underwent full factorial testing were similarly affected by three environmental factors (contact time, RH, temperature). However, other factors (organic and inorganic pollutant levels, UV light intensity) had coating-specific effects that might have been due to differences in the coating surface morphologies. Finally, long term use on road side structures could be hindered by the deactivation of the catalyst through adsorption of non water-soluble pollutants and require specific cleaning methods to overcome this issue.

6. ACKNOWLEDGEMENTS

This work was funded by the Texas Department of Transportation (TxDOT) under project 0-6636. The findings are part of an ongoing research project and the final results of the study will be considered by TxDOT before full release of the project final report. The authors would also like to thank Lisa Burris for her help in manufacturing and coating concrete samples used in this project.

7. REFERENCES

[1] Bauer MA, Utell MJ, Morrow PE, Speers DM, Gibb FR. Inhalation of 0.30 ppm nitrogen dioxide potentiates exercise-induced bronchospasm in asthmatics. Am Rev Respir Dis 1986;134:1203–8.

[2] Mohsenin V. Airway responses to nitrogen dioxide in asthmatic subjects. J Toxicol Environ Health 1987;22:371–80.

[3] Frampton MW, Morrow PE, Cox C, Gibb FR, Speers DM, Utell MJ. Effects of nitrogen dioxide exposure on pulmonary function and airway reactivity in normal humans. Am J Respir Crit Care Med 1991;143:522.

[4] Gauderman WJ, Avol E, Lurmann FW, Kuenzli N, Gilliland F, Peters J, et al. Childhood asthma and exposure to traffic and nitrogen dioxide. Epidemiology 2005;16:737–43.

[5] Clark NA, Demers PA, Karr CJ, Koehoorn M, Lencar C, Tamburic L, et al. Effect of early life exposure to air pollution on development of childhood asthma. Environ Health Perspect 2009;118:284–90.

[6] Peters A, Liu E, Verrier RL, Schwartz J, Gold DR, Mittleman MA, et al. Air pollution and incidence of cardiac arrhythmia. Epidemiology 2000;11:11–7.

[7] Nafstad P, Håheim LL, Wisløff T, Gram F, Oftedal B, Holme I, et al. Urban air pollution and mortality in a cohort of Norwegian men. Environ Health Perspect 2004;112:610–5.

[8] Raaschou-Nielsen O, Reynolds P. Air pollution and childhood cancer: A review of the epidemiological literature. Int J Cancer 2006;118:2920–9.

[9] Seinfeld JH, Pandis SN. Atmospheric Chemistry and Physics. Second edition. Wiley-Interscience; 2006.

[10] EPA. National Emissions Inventory (NEI) Air Pollutant Emissions Trends Data. Office of Air Quality Planning and US EPA Standards; 2011.

[11] Brunekreef B, Janssen NAH, de Hartog J, Harssema H, Knape M, van Vliet P. Pollution from truck traffic and lung function in children living near motorways. Epidemiology 1997;8:298–303.

[12] Thoma ED, Shores RC, Isakov V, Baldauf RW. Characterization of near-road pollutant gradients using path-integrated optical remote sensing. J Air Waste Manage Assoc 2008;58:879–90.

[13] EPA. Final Revisions to the Primary National Ambient Air Quality Standard for Nitrogen Dioxide (NO_2). Office of Air Quality Planning and Standards, 2010.

[14] Fujishima A, Honda K. Electrochemical photolysis of water at a semiconductor electrode. Nature 1972;238:37–8.

[15] Allen NS, Edge M, Sandoval G, Verran J, Stratton J, Maltby J. Photocatalytic coatings for environmental applications. Photochem Photobio 2005;81:279–90.

[16] Ballari MM, Hunger M, Hüsken G, Brouwers HJH. NO_x photocatalytic degradation employing concrete pavement containing titanium dioxide. Appl Catal, B 2010.

[17] Laufs S, Burgeth G, Duttlinger W, Kurtenbach R, Maban M, Thomas CES, et al. Conversion of nitrogen oxides on commercial photocatalytic dispersion paints. Atmos Env 2010;44:2341–9.

[18] Ballari MM, Hunger M, Hüsken G, Brouwers HJH. Modeling and experimental study of the NO_x photocatalytic degradation employing concrete pavement with titanium dioxide. Catal Today 2010;151:71–6.

[19] Dalton J, Janes P, Jones N, Nicholson J, Hallam K, Allen G. Photocatalytic oxidation of NO_x gases using TiO_2: a surface spectroscopic approach. Environ Pollut 2002;120:415–22.

[20] Ohko Y, Nakamura Y, Negishi N, Matsuzawa S, Takeuchi K. Photocatalytic oxidation of nitrogen monoxide using TiO_2 thin films under continuous UV light illumination. J Photochem Photobiol, A 2009;205:28–33.

[21] Devahasdin S, Fan C, Li K, Chen DH. TiO_2 photocatalytic oxidation of nitric oxide: transient behavior and reaction kinetics. J Photochem Photobiol, A 2003;156:161–70.

[22] Hunger M, Hüsken G, Brouwers HJH. Photocatalytic degradation of air pollutants - From modeling to large scale application. Cem Concr Res 2010;40:313–20.

[23] Hoffmann MR, Martin ST, Choi W, Bahnemann DW. Environmental applications of semiconductor photocatalysis. Chem Rev 1995;95:69–96.

[24] Chen J, Poon C-S. Photocatalytic construction and building materials: from fundamentals to applications. Build Environ 2009;44:1899–906.

[25] Maggos T, Bartzis JG, Leva P, Kotzias D. Application of photocatalytic technology for NO_x removal. Appl Phys a: Mater Sci Process 2007;89:81–4.

[26] Bengtsson N, Castellote M. Photocatalytic activity for NO degradation by construction materials: parametric study and multivariable correlations. J Adv Oxid Technol 2010;13:341–9.

[27] Lim T, Jeong S, Kim S, Gyenis J. Photocatalytic decomposition of NO by TiO_2 particles. J Photochem Photobiol, A 2000;134:209–17.

[28] Ballari MM, Yu QL, Brouwers HJH. Experimental study of the NO and NO_2 degradation by photocatalyticaly active concrete. Catal Today 2011;161:175–80.

[29] Hüsken G, Hunger M, Brouwers HJH. Experimental study of photocatalytic concrete products for air purification. Build Environ 2009;44:2463–74.

[30] Dylla H, Hassan MM, Mohammad LN, Rupnow T, Wright E. Evaluation of environmental effectiveness of titanium dioxide photocatalyst coating for concrete pavement. Trans Res Rec 2010;2164:46–51.

[31] Dylla H, Hassan MM, Schmitt M, Rupnow TS, Mohammad LN. Laboratory investigation of the effect of mixed nitrogen dioxide and nitrogen oxide gases on titanium dioxide photocatalytic efficiency in concrete pavements. J Mater Civ Eng 2011;23:1087–93.

[32] Beeldens A. An environmental friendly solution for air purification and self-cleaning effect: the application of TIO_2 as photocatalyst in concrete. Proceedings of Transport Research Arena Europe, Göteborg, Sweden: 2006.

[33] Hassan MM, Dylla H, Mohammad LN, Rupnow T. Evaluation of the durability of titanium dioxide photocatalyst coating for concrete pavement. Constr Build Mater 2010;24:1456–61.

[34] Ramirez AM, Demeestere K, De Belie N, Mantyla T, Levanen E. Titanium dioxide coated cementetious materials for air purifying purposes: preparation, characterization, and toluene removal potential. Build Environ 2010;45:832–8.

[35] Guerrini G, Peccati E. Photocatalytic cementetious roads for depollution. International RILEM Symposium on Photocatalysis, Environment and Construction Materials, Florence, Italy: 2007, pp. 179–86.

[36] Petit J. Chaussée dépolluante par photocatalyse de Vanves. 1st ed. Laboratoire Régional de l'Ouest Parisien; 2009.

[37] de Melo JVS, Trichês G, Gleize PJP, Villena J. Development and evaluation of the efficiency of photocatalytic pavement blocks in the laboratory and after one year in the field. Constr Build Mater 2012;37:310–9.

[38] Cros CJ, Terpeluk AL, Crain NE, Juenger MG, Corsi RL. Influence of environmental factors on removal of oxides of nitrogen by a photocatalytic coating. Atmospheric Environment, in Press 2013.

Appendix C

Paper 3: Clement J. Cros, Glenn C. Morrison, Jeffrey A. Siegel, Richard L. Corsi. Long-term performance of passive materials for removal of ozone from indoor air. *Indoor Air* (2011), 22, 43-53.

ABSTRACT

The health effects associated with exposure to O_3 range from respiratory irritation to increased mortality. In this paper we explore the use of three green building materials and an activated carbon mat that remove O_3 from indoor air. We studied the effects of long-term exposure of these materials to real environments on O_3 removal capability, and pre and post-ozonation emissions. A field study was completed over a six-month period and laboratory testing was intermittently conducted on material samples retrieved from the field. The results show sustained O_3 removal for all materials except recycled carpet, with greatest O_3 deposition velocity for activated carbon mat (2.5 to 3.8 m h^{-1}) and perlite-based ceiling tile (2.2 to 3.2 m h^{-1}). Carbonyl emission rates were low for activated carbon across all field sites. Painted gypsum wallboard and perlite-based ceiling tile had similar overall emission rates over the six-month period, while carpet had large initial emission rates of undesirable byproducts that decayed rapidly but remained high compared to other materials. This study confirms that activated carbon mats and perlite-based ceiling tile are viable surfaces for inclusion in buildings to remove O_3 without generating undesirable byproducts.

KEYWORDS:

activated carbon, green materials, field studies, deposition velocity, carbonyls, emissions

PRACTICAL IMPLICATIONS

The use of passive removal materials (PRM) for O_3 control could decrease the need for, or even render unnecessary, active but energy consuming control solutions. In buildings where O_3 should be controlled (high outdoor O_3 concentrations, sensitive

populations) materials specifically designed or selected for removing O_3 could be implemented, as long as O_3 removal is not associated with large emissions of harmful byproducts. We find that activated carbon mats and perlite-based ceiling tiles can provide substantial, long-lasting, O_3 control.

INTRODUCTION

Ozone is harmful to human health. Numerous studies have shown a link between exposure to O_3 and asthma, as well as decreased lung function (U.S. EPA, 2006; McDonnell et al., 1999). It is hypothesized that these effects are due to ozone induced damage to lung lining (Levy et al., 2001). Others have shown up to a 4 % increase in mortality from respiratory causes per 10-ppb increase in daily 1-hr maximum O_3 (Bell et al., 2005; Bell et al., 2006; Jerrett et al., 2009).

In the absence of indoor sources, O_3 concentrations indoors are lower than outdoors, with the indoor/outdoor O_3 concentration ratio depending on air exchange rate and the collective O_3 reactivity of indoor and building envelope surfaces (Weschler, 2000; Walker et al., 2010). However, Americans spend nearly 90 % of their time indoors (Klepeis et al., 2001), leading to significant exposure to indoor O_3. On average, indoor O_3 may account for 50 % or more of total daily O_3 exposure (Weschler, 2006).

Indoor exposure to O_3 is also accompanied by exposure to the products of ozone-initiated chemistry that also have adverse health effects (Weschler, 2004; Weschler, 2006). These products usually come from reactions between O_3 and unsaturated organic compounds. Major sources of such compounds include occupants themselves (e.g., skin oils), soft wood, carpet, linoleum, paints, cleaning products, air fresheners and soiled fabrics (Weschler, 2006).

The importance of indoor chemistry is increasing as buildings are constructed and retrofitted to be more energy efficient. To reduce energy consumption associated with space conditioning, tighter envelopes that reduce the number of air exchanges between indoors and outdoors are increasingly used. As a result, reactions that were once too slow to compete with air exchange rates may affect indoor air quality.

Removing O_3 from indoor environments could have beneficial effects on human health and comfort, as long as such removal does not create harmful by-products. Shair (1981) used an auxiliary filtration system containing nine activated charcoal filters to treat intake air on a university building when outdoor O_3 concentrations exceeded 80 ppb. The filter life to maintain at least 50 % O_3 removal was three years. Shields et al. (1999) used six panels of granular activated carbon to remove O_3 prior to ventilation of clean rooms. They observed that charcoal filters can remove O_3 for greater than five years. But the use of active systems leads to increased energy consumption. Others have tested VOC loaded activated carbon filters and showed reduced O_3 removal capacity depending on the type of adsorbed VOC and the extent of the loading (Dusenbury et al., 1996; Metts et al., 2006). However, VOC loaded carbon filters exposed to O_3 did not show increased emissions of by-products, as most of the VOC mass remained adsorbed on the activated carbon.

An alternative to conventional active (flow through) O_3 removal systems is the passive use of materials that O_3 contacts via normal air flows in the occupied space of buildings. We refer here to materials that enhance or maintain high indoor O_3 removal while forming negligible by-products, and that do so with minimal to no energy usage, as passive removal materials (PRMs). Kunkel et al. (2010) demonstrated the potential of PRMs during short-term laboratory experiments and Gall et al. (2011) investigated the possibilities and limitations associated with using such materials in homes. The study

described herein focused on evaluating how three green building materials performed as PRMs after six months in real indoor environments. Activated carbon mat was also tested for comparison.

Ozone removal to conventional and green materials has been extensively studied (Klenø et al., 2001; Grøntoft et al., 2002; Hoang et al., 2009; Kunkel et al., 2010; Morrison et al., 2000, Wang et al., 2006), as have post-ozonation emissions produced from O_3 reactions (Morrison et al., 2002; Nicolas et al., 2007; Poppendieck et al., 2007a; Wang et al., 2006, Wang and Morrison, 2010). Researchers have shown that building materials can be important sinks for O_3 indoors but that post-ozonation emissions are often significant, especially for materials covering large surface areas.

Ozone removal rates (parameterized by deposition velocities) and pre and post-ozonation emission rates of three green building materials were evaluated in this study. Activated carbon mats were also evaluated for comparison, since they have previously been shown to effectively remove O_3 from indoor air. Wall, floor and ceiling materials ("green" paint on gypsum wallboard, recycled carpet tile, and perlite-based ceiling tile) were chosen as they represent a large fraction of indoor surfaces and can therefore significantly influence indoor air quality in a building.

MATERIALS AND METHODS

Materials

The activated carbon mat (Gremarco Inc., model C0150) used in this study was a non-woven polyester based fabric (thickness = 0.5 cm) coated with activated carbon (area normalized mass = 136 g/m^2). The green ceiling tiles (Chicago Metallic Corporation, Eurostone, model Terric) were made of 100 % recyclable materials and were marketed as having no VOCs or man-made mineral fibers. The carpet (Interface FLOR, model Worn

Again) had a recycled content of 68 %-71 %. It was made of a type 6 nylon loop pile of height 0.43 cm. The recycled gypsum wallboard (USG Sheetrock, Synthetic from Galena) was obtained through a local distributor in Austin, TX. It was made of reclaimed gypsum and recycled paper. Three months before the beginning of experiments, a 100 % acrylic, low-VOC primer (Benjamin Moore, Eco Spec) was applied on the gypsum wallboard, followed by two coats of 100 % acrylic, low-VOC, flat finish paint (Benjamin Moore, Eco Spec).

All materials were new when obtained and were stored in their original packaging under ambient conditions until the beginning of experiments, except for the gypsum wallboard sheets that were painted and aired out for three months under ambient conditions in an unoccupied test house described by Novoselac et al. (2009).

Field study

Ozone deposition velocity and pre and post-ozonation emission rates were quantified for each sample prior to placement in the field. Samples were then placed in real homes and commercial/institutional buildings located in Austin, Texas, for six-months. Field locations covered a wide range of indoor environments as listed in Table 1. All residential field sites were equipped with HVAC systems but no mechanical air intakes. The office building was continuously mechanically ventilated with 10 % outdoor air. Materials were removed from the field on a monthly basis and brought back to the laboratory for analysis. New O_3 deposition velocities were determined every month. Pre and post-ozonation emission rates were determined after three and six months. Following laboratory analysis the materials were returned to their initial field locations.

Samples (20 cm × 25 cm) of activated carbon, ceiling tile and painted gypsum wallboard were mounted on metal wire stands and placed on shelves approximately 1.8 m

from the floor at each field site. Samples of carpet were placed on the floor in relatively protected areas, such as in room corners, to avoid having occupants repeatedly stepping on them during the field test. The backside and edges of samples were covered with aluminium foil to ensure that only one side of the material was directly exposed to air. This protection was also used during laboratory experiments to avoid measuring characteristics of surfaces that are not usually exposed indoors.

Indoor environmental conditions were monitored at each test location so that their effect on material properties could be analyzed. Continuous temperature and relative humidity (RH) measurements were recorded using a HOBO U12-013 datalogger (Onset Corporation, USA). As an approximate measure of dustiness, dust samples were taken monthly from the shelves on which the samples were set using adhesive Scotch Magic tape (3M, USA). The sampling area was wiped clean using a Swiffer dry cloth (Procter & Gamble, USA) after each sampling event. The tape strip was then applied to a microscope slide and analyzed using a microscope (BX40, Olympus, USA) with image processing software (Image J) to measure the percent area covered by dust. Finally, the total organic gaseous content of the air was measured using passive samplers made of large volume glass liners (SISS, Open liners, tapered, frit, 3 mm I.D.) for the injection port of a gas chromatograph (GC). The sampler was packed with Tenax-TA (Supelco Inc., 80/100 mesh), placed at each field location and replaced monthly.

Table 1. Field locations.

Building type	Room type	Age (years)	Monthly average range		Number of samples			
			Temperature	Relative humidity	Activated carbon	Carpet	Ceiling tile	Painted gypsum wallboard
Office building	Office	24	23-25°C	32-59%	1	2	1	1
Occupied by up to three students during regular business hours								
House 1	Kitchen	5	19-25°C	51-57%	1	1	2	1
Used by five residents daily								
House 2	Home Office	44	16-29°C	47-63%	1	1	1	2
Occupied by one resident and a pet daily								
House 1	Bedroom	5	19-27°C	44-60%	2	1	1	1
Occupied by one resident daily								
Unoccupied Test House	Kitchen/ Dining room	4	16-29°C	34-54%	2	1	1	1
Occupancy and operation of the Test House varied greatly depending on experiments carried out								

Laboratory testing

Experimental system

A diagram of the experimental system used to test materials is provided in Figure 1. Three identical 48-L electro-polished stainless steel chambers (25 cm × 38 cm × 50 cm) were used in parallel. Chambers were cleaned with deionized water and a heat gun before the beginning of each experiment to remove particles and chemicals that could have deposited or adsorbed to chamber walls.

Room air was dehumidified and cleaned by passing through a column containing 8 mesh Indicating Drierite (Drierite Company, USA) and an activated carbon (AC) filter. The airflow was then split into two streams, one delivered to a UV-based ozone generator (modified zero air generator, Perma Pure LLC) to introduce O_3 to the air stream (except during pre-ozonation emission rate measurements). A split stream of air was then bubbled through an impinger to achieve the desired relative humidity (RH), measured at the inlet of the chambers using an RH probe (TSI, Inc., Q-Trak 8551). Mass flow controllers (Aalborg, USA) maintained a constant volumetric flow rate entering each chamber. The air entered and exhausted from the chamber through perforated stainless steel tubes extending across the interior length of each chamber. Sampling ports for O_3 and VOC measurements were placed on the inlet and outlets of the chambers. Ozone concentrations in the inlet and exhaust streams were measured using a single UV absorbance cell ozone monitor (model 202, 2B Technologies) recalibrated three times during the experimental period using an ozone calibration source (model 306, 2B Technologies).

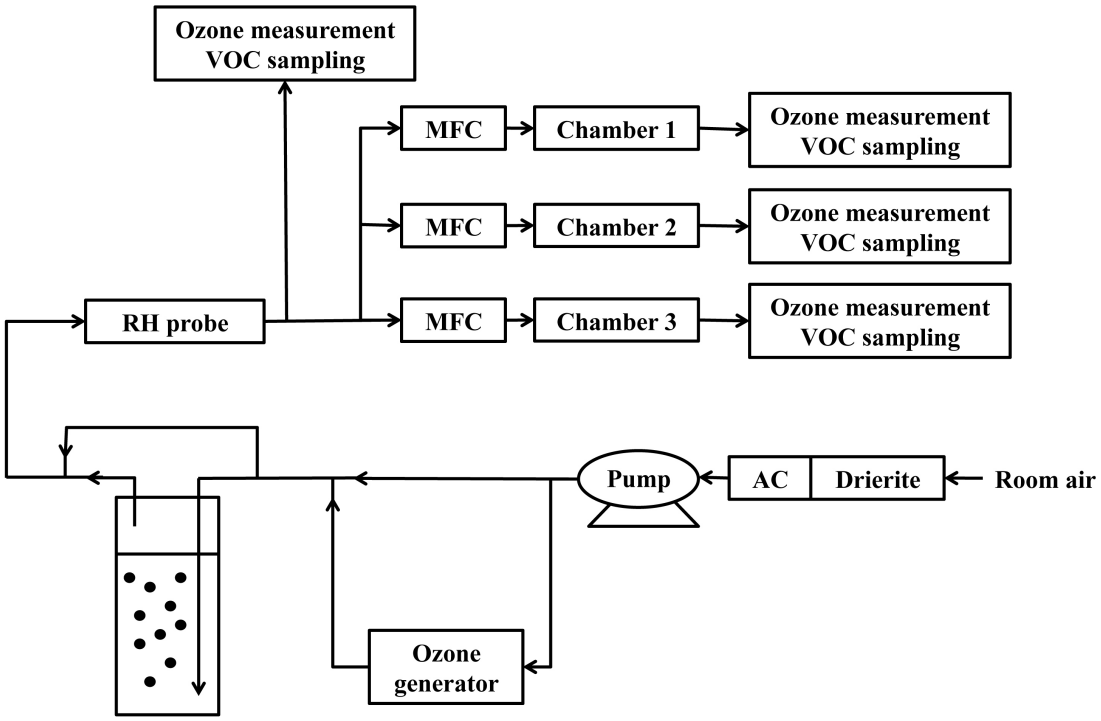

Figure 1. Diagram of the experimental system. AC = activated carbon filter, MFC = mass flow controller, RH = relative humidity.

Laboratory tests were completed under the following experimental conditions: 50 ± 2 % RH, 147 ± 10 ppb inlet O_3 concentration, two air exchanges per hour. The airflow rate through the chambers was measured using a bubble flow meter (Gilibrator 2, Gilian, Sensidyne, LP) to confirm the air exchange rate. The mean (± standard deviation) steady-state O_3 concentration (across the entire experimental program) in chambers that contained materials ranged from 51 ± 7 ppb for activated carbon to 89 ± 11 ppb for painted gypsum wallboard.

Sampling of carbonyls

Carbonyl emission rates from the materials were measured three times during the study. An initial measurement was made before samples were placed in the field.

Carbonyl measurements were then made after three and six months. Target carbonyls included C_1 to C_{10} saturated n-aldehydes, acetone, o-tolualdehyde, and benzaldehyde. Sampling methods followed those described by Morrison et al. (2002) and Poppendieck et al. (2007a). Light carbonyls (formaldehyde, acetaldehyde, acetone, propanal, butanal, pentanal) were sampled on pre-packed DNPH tubes (SKC 226-119, Silica Gel, 150/300mg sorbent). Heavy aldehydes (hexanal, heptanal, o-tolualdehyde, octanal, benzaldehyde, nonanal, decanal) were sampled on large volume glass GC injection liners (SISS, open liners, tapered, frit, 3 mm I.D.) packed with Tenax-TA (Supelco Inc., 80/100 mesh). The 400 ± 3 mL/min and 50 ± 2 mL/min airflow through the DNPH and Tenax tubes, respectively, was provided by sampling pumps (model VSS-1, A.P. Buck Inc.).

Ozone scrubbers (Supelco, LpDNPH, 505285) were used when sampling ozonated air to avoid interferences that occur because of O_3 reacting with sorbent materials and adsorbed organic compounds (Clausen et al., 1997; Pellizzari et al., 1984; Kleindienst, 1998). Ozone scrubbers were cleaned according to a previously established protocol (Poppendieck et al., 2005).

Carbonyls were sampled in chamber air before and after O_3 injection. Pre-ozonation emission rates were measured after the materials had been exposed to O_3 free air for 1.5 hours. Materials were then exposed to O_3 for four hours, and samples were collected during the fourth hour of ozonation to quantify emission rates during ozonation. For simplicity we refer to these emissions as post-ozonation for comparison with pre-ozonation.

Analysis of carbonyls

DNPH tubes used to sample light carbonyls were wrapped in aluminium foil and placed in individual plastic bags after each experiment. The tubes were kept frozen until

they were analyzed for C_1-C_5 carbonyls using high-performance liquid chromatography with UV detection (HPLC/UV) (Waters 717plus autosampler; Waters 600 controllers, Waters 996 Photodiode Array Detector; column: Gemini 5u C18 110A, 250 × 4.60 mm 5 μm).

Tenax-TA tubes were analyzed by zero-path thermal desorption followed by gas chromatography with flame ionization detection (TD/GC/FID) (Optic 2, ATAS; Agilent 6850, column: 30 m, RESTEK, Rxi-5Sil MS, 0.25 mm ID, film thickness: 0.5 μm).

The GC/FID was calibrated using a five-point external calibration curve (R^2 > 0.99) for each individual compound. Calibration curves were created using stock solutions made from pure chemicals purchased from Fisher Scientific, Inc. (pentanal, 97%, hexanal, 98%, heptanal, 95%, octanal, 99%, nonanal, 95%, decanal, 98%, benzaldehyde, 99%, tolualdehyde, 97%). One blank Tenax-TA tube and one standard were analyzed each day that experiments were run.

Data analysis

O_3 ***deposition velocity***

Ozone removal for different material samples was quantified in terms of ozone deposition velocity, a mass-transfer coefficient defined in this research as the mass flux of O_3 to the material surface divided by the O_3 concentration in the chamber exhaust. The deposition velocity is a function of fluid mechanics (transport processes) and surface O_3 decomposition kinetics. For constant fluid mechanical conditions, changes in O_3 deposition velocity with time should only be due to changes in reactivity between O_3 and material surfaces. Chamber tests were run for sufficient time that a steady-state condition with respect to O_3 concentration was reached in the chamber. For every other set of experiments (three chambers operated in parallel), one of the chambers was left empty to

allow calculation of the deposition velocity of O_3 to the chamber walls. The empty chamber was switched between experiments.

The deposition velocity of O_3 for the material tested, v_d (m h^{-1}), is based on a steady-state mass balance on a well-mixed chamber, including reaction at chamber walls:

$$v_d = \frac{\lambda V}{A_s}\left(\frac{c_{in}}{c} - 1\right) - v_{d,w}\left(\frac{A_w}{A_s} - 1\right) \quad (1)$$

where λ is the air exchange rate of the chamber (h^{-1}), V the volume of the chamber (m^3), A_w is the total area of the chamber walls (m^2), A_s is the horizontal projected area of the material sample (m^2), c_{in} is the inlet O_3 concentration (ppb), c is the O_3 concentration in a chamber containing a material sample (ppb), and $v_{d,w}$ is the O_3 deposition velocity for the chamber walls (m h^{-1}).

Mean values are expressed with a corresponding standard deviation around the mean. For all other analyses, uncertainties in the measured deposition velocities were calculated with an error propagation analysis using the maximum of instrument error, ±2% for the ozone analyzer, ±1% for the bubble flow meter and an error on horizontally-projected area measurements that was estimated to be less than 10%.

Carbonyl emission rates

One chamber in the system was left empty every other set of experiments to evaluate the carbonyl emission rates of chamber walls. The difference in carbonyl concentrations between empty chambers was on average less than 2 μg m^{-3}. Emission rates of each compound from test specimens were calculated based on a mass balance on a well-mixed flow-through chamber at steady-state, accounting for emissions from chamber walls:

$$e_{k,s} = \frac{\lambda V\left(c_k - c_{k,in}\right) - \lambda V\left(c_{k,e} - c_{k,in}\right)\left(1 - \frac{A_s}{A_w}\right)}{A_s} \quad (2)$$

where $c_{k,in}$ is the inlet concentration of compound k (μg m^{-3}), $c_{k,e}$ is the concentration of compound k in an empty chamber (μg m^{-3}), c_k is the concentration of compound k in a chamber containing a material sample (μg m^{-3}), $e_{k,s}$ is the emission rate of compound k for the material sample (μg m^{-2} h^{-1}), and all other variables are as previously described.

RESULTS AND DISCUSSION

O_3 removal

Ozone deposition velocities averaged over the six-month experimental period are shown in Figure 2. Vertical lines represent the standard deviation of deposition velocities determined across all six months. Figure 2 allows a comparison among materials and specific locations of the O_3 scavenging potential of each material. Note that since airflow conditions in test chambers did not change during the experimental program, differences in deposition velocity should have been due solely to differences in material reactivity with O_3. Higher air speeds in the chamber would have probably led to greater differences in deposition velocity between materials as transport limitations to O_3 deposition would have been reduced and effects of reactivity magnified (Cano-Ruiz et al., 1993; Grøntoft et al., 2004a). The deposition velocity for activated carbon, which is highly reactive (Kunkel et al., 2009), is within the range of O_3 transport-limited deposition velocities measured in an apartment (1.2 to 3.6 m h^{-1}) (Morrison et al., 2006). This suggests that mass-transport conditions are consistent with residential settings. Activated carbon is the most effective material at removing O_3 , with O_3 deposition velocities in laboratory chambers ranging from 2.5 to 3.8 m h^{-1}. These values are slightly lower than those

reported by Grøntoft (2002) and Kunkel et al. (2010), who observed deposition velocities ranging from 3.8 to 8.0 m h^{-1}. However, their testing methods involved the presence of mixing fans and higher air speeds adjacent to materials, which likely resulted in lower transport limitations to O_3 removal leading to higher measured deposition velocities than those in this study. Ozone deposition velocities measured for carpet were slightly less than those for activated carbon, ranging from 2.0 to 3.0 m h^{-1}. Wang et al. (2006) reported O_3 deposition velocities for aged carpet in the range of 1.5 to 5 m h^{-1} and Nicolas et al. (2007) reported deposition velocities on new carpet ranging from 1.4 to 2.7 m h^{-1}, i.e. in agreement with the results from this study. The O_3 deposition velocities for the perlite-based ceiling tile ranged from 2.2 to 3.2 m h^{-1}. Deposition velocities previously reported for ceiling tile range from 1.7 to 2.5 m h^{-1} (Hoang et al., 2009; Poppendieck et al., 2007a), similar to the range that we observed. Finally, O_3 deposition velocities for painted gypsum wallboard were about two and a half to three times lower than for the other three materials, in the range of 0.7 to 1.3 m h^{-1}. Klenø et al. (2001) reported a deposition velocity of 1.5 m h^{-1} for gypsum wallboard freshly coated with acrylic paint. Wang et al. (2006) reported deposition velocities ranging from 1.2 m h^{-1} to 0.03 m h^{-1} in three houses between 1 and 10 years old (deposition velocities decreased with age).

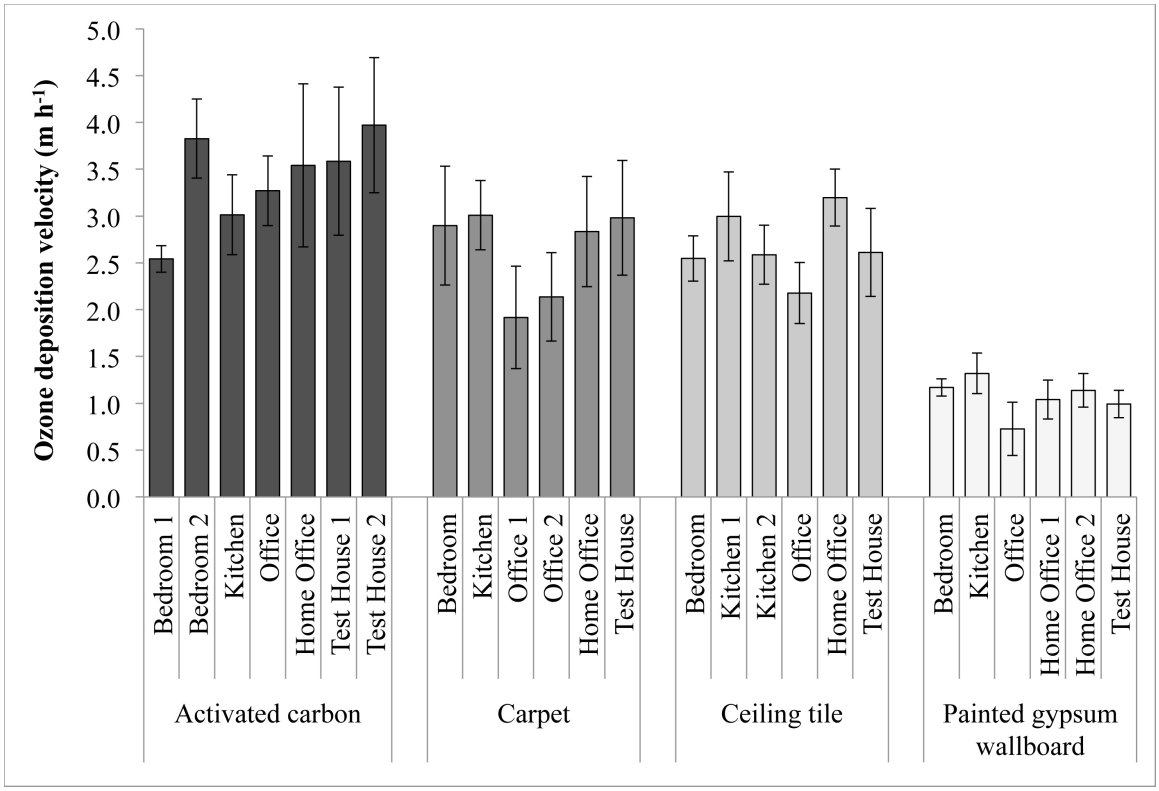

Figure 2. O_3 deposition velocity on material samples averaged over time.

All three green building materials exhibited reduced O_3 deposition velocity for samples placed in the Office field location. Ozone removal by carpet and painted gypsum wallboard samples placed in this location decreased by 36% and 53%, respectively, between the first and the following months, while the decrease was only about 10% for the ceiling tile. Environmental conditions at other locations did not affect materials in such a consistent manner. This difference could not be explicitly resolved but could be a result of consumption of reaction sites by somewhat higher O_3 concentrations in the office location, relative to residential sites, due possibly to a higher air exchange rate, higher O_3 penetration through the HVAC air intake and surfaces with lower reactivities.

Ozone deposition velocities averaged over all locations are presented in Figure 3. Vertical lines represent one standard deviation. Ozone deposition velocities averaged over all field sites for activated carbon and ceiling tile exhibited little variation over time. The deposition velocity for painted gypsum wallboard decayed by 30% for the first two months and then converged to a relatively low value. The deposition velocity for carpet started as high as the deposition velocity for activated carbon, but was lower than ceiling tiles by the end of the experimental period. After six months in the field, carpet removed about 30% less O_3 than it did initially. This result is consistent with observations by Morrison et al. (2000) who tested four carpets and found that the reactivity of each material with O_3 decreased with increasing cumulative exposure. Wang et al. (2006) also observed that O_3 removal capacity of carpet decreases with age.

Activated carbon had the highest O_3 removal capacity of all test materials and remained high even after several months at field locations. Perlite-based ceiling tile also appears to be a potentially viable PRM as its reactivity is sustained over time. Painted gypsum wallboard was the least reactive material with O_3.

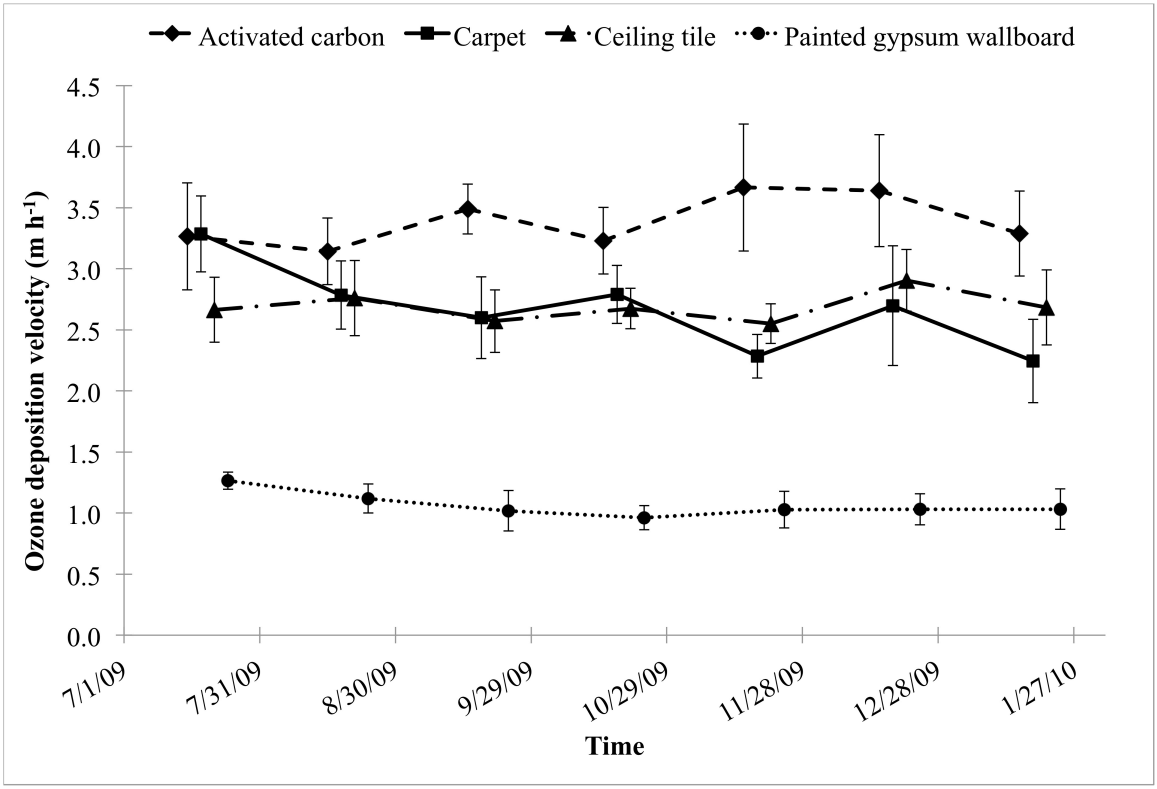

Figure 3. O_3 deposition velocity on material samples averaged over all field sites.

An entire set of results for painted gypsum wallboard is presented in Figure 4 and shows deposition velocities measured from month 0 to month 6. Some variation was observed for measurements at each location. The home office location exhibited a decreasing trend in O_3 deposition velocity for the painted gypsum wallboard, but other materials did not show a similar trend. It is not possible to ascertain whether this is only due to experimental variations or if the painted gypsum wallboard was actually affected by this particular environment. Isolated increases in reactivity could be due to changes in activity patterns at the field locations leading to a different level of soiling of the materials. For example, the UTest House (unoccupied test house facility) was heavily

used for other experimental projects during month 5, which might explain the higher sample reactivity observed for that month.

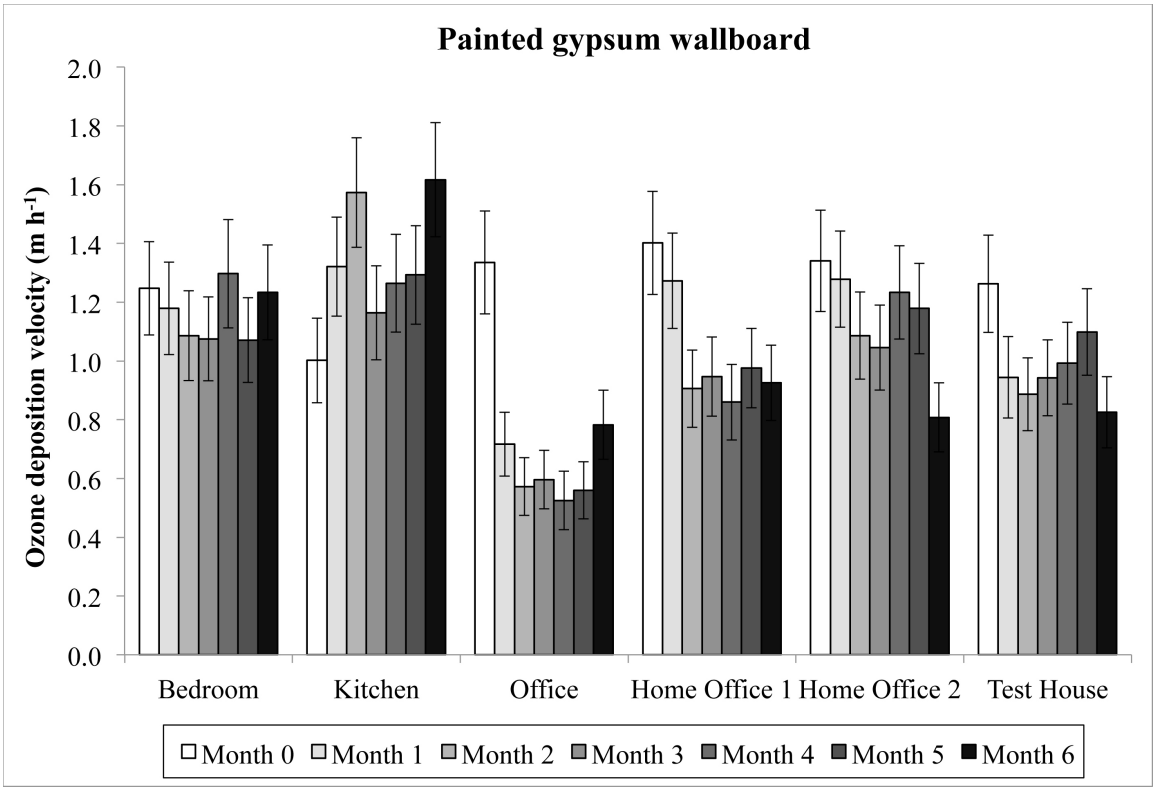

Figure 4. O_3 deposition velocity results for painted gypsum wallboard.

Carbonyl emission rates

Pre-ozonation emissions refer to emissions that occurred before ozonated air was introduced into the test chambers. Post-ozonation emission rates were measured after ozonated air was introduced into the chambers. Emission rates averaged over all locations are presented in Figure 5. Figure 5 allows a comparison of pre and post-ozonation emission rates of the materials and their evolution over time.

Both pre and post-ozonation emission rates from activated carbon were lower than the other three materials. There is a trend of decreased emission rates over time for

pre-ozonation emission rates while post-ozonation emission rates increased slightly. The relatively low emission rates from activated carbon were dominated by acetaldehyde (22% to 58% by mass) as well as formaldehyde, especially for post-ozonation emission rates (5% to 35%).

All three green materials had higher post-ozonation emission rates than pre-ozonation emission rates. In each case, post-ozonation emission rates were dominated by nonanal. This is consistent with results from Wang et al. (2006) who tested post-ozonation emission rates of various indoor surfaces in four homes between one and fourteen years old. For similar test conditions, they also observed higher post-ozonation emission rates than pre-ozonation emission rates, also dominated by nonanal.

There were also differences in emission rates among test materials. Carpet exhibited the highest pre and post-ozonation emission rates. Even though initial pre and post-ozonation emission rates for carpet were relatively high, both were characterized by a dramatic reduction in emissions between the initial measurement and the one made after three months, and was observed for all field locations. After three months, pre and post-ozonation emission rates from carpet decreased by approximately 55% from their initial level. After that period, pre-ozonation emission rates were relatively steady, while post-ozonation emission rates continued to decrease.

Results for post-ozonation emissions from carpet were compared with findings from a study by Morrison et al. (2002) who tested four different types of carpet. Some of their samples were stored in original packaging before testing, similar to our initial tests. Morrison et al. (2002) also studied carpet that had been aired out for a year prior to testing. Similar to the results of this study, they observed post-ozonation emission rates that were higher than pre-ozonation emission rates and dominated by nonanal for all

samples. Lower post-ozonation emissions also occurred from aired carpet, similar to what we observed for newly unpackaged carpet versus carpet placed in the field for six months. However, pre-ozonation emissions differed between Morrison et al. (2002) and this study. They observed pre-ozonation emission rates from aired samples that were greater than pre-ozonation emission rates from stored samples. Waring et al. (2010) also measured carbonyl emissions in a room containing carpet with O_3 and found increased levels of formaldehyde and nonanal.

Averaged results for perlite-based ceiling tile show a different temporal fingerprint of emissions relative to carpet. While pre-ozonation emission rates decreased by 50% during the six-month study period, post-ozonation emission rates averaged across all field sites more than doubled. Emission rates of samples in the kitchen location greatly influenced the average result. Emission rates in the kitchen location increased by about two orders of magnitude between the initial and final measurements. For other field locations, post-ozonation emissions decreased over the course of the experimental period. The ceiling tiles used in this study were highly porous and might have adsorbed gases or retained particles deposited on their surface during cooking events, or retained secondary products. Adsorbed gases and deposited particles could later react with O_3 during laboratory tests, explaining an increase in post-ozonation emission rates for the samples placed in the kitchen.

Finally, painted gypsum wallboard exhibited an emission pattern that was different from the other two green materials but observable for most field locations. Pre and post-ozonation emission rates were the highest initially but declined by 36% and 50%, respectively, during the first three months. However, emission rates then increased during the next three months by 23% and 30%, respectively.

Results averaged over all field locations are relevant when considering emissions by PRMs inside an entire building. However, locations where emissions were greatest, such as the kitchen or the bedroom, tend to influence the average value. This is particularly true for the perlite-based ceiling tile for which averaged results were greatly influenced by kitchen results where emissions were higher than for other locations. This result is discussed later.

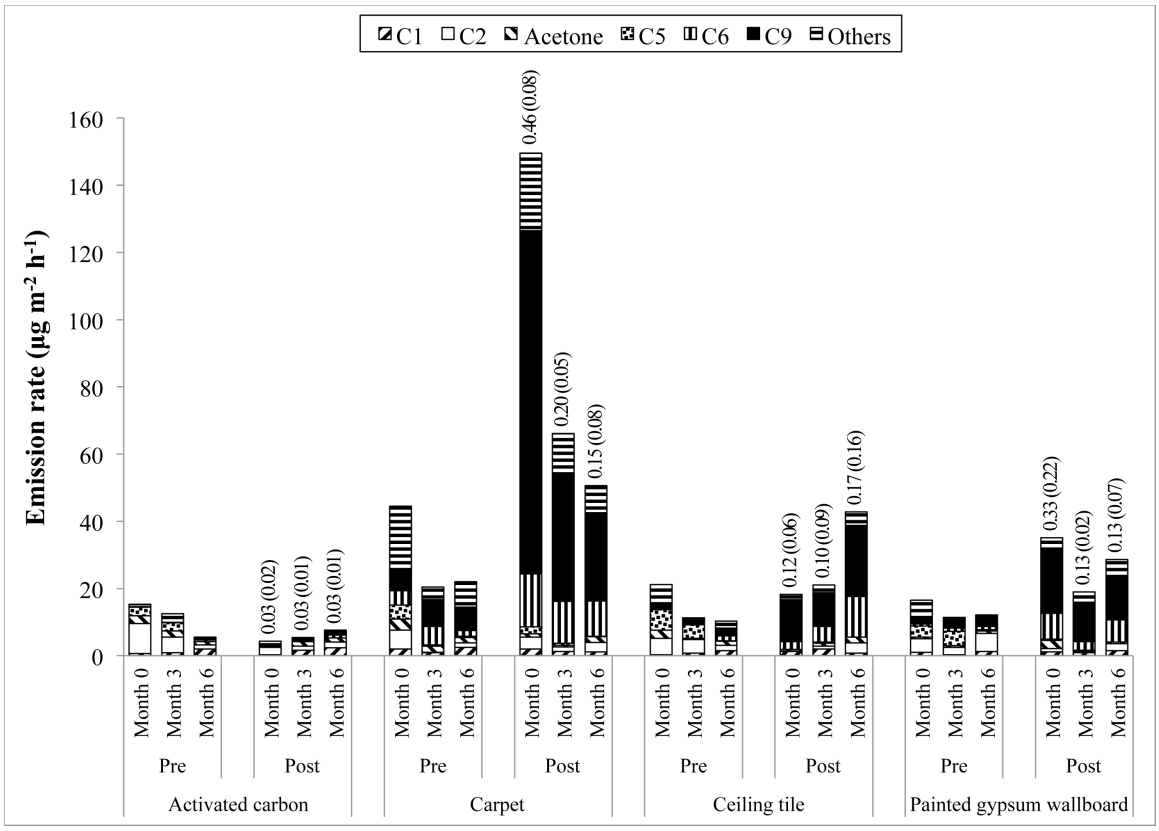

Figure 5. Emission rates for select carbonyl compounds averaged over all locations (Pre = pre-ozonation, Post = post-ozonation, mean carbonyl mass yields are presented at the top of each post-ozonation bar with standard deviation in parenthesis).

Overall carbonyl mass yields were calculated by summing the mass emission rates of all carbonyls and normalizing by the mass uptake rate of O_3. Yields (μg carbonyls / μg O_3 removed) varied from 0.01 to 0.61, 0.01 to 0.27 and 0.01 to 0.43 for measurements made at months 0, 3 and 6 respectively. The highest yields were observed for carpet, followed by painted gypsum wallboard, ceiling tile and activated carbon.

Pre-ozonation emissions were relatively consistent across locations. Greater variations were observed in post-ozonation emissions, possibly because of differences in environmental conditions, including soiling, at each field location. Over all locations post-ozonation emission rates from carpet were the highest, followed by ceiling tile, painted gypsum wallboard and finally activated carbon. As such, it appears that since the results are averaged over all locations, where all materials were placed, the nature of the material itself contributes significantly to the extent of post-ozonation emissions that will be produced. Nevertheless, samples placed in the bedroom and kitchen had noticeably higher post-ozonation emission rates than other locations. This result suggests that material soiling also affects post-ozonation emissions.

Results for pre and post-ozonation emissions at the kitchen location for all four materials are shown in Figure 6. The pre-ozonation emissions for this location did not exhibit particular trends compared to other locations. However, the post-ozonation emissions were unique to this location (results for other locations are presented in online Supporting Information). Activated carbon, ceiling tile and painted gypsum wallboard each exhibited increased overall post-ozonation emission rates over time for test materials placed in the kitchen. The ceiling tile was especially affected, with overall post-ozonation emission rates after six months that increased sixty five times compared to the initial test. Post-ozonation emission rates for painted gypsum wallboard doubled in six

months while post-ozonation emission rates for activated carbon remained very low but increased by a factor of five. One possible explanation for these results is that O_3 reacts with compounds emitted during cooking events that rise in hot cooking plumes and reach elevated materials, but that do not condense appreciably on floor materials. Vegetable cooking oils contain unsaturated fatty acids, such as oleic acid, that react with O_3 to form several oxygenated compounds including aldehydes (Sadowska, 2008). Such interactions have been observed in simulated cooking events by Wang et al. (2005) who showed increased emission rates of heavy aldehydes, especially hexanal and nonanal, from kitchen surfaces. Similar interactions between O_3 and compounds emitted during cooking events and adsorbed or condensed onto materials could explain the post-ozonation emissions observed during laboratory tests in this study. The results tend to validate this hypothesis as materials that were set on shelves high above the floor show a similar trend of increased post-ozonation emission rates. Carpet does not exhibit a strong increase of post-ozonation by-product emissions after three months. It is possible that lower amounts of unsaturated fatty acids from cooking activities were deposited on carpet, or that increases in reactivity from such deposition was offset by the otherwise lowering in reactivity of the carpet.

To a lesser extent, similar interactions between O_3 and skin oils might have occurred in the bedroom location where occupants spend approximately a third of their lives. Unsaturated fatty acids from human skin lipids have been shown to react with O_3 to produce acetone, among other by-products (Wisthaler et al., 2011). On average, acetone emission rates were highest for materials placed at the bedroom field site.

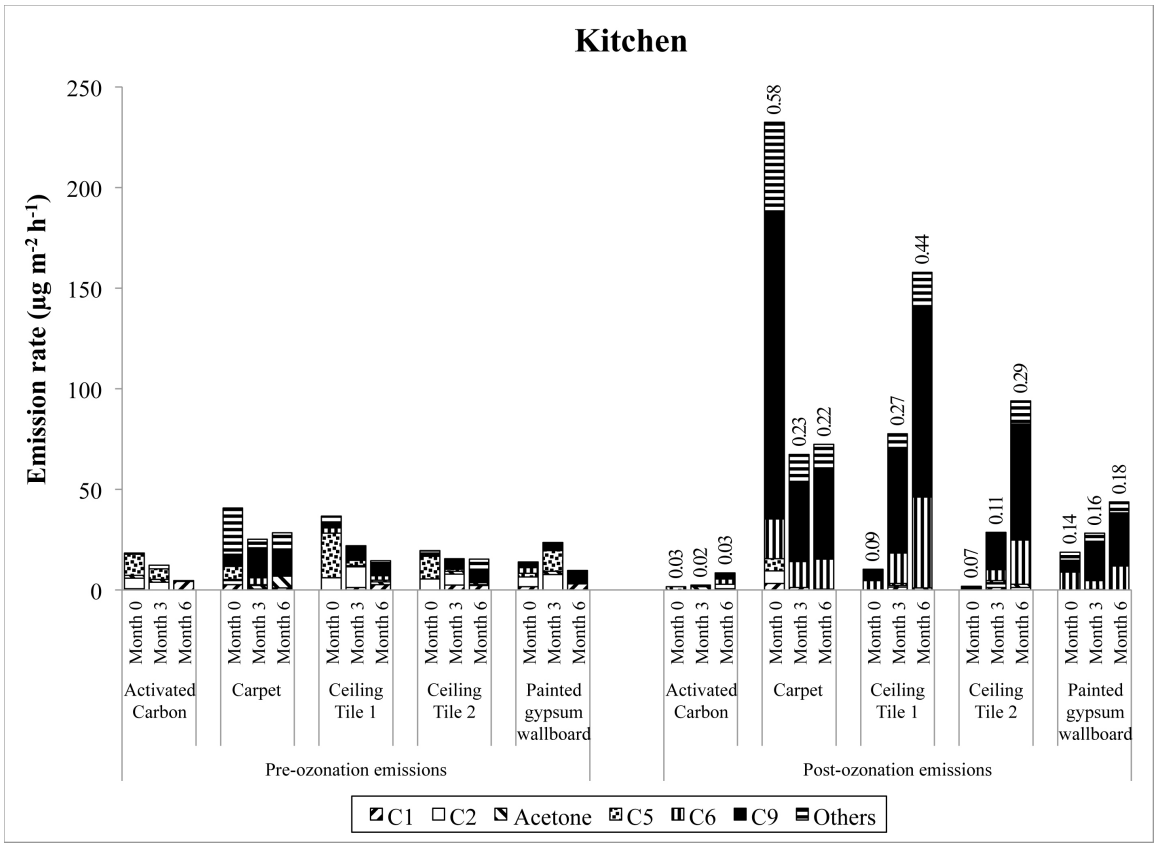

Figure 6. Carbonyl emission rates for samples from the Kitchen location (mean carbonyl mass yields are presented at the top of each post-ozonation bar).

Association with environmental parameters

Environmental parameters (temperature, RH, dustiness, TVOCs) were measured each month at field locations where material samples were installed. Single variable associations were determined using linear correlations between an environmental parameter and either O_3 deposition velocity, pre or post-ozonation carbonyl emission rates.

For all parameters measured in the field, the associations between field conditions and O_3 deposition velocities were weak, with R^2 less than 0.2 for most combinations of

environmental parameter and material. Only one correlation was found to be statistically significant: a weak positive correlation ($R^2 = 0.32$, $p < 0.05$) was observed for O_3 deposition on carpet versus VOC abundance in air at field locations.

Pre-ozonation emission rates from activated carbon had a weak but statistically significant positive association with field dustiness and temperature (R^2 values of 0.33 and 0.32, respectively, p-values < 0.01). Pre-ozonation emission rates from carpet were also positively associated with monthly VOC abundance and mean RH (R^2 values of 0.43 and 0.26 respectively, p-values < 0.05). Pre-ozonation emission rates for other materials did not exhibit a significant association (p-values greater than 0.05) with any environmental parameter.

All three green building materials exhibited strong positive associations between post-ozonation emission rates and VOC abundance in air at field sites, with R^2 of 0.50, 0.65, 0.75 for ceiling tile, painted gypsum wallboard and carpet, respectively (p-values < 0.01). Carpet also exhibited a relatively strong positive association ($R^2 = 0.55$, $p < 0.001$) between post-ozonation emission rates and RH. Post-ozonation emission rates from activated carbon did not exhibit any significant association (p-values were all above 0.05) with variations in environmental conditions. The association between increased post-ozonation emission rates and increased organic compounds in air at field sites may be due to reactive gases, e.g., unsaturated organic compounds, adsorbing to materials at field sites and reacting with O_3 during ozonation of test chambers. Additional research is warranted to further explore and understand this association, as it might be an important consideration with respect to application of PRMs in environments with high VOC concentrations.

CONCLUSIONS AND FUTURE RESEARCH

Activated carbon, perlite-based ceiling tile, recycled carpet and painted gypsum wallboard can be used to passively remove O_3 for six months and likely more, with sustained O_3 reactivity, although the deposition velocity of carpet and painted gypsum wallboard decreased by approximately 30% over six months. Painted gypsum board likely has little benefit with respect to reductions in O_3 exposure. Further, post-ozonation emission rates from carpet are sufficiently high as to preclude its use as an effective PRM. Of the materials tested in this study both activated carbon and perlite-based ceiling tile are the most promising PRMs.

The choice and placement of PRMs should be considered in relation to the type of indoor environment that they would be used in, since certain indoor environments influence O_3 deposition velocity or carbonyl emission patterns. PRMs could also be chosen according to the sensitivity to air pollution of the population occupying the building. Materials specifically designed for air purification, such as activated carbon mat, could be used around sensitive populations while more common materials such as ceiling tiles would be preferred in other settings.

This study is the first to explore the potential for long-term application of PRMs at actual field sites. Results of the study are encouraging and support the potential for sustained performance of PRMs in real buildings.

ACKNOWLEDGEMENTS

The authors thank Dr. Neil Crain, Elliott Gall, Erin Darling, Alix Broadfoot and Seth Lamble for their help during experiments. The project was funded by the United States Green Building Council grant 00021625 and by the Norm Hackerman Advanced

Research Program, Texas Higher Education Coordinating Board grant 003658-0279-2007.

REFERENCES

Bell, M.L., Dominici, F. and Samet, J.M. (2005). A meta-analysis of time-series studies of ozone and mortality with comparison to the national morbidity, mortality and air pollution study, *Epidemiology*, 16, 436-445.

Bell, M.L., Peng, R.D. and Dominici, F. (2006). The exposure-response curve for ozone and risk of mortality and the adequacy of current ozone regulations, *Environmental Health Perspectives*, 114, 532-536.

Bekö, G., Clausen, G. and Weschler, C.J. (2008). Sensory pollution from bag filters, carbon filters and combinations, *Indoor Air*, 18, 27-36.

Bekö, G., Fadeyi, M.O., Clausen, G. and Weschler, C.J. (2009). Sensory pollution from bag-type fiberglass ventilation filters: conventional filters compared with filters containing various amounts of activated carbon, *Building and Environment*, 44, 2114-2120

Cano-Ruiz, J.A., Kong, D., Balas, R.B. and Nazaroff, W.W. (1993). Removal of reactive gases at indoor surfaces: combining mass transport and surface kinetics, *Atmospheric Environment*, 27A, 2039-2050.

Clausen, P.A. and Wolkoff, P. (1996). Degradation products of Tenax TA formed during sampling and thermal desorption analysis: indicators of reactive species indoors, *Atmospheric Environment*, 31, 715-725.

Dusenbury, J.S. and Cannon, F.S. (1996). Advanced oxidant reactivity pertaining to granular activated carbon beds for air pollution control, *Carbon*, 34, 1577-1589.

Gall, E.T., Corsi, R.L., Siegel, J.A. (2011). Barriers and opportunities for passive removal of indoor ozone. *Atmospheric Environment*. Accepted for publication 11 March 2011.

Grøntoft, T. (2002). Dry deposition of ozone on building materials. Chamber measurements and modelling of the time-dependent deposition, *Atmospheric Environment*, 36, 5661-5670.

Hoang, C.P., Kinney, K.A. and Corsi, R.L. (2009). Ozone removal by green building materials, *Building and Environment*, 44, 1627-1633.

Hoang, C.P. (2009). Chemistry and microbiology of green building materials, Ph.D. dissertation, Department of Civil, Architectural and Environmental Engineering, The University of Texas at Austin, Texas, USA.

Jerrett, M., Burnett, R.T., Pope, C.A., Ito, K., Thurston, G., Krewski, D., Shi, Y., Calle, E. and Thun, M. (2009). Long-term ozone exposure and mortality, The New England Journal of Medicine, 360, 1085-1095.

Kleindienst, T.E., Corse, E.W. and Blanchard, F.T. (1998). Evaluation of the performance of DNPH-coated silica gel and C_{18} cartridges in the measurement of formaldehyde in the presence and absence of ozone, *Environmental Science and Technology*, 32, 124-130.

Klenø J.G., Clausen, P.A., Weschler, C.J. and Wolkoff, P. (2001). Determination of ozone removal rates by selected building products using the FLEC emission cell, *Environmental Science and Technology*, 35, 2548-2553.

Klepeis, N.E., Nelson, W.C., Ott, W.R., Robinson, J.P., Tsang, A.M., Switzer, P., Behar, J.V., Hern, S.C., and Engelmann, W.H. (2001). The National Human Activity Pattern Survey (NHAPS): a resource for assessing exposure to environmental pollutants, *Journal of Exposure Analysis and Environmental Epidemiology*. 11:231-252.

Kunkel, D.A., Gall, E.T., Siegel, J.A., Novoselac, A., Morrison, G.C. and Corsi, R.L. (2010). Passive reduction of human exposure to indoor ozone, *Building and Environment*, 45, 445-452.

Levy, J.I., Carrothers, T.J., Tuomisto, J.T., Hammitt, J.K. and Evans, J.S. (2001). Assessing the public health benefits of reduced ozone concentrations, *Environmental Health Perspectives*, 109, 1215-1226.

McDonnell, W.F., Abbey, D.E., Nishino, N. and Lebowitz, M.D. (1999). Long-term ambient ozone concentration and the incidence of asthma in nonsmoking adults: the Ashmog study, *Environmental Research*, 80, 110-121.

Metts, T.A. and Batterman, S.A. (2006). Effect of VOC loading on the ozone removal efficiency of activated carbon filters, *Chemosphere*, 62, 34-44.

Morrison, G.C. and Nazaroff, W.W. (2000). The rate of ozone uptake on carpet: experimental studies, *Environmental Science and Technology*, 34, 4963-4968.

Morrison, G.C. and Nazaroff, W.W. (2002). Ozone interactions with carpet: secondary emissions of aldehydes, *Environmental Science and Technology*, 36, 2185-2192.

Morrison, G.C., Zhao, P. and Kasthuri, L. (2006). The spatial distribution of pollutant transport to and from indoor surfaces, *Atmospheric Environment*, 40, 3677-3685.

Nicolas, M., Ramalho, O. and Maupetit, F. (2007). Reactions between ozone and building products: impact on primary and secondary emissions, *Atmospheric Environment*, 41, 3129-3138.

Novoselac, A., Siegel, J.A. (2009). Impact of placement of portable air cleaning devices in multizone residential environments, *Building and Environment*, 44, 2348-2356.

Pellizzari, E., Demian, B. and Krost, K. (1984). Sampling of organic compounds in the presence of reactive inorganic gases with Tenax TA, *Analytical Chemistry*, 56, 793-798.

Poppendieck, D., Hubbard, H., Ward, M. and Corsi, R.L. (2005). Building disinfection by-products (BDBPs): experimental evaluation and decision tool - Volume 2: ozone final test report, The University of Texas at Austin, USA.

Poppendieck, D., Hubbard, H., Ward, M., Weschler, C. and Corsi, R.L. (2007a). Ozone reactions with indoor materials during building disinfection, *Atmospheric Environment*, 41, 3166-3176.

Poppendieck, D., Hubbard, H., Ward, M., Weschler, C. and Corsi, R.L. (2007b). Formation and emissions of carbonyls during and following gas-phase ozonation of indoor materials, *Atmospheric Environment*, 41, 7614-7626.

Sadowska, J., Johansson, B., Johannessen, E., Friman, R., Broniarz-Press, L. and Rosenholm, J.B. (2008). Characterization of ozonated vegetable oils by spectroscopic and chromatographic methods, *Chemistry and Physics of Lipids*, 151, 85-91.

Shair, F.H. (1981). Relating indoor pollutant concentrations of ozone and sulfur dioxide to those outside: economic reduction of indoor ozone through selective filtration of the make-up air, *ASHRAE Transactions*, 87, 116-139.

Shields, H.C., Weschler, C.J., Naik, D. (1999). Ozone removal by charcoal filters after continuous extensive use (5 to 8 years). In: *Proceedings of the 8th International Conference on Indoor Air Quality and Climate*, vol. 4, pp. 49-54.

U.S. EPA. (2006). Air Quality Criteria for Ozone and Related Photochemical Oxidants (Final), EPA/600/R-05/004aF-cF. Washington, DC:US Environmental Protection Agency.

Walker, I., Sherman, M., Nazaroff, W. (2010). Ozone reductions using residential building envelopes. CEC-500-2009-101. Berkeley, CA: Lawrence Berkeley National Laboratory.

Wang, H., Springs, M. and Morrison, G. (2005). Ozone initiated secondary emissions of aldehydes from indoor surfaces, *Proceedings of the Air and Waste Association's annual conference*, number 1232, AWMA, Pittsburgh, PA, 2005.

Wang, H. and Morrison, G.C. (2006). Ozone-initiated secondary emissions rates of aldehydes from indoor surfaces in four homes, *Environmental Science and Technology*, 40, 5263-5268.

Wang, H. and Morrison, G.C. (2010). Ozone surface reactions in five homes: surface reaction probabilities, aldehyde yields, and trends, *Indoor Air*, 20, 224-234.

Waring, M.S., Siegel, J.A. (2011). The effect of an ion generator on indoor air quality in a residential room. *Indoor Air*, accepted for publication 9 October 2010.

Weschler, C.J. (2000). Ozone in indoor environments: concentration and chemistry, *Indoor Air*, 10, 269-288.

Weschler, C.J. (2004). New directions: ozone-initiated reaction products indoors may be more harmful than ozone itself, *Atmospheric Environment*, 38, 5715-5716.

Weschler C.J. (2006). Ozone's impact on public health: contributions from indoor exposures to ozone and products of ozone-initiated chemistry, *Environmental Health Perspectives*, 114, 1489-1496.

Wisthaler, A. and Weschler, C. (2010). Reactions of ozone with human skin lipids: sources of carbonyls, dicarbonyls, and hydroxycarbonyls in indoor air, *Proceedings of the National Academy of Sciences*, 107, 6568-6575.

Appendix D

Paper 4: Clement J. Cros, Atila Novoselac, Richard L. Corsi. Screening model to assess the use of indoor and outdoor reactive materials for lowering indoor levels of ozone and oxides of nitrogen. Ready for submission to *Building and Environment*.

ABSTRACT

Ozone (O_3) and oxides of nitrogen (NO_x) are pollutants mostly originating outdoors but because of the large fraction of time people spend inside buildings, most inhalation exposure to these pollutants occurs indoors. Both O_3 and nitrogen dioxide (NO_2) have been associated with a wide range of adverse health effects. Finding new, innovative ways to remove these pollutants from indoor air could have beneficial health effects. Passive removal materials (PRMs) have been studied for their long-term capacity to remove pollutants through surface reactions, with the advantage of not requiring additional energy input during operation. This paper uses a multi-zone model coupled with a computational fluid dynamics (CFD) model to estimate the possible reductions in indoor concentrations of O_3, NO and NO_2 that could be obtained through the use of indoor PRMs and a combination of both indoor and outdoor PRMs. The model shows that indoor PRMs have the potential to reduce indoor concentrations of NO_2 and O_3 (reductions up to 23 % and 18 %, respectively) while NO is not removed as efficiently. Incremental concentration reductions estimated with the addition of outdoor PRMs are much smaller (less than or equal to 2 % for all pollutants) and make the use of this solution for a detached building less attractive.

1. INTRODUCTION

Nitrogen oxides (NO_x) and ozone (O_3) are inter-related pollutants originating mostly outdoors. Nitrogen oxides are products of combustion processes taking place in power production facilities, industries and road vehicles [1] and are present at elevated levels in most urban areas. They are precursors to the formation of O_3 [2] through photochemical processes. Exposure to O_3 and nitrogen dioxide (NO_2) has been associated

with a range of adverse health effects ranging from decrease of respiratory functions [3-9], onset of asthma [10-12] and cardiovascular events [13-15]. In the absence of indoor sources, levels of these pollutants are usually lower indoors than outdoors [16,17]. However, since people in developed countries spend most of their time indoors [18], a large fraction of people's inhalation exposure to these pollutants of outdoor origin occurs indoors. Weschler [19] estimated that about half of the U.S. population's exposure to O_3 happens indoors. Similarly, Levy et al. [17] noted that personal exposures to NO_x were more strongly correlated to indoor concentrations than outdoor concentrations. When indoor sources of these pollutants, such as gas-stoves for NO_x [20] or certain types of air cleaners for O_3 [21], are present, the fraction of exposure occurring indoors is even higher.

Finding innovative ways to remove these pollutants from the indoor air could have beneficial health effects. Conventional strategies for reducing pollutant levels indoors include source control, ventilation and use of active engineered systems (e.g. devices integrated in the HVAC system or portable air cleaners). The first two strategies are not viable for pollutants mainly originating outdoors. The third strategy could be applied but often involves a tradeoff associated with increased energy use. The use of existing building surfaces indoors has long been investigated as a way to passively remove pollutants [22,23] with a recent focus on O_3 [24-27]. Inside buildings, the surface-to-volume ratio is large, which is an advantage for passive removal through building materials as it increases opportunities for removal of molecules onto surfaces.

Similarly, the façade of a building could be used in order to remove pollutants from air as it travels along the façade before entering the building through openings. The use of outdoor surfaces has been investigated for passive removal of NO_x by

photocatalytic materials [28-32]. These materials contain a semiconductor that, once activated by UV light, can catalyze water molecules adsorbed at the material surface to form hydroxyl radicals [33]. Hydroxyl radicals can in turn react with NO_x molecules adsorbed at the material surface [34]:

$$NO_{ads} + OH^{\bullet} \rightarrow HNO_2 \quad (1)$$

$$HNO_2 + OH^{\bullet} \rightarrow NO_{2,ads} + H_2O \quad (2)$$

$$NO_{2,ads} + OH^{\bullet} \rightarrow NO_{3,ads}^{-} + H^{+} \quad (3)$$

Through a modeling effort, this paper estimates possible reductions in NO_x and O_3 levels inside a model building through the use of indoor and outdoor passive removal materials (PRMs).

Several simulation models of the indoor environment are available and CONTAM is a well-validated tool (National Institute of Standards and Technology, Gaithersburg, MD, USA). CONTAM is a multi-zone airflow and contaminant transport analysis software that has been used to model tracer gas concentrations [35] and effectiveness of air cleaners [36], for example. Pollutant deposition to building materials can also be modeled through appropriate inputs in CONTAM, but deposition occurring on the outside of the building cannot. Computational fluid dynamics (CFD) modeling was used to overcome this issue. Tominaga et al. [37] studied dispersion of pollutants around a simple cubic structure using a small computational domain and well-defined wind conditions in the vicinity of the building. They showed that 2-equation k-ε turbulence models could provide results in general agreement with measured data for pollutant dispersion around a simple building structure. With respect to deposition of pollutants to

surfaces, Rim et al. [38] developed a method to determine concentrations in the vicinity of a reactive surface by adjusting concentrations obtained through CFD modeling for a perfect sink surface.

Surface deposition of reactive species is typically modeled through the use of deposition velocity [39]:

$$R = v_d c A \tag{4}$$

where R is the removal rate of the pollutant to a surface (μg h^{-1}), v_d is the deposition velocity of the pollutant to a surface (m h^{-1}), c is the bulk air concentration of the pollutant above a surface (μg m^{-3}) and A is the area of the surface on which the pollutant is depositing (m^2).

The deposition velocity is defined as the flux of pollutant to a surface divided by its concentration in the bulk air above the surface [39]:

$$v_d = \frac{J}{c} \tag{5}$$

where J is the flux of pollutant to a surface (μg h^{-1} m^{-2}), and all other variables are as previously described.

The inverse of the deposition velocity can also be expressed as an overall resistance to heterogeneous reactions and is equal to the sum of two resistances [39]: the transport resistance, which is a function of fluid dynamics conditions over the surface and the surface resistance, which is a function of reactive interactions between the surface and the pollutant.

$$\frac{1}{v_d} = r_t + r_s = \frac{1}{v_t} + \frac{4}{\gamma < v >} \quad (6)$$

where r_t is the transport limited resistance (h m^{-1}), r_s is the surface resistance (h m^{-1}), v_t is the transport-limited deposition velocity (m h^{-1}), γ is the reaction probability (-), and $<v>$ is the Boltzman velocity (m h^{-1}).

In the study presented herein, a test house at the University of Texas campus was used as model building to estimate possible reductions in NO_x and O_3 levels through the use of PRMs both indoors and outdoors. Multi-zone and CFD models were coupled in order to estimate reductions in indoor concentrations of pollutants.

2. METHODS

2.1. Modeling approach

The modeling approach used for this study is presented in Figure 1. Experimental data from a previous study by Lo et al. [40] were used to determine properties of the approach wind and to define boundary conditions for the simulation domain. Airflow around the house façade was modeled using CFD and validated by experimental data. Finally, data obtained for outdoor conditions were used as inputs to the indoor multi-zone model of the house in CONTAM.

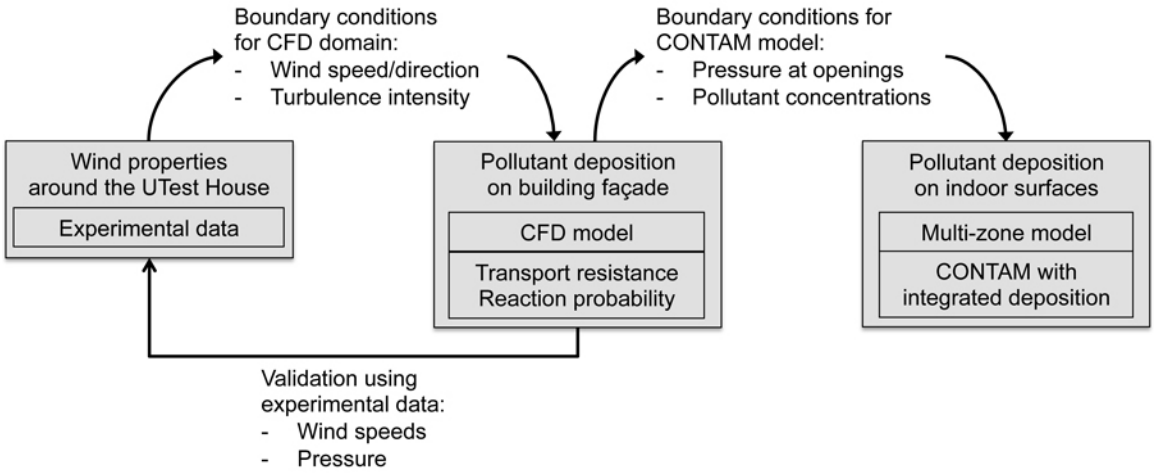

Figure 1. Modeling approach

2.2. Model building and passive removal materials

The building used for this study was the UTest House of the University of Texas campus, in Austin, TX, USA, described in detail in [40]. It is a 120 m^2 manufactured home equipped with pressure sensors on its façade and wind sensors in its vicinity (Figure 2) and is used as a test building for indoor environmental quality studies. It is oriented in the North-South direction. For the purpose of this model, the house was modeled as having two bedrooms, two bathrooms, an office and a kitchen/living area.

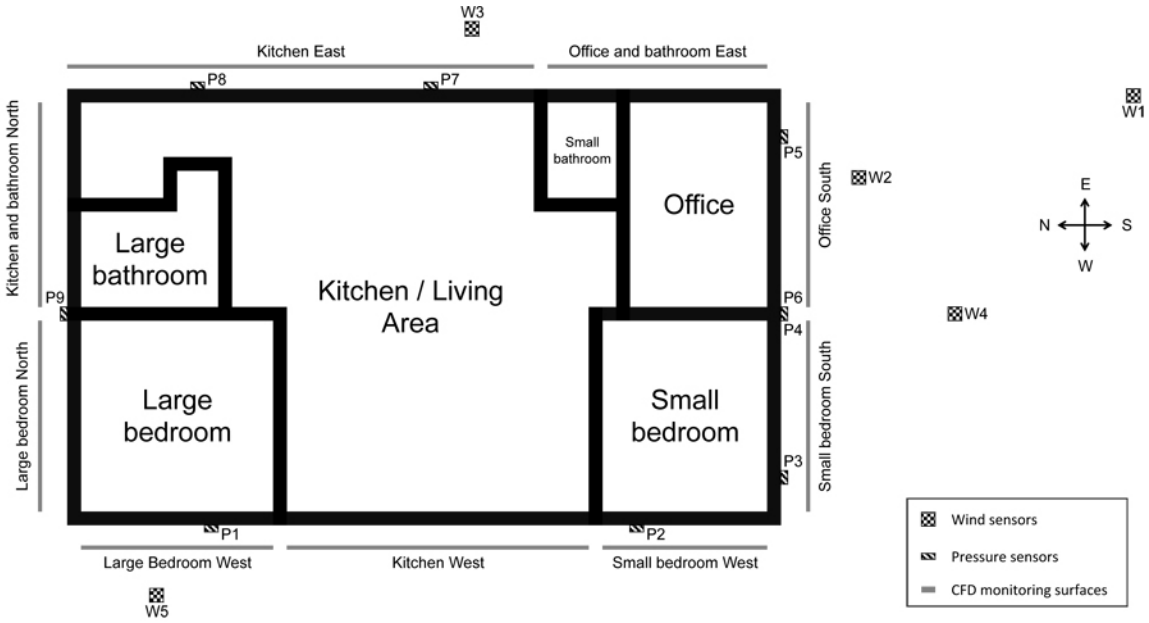

Figure 2. UTest House and location of pressure and wind velocity sensors

The model simulated the use of PRMs inside and on the façade of the model building. The indoor PRMs included in the model were an activated carbon mat, made of a non-woven polyester-based fabric (thickness = 0.5 cm) coated with AC (area normalized mass = 136 g m^{-2}) and a green ceiling tile made of 100 % recyclable materials and marketed as having no VOCs or man-made mineral fibers. Both these materials were previously tested for O_3 removal as described in [27], and for NO and NO_2 removal as described in Supplementary Materials. Deposition velocities for realistic indoor air conditions [27] were determined through laboratory testing and used for modeling purposes. The outdoor PRM included in this study was a photocatalytic stucco, composed of portland cement, admixtures and 4.98 % TiO_2 by mass of solids, mainly in the anatase form, described in more details by Cros et al. [30]. Reaction probabilities of each pollutant with the photocatalytic stucco in the environmental conditions used for the

model were determined from data collected during the experimental program described by Cros et al. [30] and analyzed as described in Supplementary Materials.

2.3. Modeling conditions and scenarios

The model was run for specific outdoor wind conditions that had been monitored during a previous experimental investigation by Lo et al. [40] at the UTest House. Wind speed and pressure data around the UTest House were collected during experiments by Lo et al. [40] and were used in this modeling effort to validate CFD airflow results. The case considered an approach wind velocity (recorded at sensor W1 on Figure 2) of 7.9 m s^{-1} measured 4 m above the ground, with an azimuth angle of 163°. The wind profile power law ($\alpha = 0.125$ [40]) was used to determine the approach wind velocity at various heights. Wind velocity data at sensor W1 (Figure 2) was also used to determine the turbulence intensity of the incoming air flow.

Three scenarios including different amounts of PRMs were modeled and compared. Scenario 0 was a base case scenario where no PRMs were installed, either indoors or outdoors. Scenario 1 included indoor PRMs only while Scenario 2 used a combination of both indoor and outdoor PRMs. The amounts of PRMs used for each scenario are presented in Table 1. For indoor PRMs, ceiling tiles were chosen for all bedrooms and the office but not the kitchen because of possibly large ozone-initiated emissions observed for this material in a kitchen location [27]. Activated carbon mat was placed in the kitchen instead. The bathrooms were not equipped with PRMs. The stucco included in this study was chosen as outdoor PRM because it exhibited a good capacity to remove NO_x and O_3 in laboratory experiments and weathered outdoor exposure well [41].

Table 1. Description of PRMs installations for each scenario

<table>
<tr><th></th><th>AC mat</th><th>Ceiling tiles</th><th>Photocatalytic stucco</th></tr>
<tr><td>Scenario 0</td><td>None</td><td>None</td><td rowspan="2">None</td></tr>
<tr><td>Scenario 1</td><td rowspan="2">Covers half of the ceiling of the kitchen/living area. Total area: 23 m^2</td><td rowspan="2">Covers the ceiling of all three bedrooms. Total area: 36 m^2</td></tr>
<tr><td>Scenario 2</td><td>Covers all four exterior walls. Total area: 160 m^2</td></tr>
</table>

Relative pollutant concentration reductions between two scenarios were calculated as follows:

$$R_{i,j} = 100\times\left(1-\frac{c_i}{c_j}\right) \quad (7)$$

where $R_{i,j}$ is the relative pollutant concentration reduction in scenario i relative to scenario j (%), c_i and c_j are the average pollutant concentrations over a day in scenario i and j, respectively (ppb).

2.4. Modeling of outdoor concentrations infiltrating into the building

2.4.1. CFD model of the UTest House

Outdoor concentrations of NO, NO_2 and O_3 in the vicinity of the house walls were modeled using CFD analysis and heterogeneous deposition theory. The CFD simulation used the Reynolds Averaged Navier-Stokes Equations (RANS) with the two-layer Realizable k-ε turbulence model for steady-state calculations. The CFD model was developed using the commercially available ANSYS Fluent 12.1 code and run on a computer with 4 core processors at 3.06 GHz and running on a Windows 7 operating

system. The validity of the model was tested by comparing model results to experimentally measured data from Lo et al. [40].

The mesh used in this study was composed of 500,000 tetrahedral cells. The cells closest to the house façade were 5 mm deep, with a growth factor of 1.2 for the first five layers of cells adjacent to the façade. Grid independence was investigated by comparing simulated pressures and wind speeds between the mesh used and one with cells twice as coarse at the façade boundary and in the vicinity of the façade.

The study domain was a rectangular prism with dimensions 40 m × 30 m × 15 m with the UTest House at its center. The size of the computational domain was chosen so that properties of the approach wind would not be simulated through CFD but rather implemented at the boundary conditions from experimentally measured data. The south and east faces of the computational domain were set with velocity inlet boundary conditions. Turbulence intensity at these boundaries was implemented using the value determined from experimental data (see section 2.3). The west and north faces were set with pressure outlet boundary conditions. The top face of the computational domain (sky) was set with a symmetry boundary condition and the bottom face of the domain (ground) was set with a wall boundary condition. Domain independence was investigated as well by comparing simulated pressures and wind speed between the domain used and a domain with dimensions 150 m × 40 m × 35 m.

Monitoring surfaces and points were used in the CFD model to calculate scalars related to this investigation. Monitoring points were placed at locations corresponding to the pressure and wind sensors used in experimental data acquisition (Figure 2). Control surfaces corresponding to the rooms inside the house were placed on the UTest House

façade. These surfaces were used to extract simulated pollutant concentrations on the façade.

2.4.2. Ambient outdoor conditions

Ambient outdoor pollutant concentrations were defined for three conditions: morning (from 8 am to 12 pm), afternoon (from 2 pm to 6 pm) and night (from 8 pm to 6 am). Ambient outdoor concentrations between these periods were linearly interpolated. Morning and afternoon conditions were defined as explained in [30] with NO = 150 ppb and NO_2 = 20 ppb for the morning condition and NO_2 = 50 ppb and O_3 = 150 ppb for the afternoon condition. The nighttime condition was determined by taking the average of nighttime concentrations of all three pollutants (between 8 pm and 6 am) as measured in Houston, TX for the months of August and September 2009 [42]. The nighttime condition was adjusted to NO = 5 ppb, NO_2 = 15 ppb, O_3 = 15 ppb. During the nighttime condition, the photocatalytic stucco was assumed to be non-reactive since UV light was absent.

2.4.3. Inclusion of outdoor PRM in CFD model

In order to determine concentrations of pollutants in the vicinity of the UTest House façade, deposition of pollutants to the house façade coated with a photocatalytic stucco needed to be integrated in the model. A two-step process was used.

First, the CFD model was run with the house façade assumed to be a perfect sink for the pollutants studied. In that case, only the effect of pollutant transport limitations to the surface was simulated, since surface resistance was zero. Pollutant concentrations in the vicinity of the perfect sink façade (first layer of cells adjacent to the façade) were determined for each section of the façade (Figure 2) through the CFD model. Average

free stream velocities above each section of the façade were determined as well through the CFD model. Simulated velocities were used to estimate the average transport-limited deposition velocities for each façade section using mass transfer correlations reported by Morrison et al. [43] for turbulent flow over a flat plate.

Secondly, concentrations in the vicinity of the façade calculated in the case of a perfect sink façade had to be adjusted for the actual photocatalytic stucco coating, which is not a perfect sink for O_3, NO and NO_2. The method described by Rim et al. [38] was utilized and the actual concentration in the vicinity of the façade was determined as:

$$c_{actual} = \left(\frac{4v_t}{4v_t + \langle v_b \rangle \gamma}\right) c_{bulk} + \left(\frac{\langle v_b \rangle \gamma}{4v_t + \langle v_b \rangle \gamma}\right) c_{perfect} \qquad (8)$$

where c_{actual} is the pollutant concentration in the vicinity of the façade with the outdoor PRM present (ppb), c_{bulk} is the pollutant concentration in the bulk air (ppb), $c_{perfect}$ is the pollutant concentration in the vicinity of the façade when it is considered to be a perfect sink for the pollutant (ppb), $<v_b>$ is the pollutant Boltzmann velocity (m h^{-1}), γ is the pollutant reaction probability with the outdoor PRM (-), v_t is the pollutant transport-limited deposition velocity on the façade (m h^{-1}).

In the morning condition, concentration of NO_2 had to be adjusted differently. In effect, in the morning condition, experiments conducted to determine NO_x removal by the photocatalytic coating showed that a fraction of the NO oxidized on the photocatalytic surface was converted to NO_2 rather than the expected final product, nitric acid. It is possible that, during the photocatalytic oxidation process presented in equations (1) through (3), some adsorbed NO_2 molecules formed during the second step of the process (equation 2) could not be oxidized further and desorbed into the air. The NO_2 yield for

the morning conditions used in this study is $y_{NO2} = 0.24$ moles of NO_2 formed per mole of NO reacted. Hence, in the morning condition, NO_2 concentration is calculated as:

$$c_{NO2,m,actual} = c_{NO2,bulk} + 0.24 \times \left(c_{NO,bulk} - c_{NO,m,actual}\right) \quad (9)$$

where $c_{NO2,m,actual}$ is the NO_2 concentration in the morning condition in the vicinity of the façade with the outdoor PRM present (ppb), $c_{NO2,bulk}$ is the NO_2 concentration in the bulk air (ppb), $c_{NO,m,actual}$ is the NO concentration in the morning condition in the vicinity of the façade with the outdoor PRM present (ppb), $c_{NO,bulk}$ is the NO concentration in the bulk air (ppb)

2.5. Modeling of indoor concentrations

2.5.1. Multi-zone model

Indoor concentrations of NO, NO_2 and O_3 inside the UTest House were modeled using CONTAM3.0 software developed by the National Institute of Standards and Technology (NIST). The house was modeled through 3 levels: crawl space, living space and attic. Infiltration into and leakage between the various zones of the house were modeled using flow paths with characteristics obtained for a manufactured home from Persily and Martin [44].

Outdoor air concentrations at each opening were used as inputs to the CONTAM model. By adjusting outdoor air concentration at openings, it was possible to take into account the absence or presence of the photocatalytic stucco on the UTest House façade. For scenarios 0 and 1, pollutant concentrations at each opening were equal to the ambient air concentrations. For scenario 2, the average pollutant concentration calculated for each section of the UTest House façade (section 2.4) was used for all openings located on that

section of the façade in the CONTAM model. Similarly, pressure values at each opening determined through CFD modeling were used as input for the CONTAM model.

The model was run for two consecutive and identical days. The first day was used to obtain reasonable initial concentrations by the beginning of day 2. Results presented in this paper used concentration data obtained for day 2 only.

A very simple occupancy scenario of the house was implemented. Occupants were assumed to be in the house until 8 am in the morning and come back by 6 pm. An HVAC schedule was implemented to take into account effects of air recirculation and changes in indoor/outdoor air exchange rate due to HVAC operation. It was assumed that no pollutant removal occurred in the HVAC system, a reasonable assumption for ozone and likely for NO_x [45,46]. The HVAC was off during the night, when occupants were sleeping, and during the day, when occupants were assumed to be away from the house. The HVAC was on for ten minutes at 7 am after occupants woke up and then was on for ten minutes every thirty minutes from 6 pm to 11 pm.

2.5.2. Deposition to indoor surfaces

Removal of pollutants to the background (existing materials, before inclusion of PRMs) was modeled using sink elements characterized by a deposition velocity. Deposition velocities to background surfaces for O_3 and NO_x were determined using literature values for O_3 decay rates in homes reported by Lee et al. [47] and NO_x decay rates in a home reported by Wade et al. [48]. Decay rates correspond to $v_{d,background} \times A_{whole\ house}/V_{whole\ house}$, where $v_{d,background}$ is the average pollutant deposition velocity to background surfaces ($m\ h^{-1}$), $A_{whole\ house}$ is the total area of indoor surfaces (m^2), $V_{whole\ house}$ is the total air volume in the house (m^3). For this study, the surface-to-volume

ratio in the house ($A_{whole\ house}/V_{whole\ house}$) was assumed to be 3 m^{-1} [49,50]. By multiplying the decay rate to background surfaces (values of 2.8 h^{-1}, 0.06 h^{-1}, 0.83 h^{-1} for O_3, NO and NO_2, respectively) by the inverse of the surface-to-volume ratio, the values of average deposition velocities of O_3, NO and NO_2 to background surfaces were determined for inclusion in the model, and are presented in Table 2.

Table 2. Deposition velocities of O_3, NO and NO_2 to indoor surfaces included in the model

	O_3	NO	NO_2
$v_{d,background}$ (m h^{-1})	0.93	0.02	0.28
$v_{d,ceiling\ tile}$ (m h^{-1})	2.69	0.12	0.48
$v_{d,activated\ carbon}$ (m h^{-1})	3.39	0.92	3.20

Indoor PRMs were modeled as sinks for scenarios 1 and 2, and their removal capacity was described using experimentally measured deposition velocities for O_3, NO and NO_2 as described in section 2.1. Deposition velocities to indoor PRMs used in this model are also presented in Table 2.

3. RESULTS AND DISCUSSION

3.1. Validation of CFD model

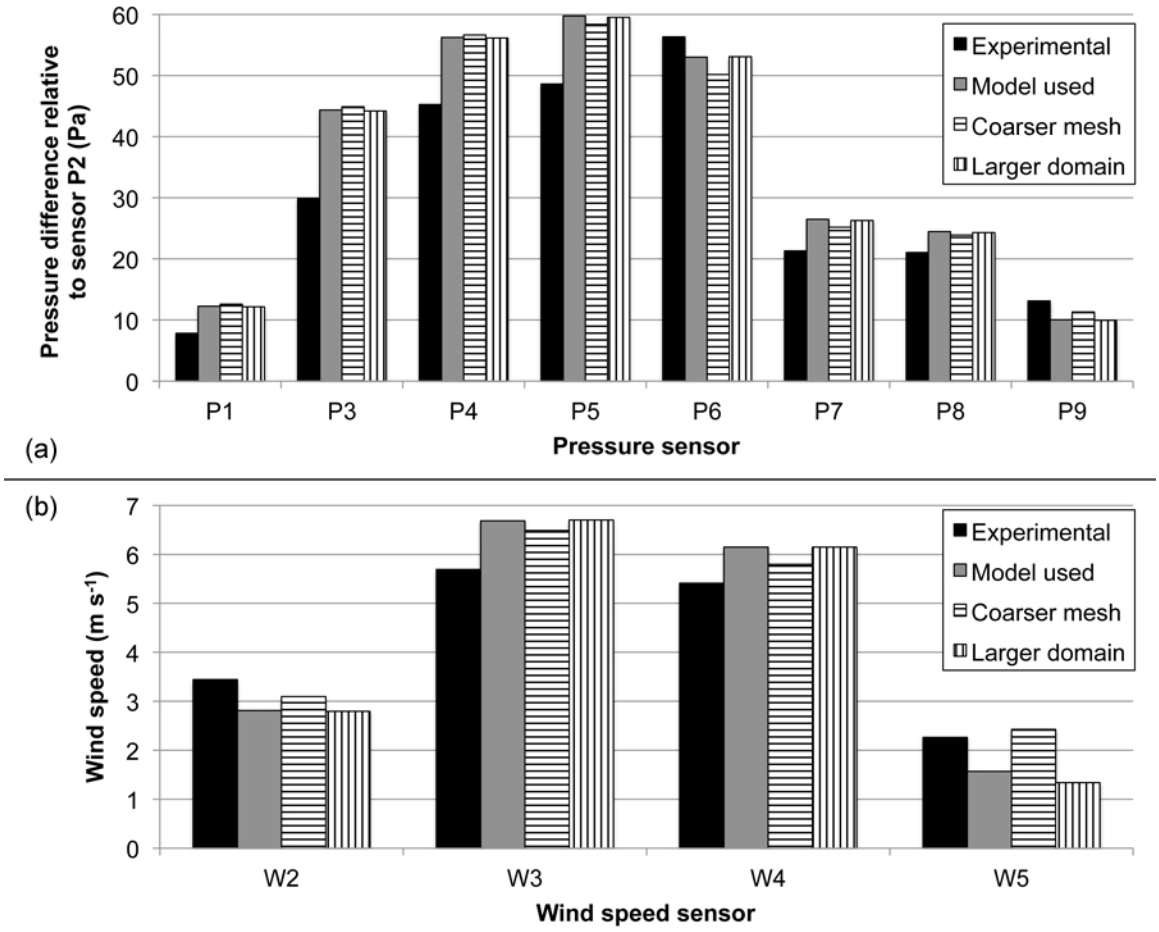

Figure 3. Pressure (a) and wind speed (b) simulation results compared to experimental measurements

Results of the wind velocity and pressure simulation are presented in Figure 3. Pressure results are presented relative to a reference point (pressure sensor P2). In effect, experimentally measured pressures were measured as outdoor/indoor pressure differences while modeling results were absolute pressures. Results show that there is fairly good agreement between the experimentally measured data and the wind velocity and pressure estimates obtained through CFD simulation. The model captures important features of the airflow around the house. Moreover, results obtained through the use of a coarser mesh or

larger simulation domain are also consistent with results obtained using a finer mesh and smaller computational domain suggesting that grid independence and domain independence are verified.

3.2. Outdoor wall concentrations estimates with photocatalytic stucco

Transport limited deposition velocities calculated for each section of the UTest House façade are presented in Table 2. Free stream velocity above each wall section was obtained from the CFD model and used to calculate v_t using mass transfer correlations as described in section 2.4.3. Differences in transport-limited deposition velocities for each gas were due to differences in their diffusivity in air.

Table 3. Transport-limited deposition velocities for the sections of the UTest House façade

	$v_{t,O3}$ (m h^{-1})	$v_{t,NO}$ (m h^{-1})	$v_{t,NO2}$ (m h^{-1})
Office South	12.4	14.5	11.5
Small bedroom South	21.8	25.4	20.2
Small bedroom West	14.9	17.4	13.8
Kitchen West	13.4	15.6	12.4
Large bedroom West	11.5	13.4	10.7
Large bedroom North	7.1	8.3	6.6
Kitchen North	9.4	11.0	8.7
Kitchen East	28.9	33.8	26.8
Office and bathroom East	28.7	33.6	26.7

In an unpublished study conducted within the framework of a previous experimental program [51], Poppendieck et al. measured transport-limited deposition velocity of O_3 on the UTest House façade. They found O_3 transport-limited deposition velocities in the range of 5 m h^{-1} to 20 m h^{-1}, similar to O_3 transport-limited velocities estimated here.

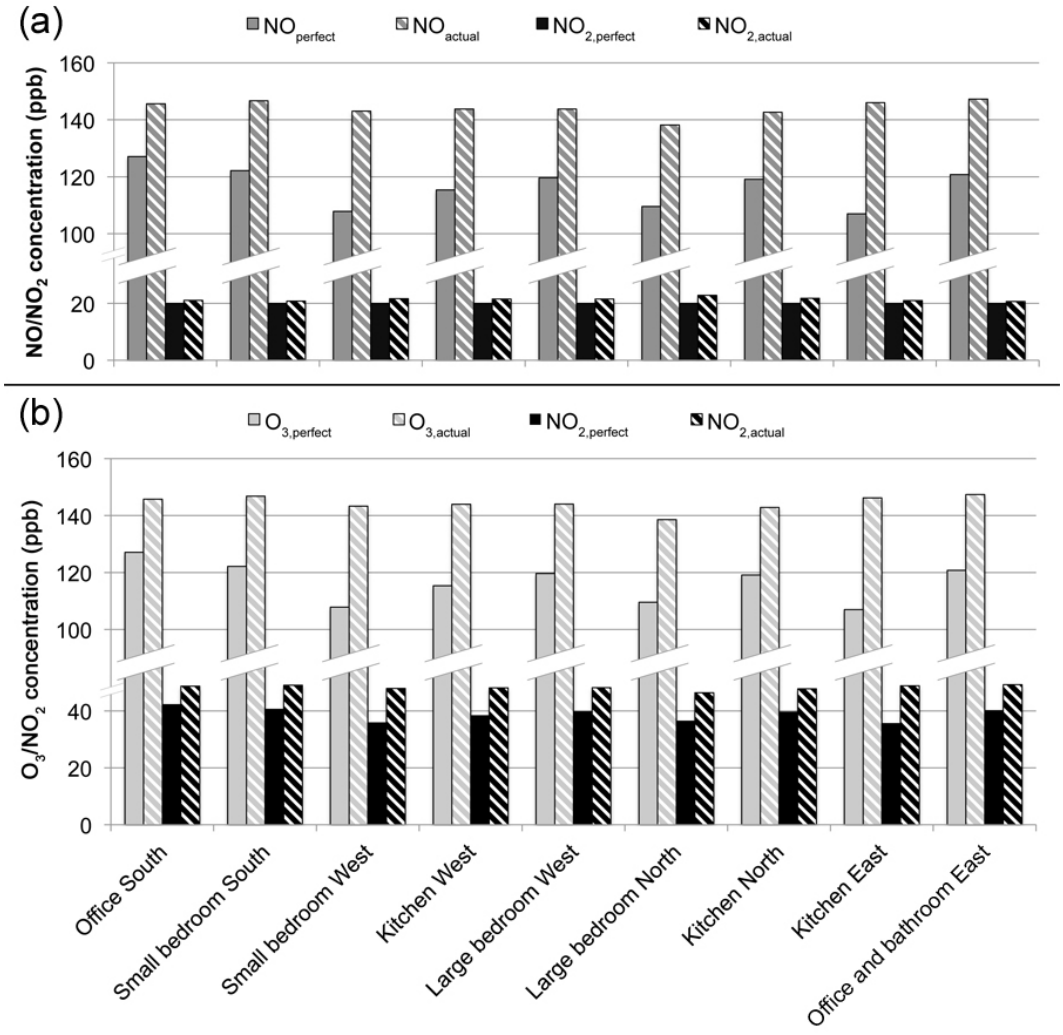

Figure 4. Pollutant concentrations in the vicinity of the UTest House façade in (a) the morning condition, (b) the afternoon condition

Estimated concentrations of pollutants in the vicinity of the UTest House façade for a perfect sink and adjusted for the presence of the photocatalytic stucco are presented in Figure 4. In the case for which the UTest House façade was considered to be a perfect sink, pollutant concentrations in the vicinity of the façade were 15 % to 29 % lower than ambient pollutant concentrations. Taking into account the surface resistance to deposition

of the photocatalytic stucco, actual pollutant concentrations in the vicinity of the façade were 7 % to 15 % lower than ambient concentrations. Formation of NO_2 during the photocatalytic oxidation of NO in the morning condition led to small increases in NO_2 concentrations in the vicinity of the façade, for the morning condition only. Absolute NO_2 concentration increases ranged from 0.7 to 2.8 ppb. Despite some NO_2 being formed in the morning, overall NO_x concentrations in the vicinity of the façade were lower than ambient concentrations.

Reductions observed on the windward side of the house (South and East walls) were generally lower than reductions obtained on the leeward side (North and West walls). It is possible that lower air speeds on the leeward side of the house allowed more time for reaction between pollutant molecules and the reactive surface to take place. Moreover, a fraction of the air on the leeward side of the house might have come in contact with the reactive surface while traveling along the building façade.

Moussiopoulos et al. [52] reported NO_x concentration reductions of up to 60 % in the vicinity of walls covered with a photocatalytic material in an experimental street canyon, much higher than reductions estimated in this study. The street canyon configuration offers a much higher surface-to-volume ratio for reaction and lower air speeds that might explain the higher reductions observed.

3.3. Comparison of scenario results

Results of the CONTAM simulation are presented in Figure 5 and Figure 6. The figures show average concentration reductions over the course of a day. Comparison between scenario 1 (indoor PRMs only) and 0 (no PRMs) indicates that indoor PRMs can effectively reduce indoor concentrations of O_3 and NO_2 (Figure 5). Overall, the largest

reductions in pollutant concentrations were observed in the leeward rooms of the house. It is possible that, since pressures were higher on the windward side of the house and lowest on the leeward side, the overall air movement inside the house was in the same direction as outdoors. Hence, a portion of the air present in the leeward rooms of the house had traveled through other rooms where it encountered PRMs and pollutants could be reacted away, explaining the lower concentrations observed on the leeward side.

Reduction in NO_2 concentration for the entire house was 18 % with reductions in the rooms of the house varying from 4 % to 23 %. Reductions ranged from 9 % to 23 % in rooms outfitted with PRMs. The largest reduction was obtained in the kitchen location, outfitted with activated carbon. Deposition of NO_2 to activated carbon was very high compared to other surfaces indoors: NO_2 deposition velocity to activated carbon was eleven and six times higher than to background surfaces and perlite-based ceiling tile, respectively. This explains why, even though only half the ceiling of the kitchen/living area was covered with activated carbon versus the entire ceiling for rooms outfitted with perlite-based ceiling tiles, this was the room that experienced the highest reduction in NO_2 concentration.

Reductions in O_3 concentration in the rooms of the house varied between 2 % and 18 % with reductions ranging from 13 % to 18 % in rooms equipped with PRMs. Overall O_3 concentration reduction for the house was 13 %. For comparison, this overall O_3 concentration reduction could be obtained by continuously operating an air cleaner with 100 % O_3 removal efficiency and an airflow of 120 $m^3 h^{-1}$. Differences in deposition velocities on the various indoor surfaces were smaller for O_3 than for NO_2. Deposition velocity of ozone to activated carbon was only 3.6 and 1.3 times higher than to background surfaces and perlite-based ceiling tile. For that reason, O_3 concentration

reduction in the kitchen/living area equipped with activated carbon on half of its ceiling was smaller than in other rooms equipped with PRMs on the entire ceiling. The reductions estimated in this study are lower than concentration reductions estimated by Gall et al. [25] using activated carbon or gypsum wallboard as PRMs. They used values of deposition velocities determined in experimental conditions offering better transport of air to the material surface and are valid when materials are strategically placed inside homes to take advantage of surfaces experiencing low transport-resistance.

Finally, reduction in NO concentration for the entire house was 6 % with reductions in the rooms of the house varying from 0.3 % to 8 %. Reductions ranged from 2 % to 8 % in rooms equipped with PRMs. Reductions are smaller than for the other pollutants studied here because NO is less reactive with building materials. However, O_3 and NO_2 are the most potent pollutants considered in this study in terms of health effects. Their efficient removal by the indoor PRMs makes this solution attractive from a health standpoint.

Relative pollutant concentration reductions between scenarios 2 (indoor and outdoor PRMs) and 1 (indoor PRMs only) are presented in Figure 6. Relative changes observed between scenarios 2 and 1 are much smaller than changes observed between scenarios 1 and 0. Incremental concentration reductions for NO, NO_2 and O_3 over scenario 1 range from 0.1 % to 2.0 %. It appears that outdoor PRMs do not have as good a potential for reducing occupants' inhalation exposure to pollutants from outdoor origin as indoor PRMs. Not only are reductions in outdoor concentrations small but, because outdoor air mainly penetrates the house on the windward side, it is not possible to take advantage of the lower pollutant concentrations obtained through photocatalysis on the

leeward side of the house, unless mechanical ventilation with an outdoor intake of air is used.

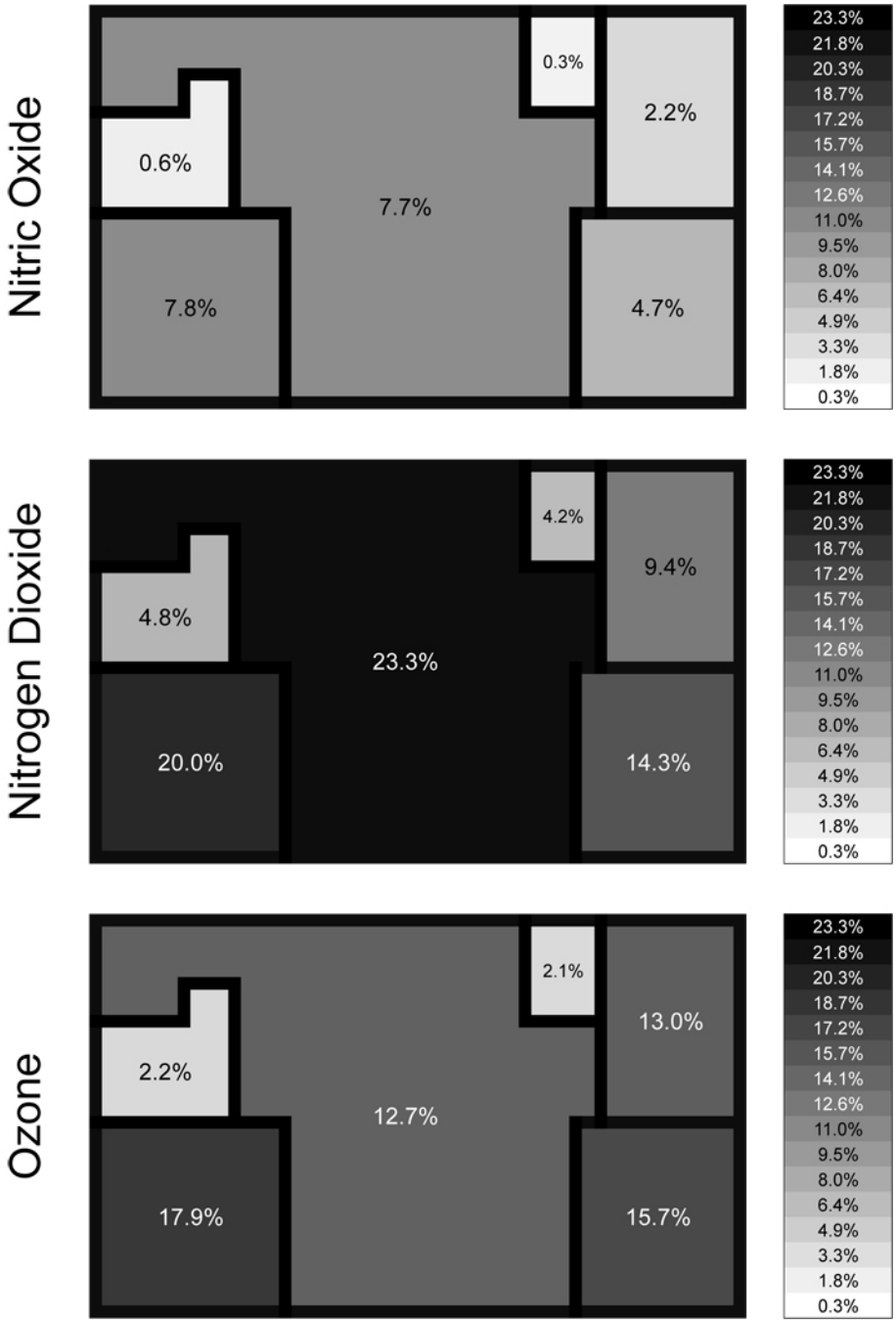

Figure 5. Relative change in whole day average room concentrations in scenario 1 (indoor PRMs only) relative to scenario 0 (no PRMs).

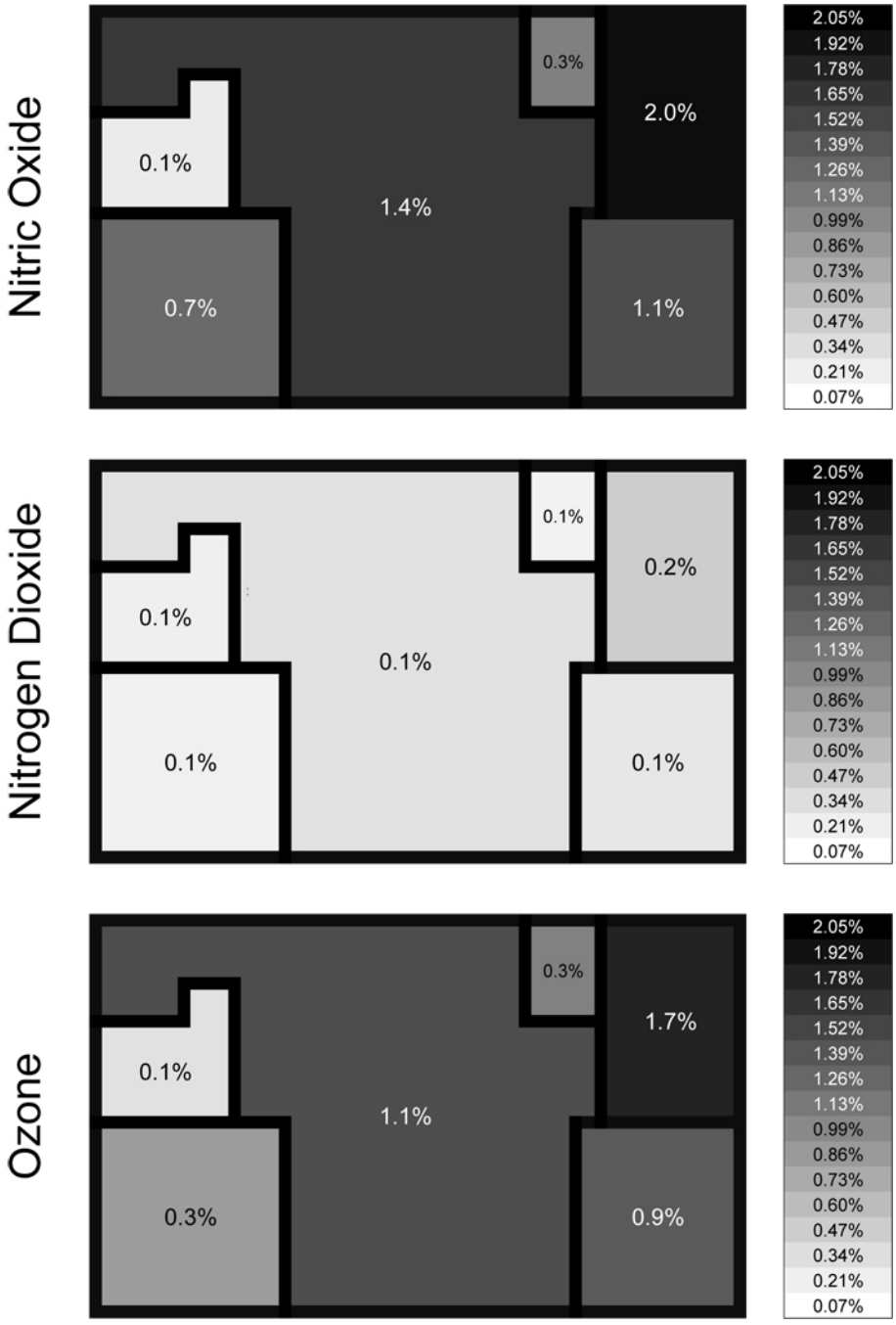

Figure 6. Relative change in whole day average room concentrations in scenario 2 (indoor and outdoor PRMs) relative to scenario 1 (indoor PRMs only).

4. Conclusion

The model presented in this paper estimated possible reductions in indoor NO_x and O_3 concentrations through the use of PRMs placed on both indoor and outdoor building surfaces. Indoor PRMs, perlite-based ceiling tiles and activated carbon mat, proved to be efficient at reducing indoor levels of O_3 and NO_2, with reductions in indoor concentrations of up to 18 % and 23 %, respectively. Reductions in indoor NO levels were smaller. Application of an outdoor PRM, a photocatalytic stucco, on the outside of the model house did not appreciably change indoor levels of any of the three pollutants studied. Other urban structures such as street canyons, might benefit more from outdoor PRM installation because of more favorable airflow conditions.

5. Acknowledgements

The authors would like to thank Priscilla Guerrero for her help in creating the CONTAM model of the UTest House.

6. References

[1] EPA, National Emissions Inventory (NEI) Air Pollutant Emissions Trends Data, Office of Air Quality Planning and US EPA Standards, 2011.

[2] J.H. Seinfeld, S.N. Pandis, Atmospheric Chemistry and Physics, Second edition, Wiley-Interscience, 2006.

[3] J.I. Levy, T.J. Carrothers, J. Tuomisto, J. Hammitt, J. Evans, Assessing the public health benefits of reduced ozone concentrations, Environ. Health Perspect. 109 (2001) 1215.

[4] W.M. Foster, D.L. Costa, E.G. Langenback, Ozone exposure alters tracheobronchial mucociliary function in humans, J. Appl. Physiol. 63 (1987) 996–1002.

[5] J.R. Balmes, L.L. Chen, C. Scannell, I. Tager, D. Christian, P.Q. Hearne, et al., Ozone-induced decrements in FEV1 and FVC do not correlate with measures of inflammation, Am. J. Respir. Crit. Care Med. 153 (1996) 904–909.

[6] R.B. Devlin, W.F. McDonnell, R. Mann, S. Becker, D.E. House, D. Schreinemachers, et al., Exposure of humans to ambient levels of ozone for 6.6 hours causes cellular and biochemical changes in the lung, Am. J. Respir. Cell Mol. Biol. 4 (1991) 72–81.

[7] M.A. Bauer, M.J. Utell, P.E. Morrow, D.M. Speers, F.R. Gibb, Inhalation of 0.30 ppm nitrogen dioxide potentiates exercise-induced bronchospasm in asthmatics, Am. Rev. Respir. Dis. 134 (1986) 1203–1208.

[8] V. Mohsenin, Airway responses to nitrogen dioxide in asthmatic subjects, J. Toxicol. Environ. Health. 22 (1987) 371–380.

[9] M.W. Frampton, P.E. Morrow, C. Cox, F.R. Gibb, D.M. Speers, M.J. Utell, Effects of nitrogen dioxide exposure on pulmonary function and airway reactivity in normal humans, Am. J. Respir. Crit. Care Med. 143 (1991) 522.

[10] W.F. McDonnell, D.E. Abbey, N. Nishino, M.D. Lebowitz, Long-term ambient ozone concentration and the incidence of asthma in nonsmoking adults: the AHSMOG Study, Environ. Res. 80 (1999) 110–121.

[11] W.J. Gauderman, E. Avol, F.W. Lurmann, N. Kuenzli, F. Gilliland, J. Peters, et al., Childhood asthma and exposure to traffic and nitrogen dioxide, Epidemiology. 16 (2005) 737–743.

[12] N.A. Clark, P.A. Demers, C.J. Karr, M. Koehoorn, C. Lencar, L. Tamburic, et al., Effect of early life exposure to air pollution on development of childhood asthma, Environ. Health Perspect. 118 (2009) 284–290.

[13] J.I. Halonen, T. Lanki, P. Tiittanen, J.V. Niemi, M. Loh, J. Pekkanen, Ozone and cause-specific cardiorespiratory morbidity and mortality, J. Epidemiol. Community Health. 64 (2010) 814–820.

[14] S. Cakmak, R. Dales, J. Leech, L. Liu, The influence of air pollution on cardiovascular and pulmonary function and exercise capacity: Canadian Health Measures Survey (CHMS), Environ. Res. 111 (2011) 1309–1312.

[15] A. Peters, E. Liu, R.L. Verrier, J. Schwartz, D.R. Gold, M.A. Mittleman, et al., Air pollution and incidence of cardiac arrhythmia, Epidemiology. 11 (2000) 11–17.

[16] C.J. Weschler, H.C. Shields, D.V. Naik, Indoor ozone exposures, Japca. 39 (1989) 1562–1568.

[17] J.I. Levy, Impact of residential nitrogen dioxide exposure on personal exposure: an international study, J. Air Waste Manage. Assoc. 48 (1998) 553–560.

[18] N.E. Klepeis, W.C. Nelson, W.R. Ott, J.P. Robinson, A.M. Tsang, P. Switzer, et al., The National Human Activity Pattern Survey (NHAPS), Lawrence Berkeley National Laboratory, 2001.

[19] C.J. Weschler, Ozone's impact on public health: contributions from indoor exposures to ozone and products of ozone-initiated chemistry, Environ. Health Perspect. 114 (2006) 1489–1496.

[20] J.D. Spengler, C.P. Duffy, R. Letz, T. Tibbitts, B.G. Ferris, Nitrogen dioxide inside and outside 137 homes and implications for ambient air quality standards and health effects research, Environ. Sci. Technol. 17 (1983) 164–168.

[21] M.S. Waring, J.A. Siegel, The effect of an ion generator on indoor air quality in a residential room, Indoor Air. 21 (2011) 267–276.

[22] J. Yu, Deactivation and regeneration of environmentally exposed titanium dioxide based products, Prepared for the environmental protection department, HKSAR, 2003.

[23] Y. Sekine, A. Nishimura, Removal of formaldehyde from indoor air by passive type air-cleaning materials, Atmos. Env. 35 (2001) 2001–2007.

[24] D.A. Kunkel, E.T. Gall, J.A. Siegel, A. Novoselac, G.C. Morrison, R.L. Corsi, Passive reduction of human exposure to indoor ozone, Build. Environ. 45 (2010) 445–452.

[25] E.T. Gall, R.L. Corsi, J.A. Siegel, Barriers and opportunities for passive removal of indoor ozone, Atmos. Env. 45 (2011) 3338–3341.

[26] E.K. Darling, C.J. Cros, P. Wargocki, J. Kolarik, G.C. Morrison, R.L. Corsi, Impacts of a clay plaster on indoor air quality assessed using chemical and sensory measurements, Build. Environ. 57 (2012) 370–376.

[27] C.J. Cros, G.C. Morrison, J.A. Siegel, R.L. Corsi, Long-term performance of passive materials for removal of ozone from indoor air, Indoor Air. 22 (2011) 43–53.

[28] S. Laufs, G. Burgeth, W. Duttlinger, R. Kurtenbach, M. Maban, C.E.S. Thomas, et al., Conversion of nitrogen oxides on commercial photocatalytic dispersion paints, Atmos. Env. 44 (2010) 2341–2349.

[29] H. Chen, C.E. Nanayakkara, V.H. Grassian, Titanium Dioxide Photocatalysis in Atmospheric Chemistry, Chem. Rev. 112 (2012) 5919–5948.

[30] C.J. Cros, A.L. Terpeluk, N.E. Crain, M.G. Juenger, R.L. Corsi, Influence of environmental factors on removal of oxides of nitrogen by a photocatalytic coating, Atmospheric Environment, in Press. (2013).

[31] G. Hüsken, M. Hunger, H.J.H. Brouwers, Experimental study of photocatalytic concrete products for air purification, Build. Environ. 44 (2009) 2463–2474.

[32] H. Dylla, M.M. Hassan, L.N. Mohammad, T. Rupnow, E. Wright, Evaluation of environmental effectiveness of titanium dioxide photocatalyst coating for concrete pavement, Trans. Res. Rec. 2164 (2010) 46–51.

[33] A. Fujishima, K. Honda, Electrochemical photolysis of water at a semiconductor electrode, Nature. 238 (1972) 37–38.

[34] M.M. Ballari, Q.L. Yu, H.J.H. Brouwers, Experimental study of the NO and NO_2 degradation by photocatalyticaly active concrete, Catal. Today. 161 (2011) 175–180.

[35] S.J. Emmerich, S.J. Nabinger, A. Gupte, C. Howard-Reed, L. Wallace, Comparison of measured and predicted tracer gas concentrations in a townhouse, NIST, Gathersburg, MD, USA, 2003.

[36] C. Howard-Reed, S.J. Nabinger, S.J. Emmerich, Measurement and simulation of the indoor air quality impact of gaseous air cleaners in a test house, in: Indoor Air 2002, Monterey, CA, USA, 2002: pp. 652–657.

[37] Y. Tominaga, T. Stathopoulos, Numerical simulation of dispersion around an isolated cubic building: Comparison of various types of k–ε models, Atmos. Env. 43 (2009) 3200–3210.

[38] D. Rim, A. Novoselac, G.C. Morrison, The influence of chemical interactions at the human surface on breathing zone levels of reactants and products, Indoor Air. 19 (2009) 324–334.

[39] J.A. Cano-Ruiz, D. Kong, R. Balas, W.W. Nazaroff, Removal of reactive gases at indoor surfaces: combining mass transport and surface kinetics, Atmos. Env. 27 (1993) 2039–2050.

[40] L.J. Lo, A. Novoselac, Cross ventilation with small openings: measurements in a multi-zone test building, Build. Environ. 57 (2012) 377–386.

[41] C.J. Cros, A.L. Terpeluk, N.E. Crain, R.L. Corsi, M.G. Juenger, Removal of oxides of nitrogen by photocatalytic coatings: influence of environmental parameters and outdoor exposure, Submitted to Construction and Building Materials. (2013).

[42] TCEQ, ed., Hourly air pollution data, (n.d.).

[43] G.C. Morrison, P. Zhao, L. Kasthuri, The spatial distribution of pollutant transport to and from indoor surfaces, Atmos. Env. 40 (2006) 3677–3685.

[44] A.K. Persily, S.R. Martin, A modeling study of ventilation in manufactured houses, NIST, Gaithersburg, MD, USA, 2000.

[45] P. Zhao, J.A. Siegel, R.L. Corsi, Ozone removal by HVAC filters, Atmos. Env. 41 (2007) 3151–3160.

[46] G.C. Morrison, W.W. Nazaroff, J.A. Cano-Ruiz, A.T. Hodgson, M.P. Modera, Indoor air quality impacts of ventilation ducts: ozone removal and emissions of volatile organic compounds, J. Air Waste Manage. Assoc. 48 (1998) 941–952.

[47] K. Lee, J. Vallarino, T. Dumyahn, H. Ozkaynak, J.D. Spengler, Ozone decay rates in residences, J. Air Waste Manage. Assoc. 49 (1999) 1238–1244.

[48] W.A. Wade, W.A. Cote, J.E. Yocom, A study of indoor air quality, J. Air. Pollut. Control Assoc. 25 (1975) 933–939.

[49] C.S. Mitchell, J. Zhang, T. Sigsgaard, M. Jantunen, P.J. Lioy, R. Samson, et al., Current State of the Science: Health Effects and Indoor Environmental Quality, Environ. Health Perspect. 115 (2007) 958–964.

[50] T.L. Thatcher, A.C.K. Lai, R. Moreno-Jackson, R.G. Sextro, W.W. Nazaroff, Effects of room furnishings and air speed on particle deposition rates indoors, Atmos. Env. 36 (2002) 1811–1819.

[51] D.G. Poppendieck, E.K. Darling, E. McDonald Buller, Y. Kimura, R.L. Corsi, Dry deposition of ozone to built environment surfaces, Center for Energy and Environmental Resources, University of Texas at Austin, 2011.

[52] N. Moussiopoulos, P. Barmpas, I. Ossanlis, J. Bartzis, Comparison of numerical and experimental results for the evaluation of the depollution effectiveness of photocatalytic coverings in street canyons, Environ. Model. Assess. 13 (2007) 357–368.

Supplementary Materials

S1. NO AND NO_2 REMOVAL BY INDOOR MATERIALS

S1.1. Methods

Deposition velocities of NO and NO_2 were measured for the activated carbon mat and ceiling tile selected for this study. The experimental system used by Cros et al. [1] was used, with some modifications:

- the ozone analyzer was replaced by a NO_x chemiluminescence analyzer (model 200E; Teledyne, Thousands Oaks, CA, USA),
- NO and NO_2 gases were obtained in cylinders (Praxair, Danbury, CT, USA) and introduced into the inlet air stream through mass flow controllers (Series FMA 5500; Omega Engineering, Inc., Stamford, CT, USA),
- only one test chamber was used.

Tests were run with and without materials inside the chamber to determine and separate deposition to both the chamber walls and the material sample. Inlet concentrations of NO or NO_2 were 150 ppb. Other test conditions were identical to conditions used for measurement of ozone deposition velocities by Cros et al. [1].

Each test was run until steady-state conditions were reached inside the reactor. Deposition velocity was calculated using a steady-state mass balance on the continuous flow reactor:

$$v_d = \frac{\lambda V}{A_s}\left(\frac{c_{inlet}}{c} - 1\right) - v_{d,w}\left(\frac{A_w}{A_s} - 1\right) \quad \text{(S1)}$$

where v_d is the pollutant deposition velocity on the material sample (m h^{-1}), λ is the air exchange rate of the chamber (h^{-1}), V is the volume of the chamber (m^3), A_w is the total area chamber walls (m^2), A_s is the horizontal projected area of the material sample (m^2), c_{inlet} is the inlet pollutant concentration (ppb), c is the pollutant concentration in the outlet of the chamber (ppb), and $v_{d,w}$ is the pollutant deposition velocity for the chamber walls (m h^{-1}).

S1.2. Results

Deposition velocities of NO and NO_2 on the selected indoor materials are presented in Table 1.

Table 1. Deposition velocities of NO and NO_2 on indoor PRMs

	$v_{d,NO}$ (m h^{-1})	$v_{d,NO2}$ (m h^{-1})
Ceiling tile	0.12	0.48
Activated carbon mat	0.92	3.2

S2. NO, NO_2 AND O_3 REMOVAL BY OUTDOOR MATERIALS

S2.1. Methods

The experimental system described in [2] was used to obtain the parameters necessary for inclusion of the photocatalytic stucco in the modeling effort. It was necessary to determine the reaction probability of O_3, NO and NO_2 with the selected stucco for the modeling conditions chosen. From Cano-Ruiz et al. [3], the reaction probability can be calculated as:

$$\gamma = \frac{4}{< v >}\left(\frac{1}{v_d} - \frac{1}{v_t}\right)^{-1} \quad \text{(S2)}$$

where γ is the pollutant reaction probability with the reactive surface (-), $<v>$ is the pollutant Boltzmann velocity (m h^{-1}), v_d is the pollutant deposition velocity on the reactive surface (m h^{-1}), v_t is the pollutant transport-limited deposition velocity on the reactive surface (m h^{-1}).

S2.2. Determination of the transport-limited deposition velocity in the test reactor

For each pollutant, the transport-limited deposition velocity is a function of the fluid mechanics inside the reactor, which were held constant for these experiments. The transport-limited deposition velocity in the reactor was calculated using ozone deposition to a highly reactive surface: concrete coated with a potassium iodide solution (125 mg KI / 100 mL distilled water). In this specific case, the surface resistance to the deposition of ozone on the material is assumed to be negligible so the transport resistance is the only resistance to deposition. In this case, the deposition velocity on the potassium iodide-coated concrete is:

$$\frac{1}{v_{d,O3,KI}} = \frac{1}{v_{t,O3}} + \frac{4}{< v_{O3} > \gamma_{O3,KI}} \qquad \lim_{\gamma_{O3,KI} \to 1} \frac{1}{v_{t,O3}} \quad \text{(S3)}$$

$v_{d,O3,KI}$ is the deposition velocity of ozone on the potassium iodide coated sample (m h^{-1}), $v_{t,O3}$ is the transport-limited deposition velocity of ozone in the reactor (m h^{-1}), $\gamma_{O3,KI}$ is the reaction probability of ozone with the potassium iodide coated sample (-), $<v_{O3}>$ is the Boltzmann velocity for ozone (m h^{-1}).

The deposition velocity of ozone on the potassium iodide coated concrete is determined using a mass balance on the well-mixed reactor:

$$v_{t,O3} = v_{d,O3,KI} = \frac{\lambda V_{sample}}{A_{sample}}\left(\frac{c_{O3,in,KI}}{c_{O3,KI}} - 1\right) - v_{d,O3,w}\frac{A_{w,sample}}{A_{sample}} \quad \text{(S4)}$$

λ is the testing reactor air exchange rate (h^{-1}), $c_{O3,in,KI}$ and $c_{O3,KI}$ are the ozone inlet and outlet concentrations, respectively, when testing the potassium iodide coated sample (ppb), V_{sample} is the air volume of the reactor in the presence of a concrete sample (m^3), A_{sample} is the projected area of the concrete sample tested (m^2), $A_{w,sample}$ is the area of exposed reactor walls in the presence of a concrete sample (m^2), $v_{d,O3,w}$ is the ozone deposition velocity to the chamber walls (m h^{-1}).

The measured value for the transport-limited deposition velocity of ozone in the reactor was used to estimate the transport-limited deposition velocities in the reactor for NO and NO_2 , $v_{t,NO}$ and $v_{t,NO2}$, respectively. Mass transfer correlations for gas flow above a flat plate were used to determine the relationship between $v_{t,O3}$ and $v_{t,NO}$ and $v_{t,NO2}$ [4]:

$$v_{t,NO} = \left(\frac{D_{NO}}{D_{O3}}\right)^{2/3} \times v_{t,O3} \quad \text{(S5)}$$

$$v_{t,NO2} = \left(\frac{D_{NO2}}{D_{O3}}\right)^{2/3} \times v_{t,O3} \quad \text{(S6)}$$

where D_{NO}, D_{NO2}, D_{O3} are the NO, NO_2 and O_3 diffusion coefficients, respectively (m^2 h^{-1}).

S2.3. Determination of the deposition velocity of ozone, NO and NO_2 on the photocatalytic stucco

Deposition velocities were calculated using a steady-state mass balance on the continuous flow reactor:

$$v_d = \frac{\lambda V_{sample}}{A_{sample}}\left(\frac{c_{in}}{c} - 1\right) - v_{d,w}\frac{A_{w,sample}}{A_{sample}} \quad \text{(S7)}$$

where v_d is the pollutant deposition velocity on the photocatalytic stucco (m h^{-1}), λ is the test reactor air exchange rate (h^{-1}), $v_{d,w}$ is the pollutant deposition velocity to the chamber walls (m h^{-1}), and all other variables are as previously described.

Using calculated values of v_d and v_t, γ could be calculated using equation (S2).

S2.4. Results

Reaction probabilities for O_3, NO and NO_2 with the photocatalytic stucco in the morning and afternoon conditions described in the model are presented in Table 2.

Table 2. Reaction probabilities for O_3, NO and NO_2 with the photocatalytic stucco in the model conditions

	Morning condition			Afternoon condition		
	O_3	NO	NO_2	O_3	NO	NO_2
Reaction probability	N/A	8.31×10^{-6}	N/A	8.59×10^{-6}	N/A	7.28×10^{-6}

S3. References

[1] C.J. Cros, G.C. Morrison, J.A. Siegel, R.L. Corsi, Long-term performance of passive materials for removal of ozone from indoor air, Indoor Air. 22 (2011) 43–53.

[2] C.J. Cros, A.L. Terpeluk, N.E. Crain, M.G. Juenger, R.L. Corsi, Influence of environmental factors on removal of oxides of nitrogen by a photocatalytic coating, Atmospheric Environment, in Press. (2013).

[3] J.A. Cano-Ruiz, D. Kong, R. Balas, W.W. Nazaroff, Removal of reactive gases at indoor surfaces: combining mass transport and surface kinetics, Atmospheric Environment. 27 (1993) 2039–2050.

[4] K. Asano, Mass Transfer: From Fundamentals to Modern Industrial Applications, Wiley-VCH, 2007.

Appendix E

PRACTICAL ASSESSMENT OF FEASIBILITY: PHOTOCATALYTIC ROAD BARRIERS/SOUND WALLS FOR REMOVAL OF NO_x FROM ROADWAYS

Methodology

Application of barriers/sound walls coated with a photocatalytic stucco was evaluated in a screening model in order to determine an order magnitude of possible removal of NO_x from roadways.

The model used a succession of well-mixed cells. Two scenarios were considered:

- Wind perpendicular to the roadway (Figure 1a)
- Wind parallel to the roadway (Figure 1b)

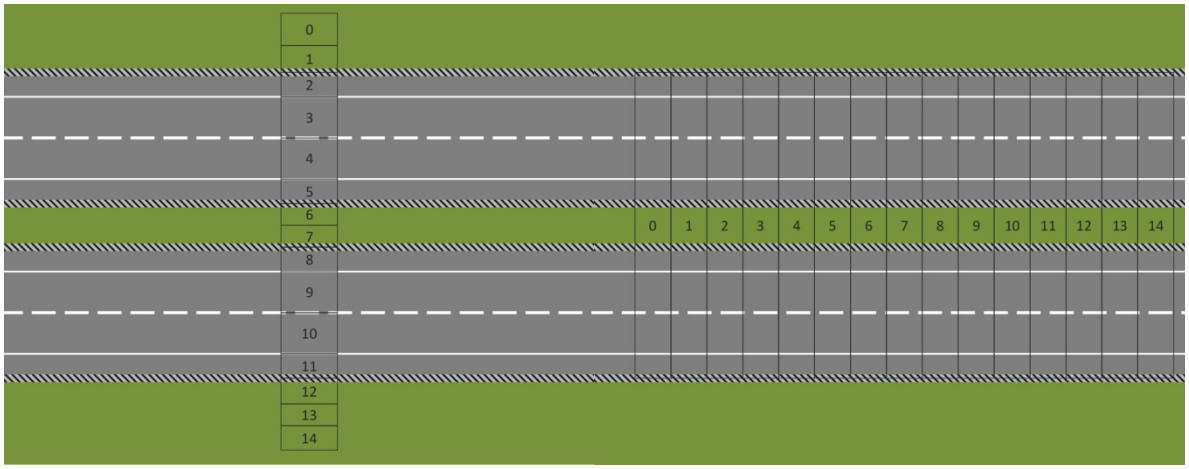

(a) (b)

Figure 1. Schematic of model set up for (a) perpendicular wind case (b) parallel wind case. Well-mixed cells used for the model are indicated.

Air was assumed to flow from one cell to the next only. Each cell is assumed to be at steady state and well mixed. The mixing height for the cells was taken from [104]. Both homogeneous and heterogeneous chemistry were taken into account. Deposition to

surfaces was modeled through the use of deposition velocities. A simple homogeneous chemistry model for O_3 and NO_x was used, as described by [105].

$$NO_2 \overset{k_1}{\rightarrow} NO + O$$

$$O_2 + O + M \overset{k_2}{\rightarrow} O_3 + M$$

$$NO + O_3 \overset{k_3}{\rightarrow} NO_2 + O_2$$

Assuming pseudo steady-state on O, $\frac{\partial[O]}{\partial t} = 0 \Rightarrow [O] = \left(\frac{k_1}{k_2}\right)\frac{[NO_2]}{[O_2][M]}$

For each cell, the following set of steady-state equations was used:

NO

$$0 = \lambda c_{NO,in} - \lambda c_{NO} + \frac{E_{NO}}{V} - v_{d,p,NO} c_{NO} \frac{A_p}{V} - v_{d,g,NO} c_{NO} \frac{A_g}{V} + k_1 c_{NO_2} - k_3 c_{NO} c_{O_3}$$

NO_2

$$0 = \lambda c_{NO_2,in} - \lambda c_{NO_2} + \frac{E_{NO_2}}{V} - v_{d,p,NO_2} c_{NO_2} \frac{A_p}{V} - v_{d,g,NO_2} c_{NO_2} \frac{A_g}{V} - k_1 c_{NO_2} + k_3 c_{NO} c_{O_3}$$

O_3

$$0 = \lambda c_{O_3,in} - \lambda c_{O_3} + \frac{E_{O_3}}{V} - v_{d,p,O_3} c_{O_3} \frac{A_p}{V} - v_{d,g,O_3} c_{O_3} \frac{A_g}{V} + k_1 c_{NO_2} - k_3 c_{NO} c_{O_3}$$

$c_{k,in}$ is the concentration of pollutant k at the cell inlet (ppb), c_k is the concentration of pollutant k in the cell (ppb), λ is the cell air exchange rate (hr^{-1}), E_k is the pollutant k emission rate inside the cell (g hr^{-1}), V is the cell volume (m^3), $v_{d,p,k}$ is the deposition velocity of pollutant k to the photocatalytic coating (m hr^{-1}), A_p is the surface of photocatalytic coating in the cell (m^2), $v_{d,g,k}$ is the deposition velocity of pollutant k to the ground (m hr^{-1}), A_g is the surface of ground in the cell (m^2).

The equations were solved sequentially for each cell until reaching the last cell of the model.

Emissions from vehicles traveling on the road were calculated using emission factors from McGaughey et al. [106] and traffic count from Wang et al. [104]. The traffic count is for a highway section in the vicinity of Austin, TX and that was used as the basis for the model set up. It was also the subject of other investigations for which a mixing height of 2.5 m was used over the roadway. This is the height that was used for the model cells. These numbers are representative for a highway in Texas. The emission factors may be somewhat lower today since improvements in engine efficiency of new vehicles have been made but the number used in the model are the most recent that could be found (2004).

The model was run for a best case scenario, in order to evaluate the feasibility of application of photocatalytic coating s for pollution reduction near roadways. Wind speed in the bulk air was taken to be only 1 m/s, leaving more time for pollutants to react with the photocatalytic surface. The walls covered with photocatalytic stucco were 2 m high offering more surface area for reaction. Deposition velocity of the pollutants to the photocatalytic coating was taken to be equal to the inverse of the surface resistance, hence assuming no transport resistance (in reality, the transport resistance would be low because of the high air speeds and turbulence near barrier surfaces due to the vehicular traffic on the road).

Results

The reduction estimates obtained through the modeling effort (Table 1) show fairly low overall removals for all pollutants, even in this best case scenario model. More realistic conditions would probably lead to actually lower removals. This suggests that

more detailed modeling of the airflow around road elements, and specifically the highway barriers, is not necessary.

Table 1. Results of the preliminary assessment of use of road barriers coated with a photocatalytic stucco for reduction of NO_x emissions from roadways

	Perpendicular wind			Parallel wind		
	NO	NO_2	O_3	NO	NO_2	O_3
Outlet concentrations with photocatalytic barriers (ppb)	214.3	191.4	21.7	982.9	261.2	5.5
Outlet concentration without barriers (ppb)	221.3	203.8	22.0	1026	286.5	5.8
Relative reduction (%)	3.14	6.10	1.56	4.22	8.83	4.49

References

[1] EPA, National Emissions Inventory (NEI) Air Pollutant Emissions Trends Data, Office of Air Quality Planning and US EPA Standards, 2011.

[2] J.H. Seinfeld, S.N. Pandis, Atmospheric Chemistry and Physics, Second edition, Wiley-Interscience, 2006.

[3] J.I. Levy, T.J. Carrothers, J. Tuomisto, J. Hammitt, J. Evans, Assessing the public health benefits of reduced ozone concentrations, Environ. Health Perspect. 109 (2001) 1215.

[4] W.M. Foster, D.L. Costa, E.G. Langenback, Ozone exposure alters tracheobronchial mucociliary function in humans, J. Appl. Physiol. 63 (1987) 996–1002.

[5] J.R. Balmes, L.L. Chen, C. Scannell, I. Tager, D. Christian, P.Q. Hearne, et al., Ozone-induced decrements in FEV1 and FVC do not correlate with measures of inflammation, Am. J. Respir. Crit. Care Med. 153 (1996) 904–909.

[6] R.B. Devlin, W.F. McDonnell, R. Mann, S. Becker, D.E. House, D. Schreinemachers, et al., Exposure of humans to ambient levels of ozone for 6.6 hours causes cellular and biochemical changes in the lung, Am. J. Respir. Cell Mol. Biol. 4 (1991) 72–81.

[7] M.A. Bauer, M.J. Utell, P.E. Morrow, D.M. Speers, F.R. Gibb, Inhalation of 0.30 ppm nitrogen dioxide potentiates exercise-induced bronchospasm in asthmatics, Am. Rev. Respir. Dis. 134 (1986) 1203–1208.

[8] V. Mohsenin, Airway responses to nitrogen dioxide in asthmatic subjects, J. Toxicol. Environ. Health. 22 (1987) 371–380.

[9] M.W. Frampton, P.E. Morrow, C. Cox, F.R. Gibb, D.M. Speers, M.J. Utell, Effects of nitrogen dioxide exposure on pulmonary function and airway reactivity in normal humans, Am. J. Respir. Crit. Care Med. 143 (1991) 522.

[10] W.F. McDonnell, D.E. Abbey, N. Nishino, M.D. Lebowitz, Long-term ambient ozone concentration and the incidence of asthma in nonsmoking adults: the AHSMOG Study, Environ. Res. 80 (1999) 110–121.

[11] W.J. Gauderman, E. Avol, F.W. Lurmann, N. Kuenzli, F. Gilliland, J. Peters, et al., Childhood asthma and exposure to traffic and nitrogen dioxide, Epidemiology. 16 (2005) 737–743.

[12] N.A. Clark, P.A. Demers, C.J. Karr, M. Koehoorn, C. Lencar, L. Tamburic, et al., Effect of early life exposure to air pollution on development of childhood asthma, Environ. Health Perspect. 118 (2009) 284–290.

[13] J.I. Halonen, T. Lanki, P. Tiittanen, J.V. Niemi, M. Loh, J. Pekkanen, Ozone and cause-specific cardiorespiratory morbidity and mortality, J. Epidemiol. Community Health. 64 (2010) 814–820.

[14] S. Cakmak, R. Dales, J. Leech, L. Liu, The influence of air pollution on cardiovascular and pulmonary function and exercise capacity: Canadian Health Measures Survey (CHMS), Environ. Res. 111 (2011) 1309–1312.
[15] A. Peters, E. Liu, R.L. Verrier, J. Schwartz, D.R. Gold, M.A. Mittleman, et al., Air pollution and incidence of cardiac arrhythmia, Epidemiology. 11 (2000) 11–17.
[16] C.J. Weschler, H.C. Shields, D.V. Naik, Indoor ozone exposures, Japca. 39 (1989) 1562–1568.
[17] J.I. Levy, Impact of residential nitrogen dioxide exposure on personal exposure: an international study, J. Air Waste Manage. Assoc. 48 (1998) 553–560.
[18] N.E. Klepeis, W.C. Nelson, W.R. Ott, J.P. Robinson, A.M. Tsang, P. Switzer, et al., The National Human Activity Pattern Survey (NHAPS), Lawrence Berkeley National Laboratory, 2001.
[19] C.J. Weschler, Ozone's impact on public health: contributions from indoor exposures to ozone and products of ozone-initiated chemistry, Environ. Health Perspect. 114 (2006) 1489–1496.
[20] J.D. Spengler, C.P. Duffy, R. Letz, T. Tibbitts, B.G. Ferris, Nitrogen dioxide inside and outside 137 homes and implications for ambient air quality standards and health effects research, Environ. Sci. Technol. 17 (1983) 164–168.
[21] M.S. Waring, J.A. Siegel, The effect of an ion generator on indoor air quality in a residential room, Indoor Air. 21 (2011) 267–276.
[22] CAFE, Milieu Ltd, Danish National Environmental Research Institute, Center for Clean Air Policy, Comparison of the EU and US air quality standard and planning requirements, DG Environment, 2013.
[23] M.E. Sather, K. Cavender, Trends analysis of ambient 8 hour ozone and precursor monitoring data in the south central U.S, J. Environ. Monitor. 9 (2007) 143–150.
[24] R.G. Derwent, C.S. Witham, S.R. Utembe, M.E. Jenkin, N.R. Passant, Ozone in Central England: the impact of 20 years of precursor emission controls in Europe, Environmental Science and Policy. 13 (2010) 195–204.
[25] C.J. Weschler, Ozone in indoor environments: concentration and chemistry, Indoor Air. 10 (2000) 269–288.
[26] C.J. Weschler, New directions: Ozone-initiated reaction products indoors may be more harmful than ozone itself, Atmos. Env. 38 (2004) 5715–5716.
[27] J. Yu, Deactivation and regeneration of environmentally exposed titanium dioxide based products, Prepared for the environmental protection department, HKSAR, 2003.
[28] Y. Sekine, A. Nishimura, Removal of formaldehyde from indoor air by passive type air-cleaning materials, Atmos. Env. 35 (2001) 2001–2007.
[29] D.A. Kunkel, E.T. Gall, J.A. Siegel, A. Novoselac, G.C. Morrison, R.L. Corsi, Passive reduction of human exposure to indoor ozone, Build. Environ. 45

(2010) 445–452.
[30] E.T. Gall, R.L. Corsi, J.A. Siegel, Barriers and opportunities for passive removal of indoor ozone, Atmos. Env. 45 (2011) 3338–3341.
[31] E.K. Darling, C.J. Cros, P. Wargocki, J. Kolarik, G.C. Morrison, R.L. Corsi, Impacts of a clay plaster on indoor air quality assessed using chemical and sensory measurements, Build. Environ. 57 (2012) 370–376.
[32] C.J. Cros, G.C. Morrison, J.A. Siegel, R.L. Corsi, Long-term performance of passive materials for removal of ozone from indoor air, Indoor Air. 22 (2011) 43–53.
[33] S. Laufs, G. Burgeth, W. Duttlinger, R. Kurtenbach, M. Maban, C.E.S. Thomas, et al., Conversion of nitrogen oxides on commercial photocatalytic dispersion paints, Atmos. Env. 44 (2010) 2341–2349.
[34] H. Chen, C.E. Nanayakkara, V.H. Grassian, Titanium Dioxide Photocatalysis in Atmospheric Chemistry, Chem. Rev. 112 (2012) 5919–5948.
[35] C.J. Cros, A.L. Terpeluk, N.E. Crain, M.G. Juenger, R.L. Corsi, Influence of environmental factors on removal of oxides of nitrogen by a photocatalytic coating, Atmospheric Environment, in Press. (2013).
[36] G. Hüsken, M. Hunger, H.J.H. Brouwers, Experimental study of photocatalytic concrete products for air purification, Build. Environ. 44 (2009) 2463–2474.
[37] H. Dylla, M.M. Hassan, L.N. Mohammad, T. Rupnow, E. Wright, Evaluation of environmental effectiveness of titanium dioxide photocatalyst coating for concrete pavement, Trans. Res. Rec. 2164 (2010) 46–51.
[38] A. Fujishima, K. Honda, Electrochemical photolysis of water at a semiconductor electrode, Nature. 238 (1972) 37–38.
[39] M.M. Ballari, Q.L. Yu, H.J.H. Brouwers, Experimental study of the NO and NO2 degradation by photocatalyticaly active concrete, Catal. Today. 161 (2011) 175–180.
[40] A. Chaloulakou, I. Mavroidis, I. Gavriil, Compliance with the annual NO2 air quality standard in Athens. Required NOx levels and expected health implications, Atmos. Env. 42 (2008) 454–465.
[41] L. Pilotto, R. Douglas, R. Attewell, S. Wilson, Respiratory effects associated with indoor nitrogen dioxide exposure in children, Int. J. Epidemiol. 26 (1997) 788–796.
[42] Z.J. Andersen, L.C. Kristiansen, K.K. Andersen, T.S. Olsen, M. Hvidberg, S.S. Jensen, et al., Stroke and Long-Term Exposure to Outdoor Air Pollution From Nitrogen Dioxide: A Cohort Study, Stroke. (2011) 1–7.
[43] P. Nafstad, L.L. Håheim, T. Wisløff, F. Gram, B. Oftedal, I. Holme, et al., Urban air pollution and mortality in a cohort of Norwegian men, Environ. Health Perspect. 112 (2004) 610–615.
[44] O. Raaschou-Nielsen, Z.J. Andersen, M. Hvidberg, S.S. Jensen, M. Ketzel, M. Sørensen, et al., Lung cancer incidence and long-term exposure to air pollution from traffic, Environ. Health Perspect. 119 (2011) 860–865.

[45] P. Vineis, G. Hoek, M. Krzyzanowski, F. Vigna-Taglianti, F. Veglia, L. Airoldi, et al., Air pollution and risk of lung cancer in a prospective study in Europe, Int. J. Cancer. 119 (2006) 169–174.
[46] W. Foster, P. Stetkiewicz, Regional clearance of solute from the respiratory epithelia: 18-20 h postexposure to ozone, J. Appl. Physiol. 81 (1996) 1143–1149.
[47] R.M. Aris, D. Christian, P.Q. Hearne, K. Kerr, W.E. Finkbeiner, J.R. Balmes, Ozone-induced airway inflammation in human subjects as determined by airway lavage and biopsy, Am. Rev. Respir. Dis. 148 (1993) 1363–1372.
[48] R.L. Auten, W.M. Foster, Biochemical effects of ozone on asthma during postnatal development, Biochim. Biophys. Acta. 1810 (2011) 1114–1119.
[49] M.T. Salam, J. Millstein, Y.-F. Li, F.W. Lurmann, H.G. Margolis, F.D. Gilliland, Birth outcomes and prenatal exposure to ozone, carbon monoxide, and particulate matter: results from the children's health study, Environ. Health Perspect. 113 (2005) 1638–1644.
[50] A.J. Krupnick, W. Harrington, B. Ostro, Ambient ozone and acute health effects: Evidence from daily data, J. Env. Econ. Manage. 18 (1990) 1–18.
[51] A. Gryparis, B. Forsberg, K. Katsouyanni, A. Analitis, G. Touloumi, J. Schwartz, et al., Acute effects of ozone on mortality from the "air pollution and health: a European approach" project, Am. J. Respir. Crit. Care Med. 170 (2004) 1080–1087.
[52] P. Garrett, E. Casimiro, Short-term effect of fine particulate matter (PM2.5) and ozone on daily mortality in Lisbon, Portugal, Environ. Sci. Pollut. Res. 18 (2011) 1585–1592.
[53] B. Revich, D. Shaposhnikov, The effects of particulate and ozone pollution on mortality in Moscow, Russia, Air Qual. Atmos. Health. 3 (2010) 117–123.
[54] M.L. Bell, F. Dominici, J. Samet, A meta-analysis of time-series studies of ozone and mortality with comparison to the national morbidity, mortality, and air pollution study, Epidemiology. 16 (2005) 436–445.
[55] T. Grøntoft, Dry deposition of ozone on building materials. Chamber measurements and modelling of the time-dependent deposition, Atmos. Env. 36 (2002) 5661–5670.
[56] C.P. Hoang, K.A. Kinney, R.L. Corsi, Ozone removal by green building materials, Build. Environ. 44 (2009) 1627–1633.
[57] J. Klenø, P.A. Clausen, C.J. Weschler, P. Wolkoff, Determination of ozone removal rates by selected building products using the FLEC emission cell, Environ. Sci. Technol. 35 (2001) 2548–2553.
[58] G.C. Morrison, W.W. Nazaroff, The rate of ozone uptake on carpets: experimental studies, Environ. Sci. Technol. 34 (2000) 4963–4968.
[59] H. Wang, G.C. Morrison, Ozone-initiated secondary emission rates of aldehydes from indoor surfaces in four homes, Environ. Sci. Technol. 40 (2006) 5263–5268.

[60] G.C. Morrison, W.W. Nazaroff, Ozone interactions with carpet: secondary emissions of aldehydes, Environ. Sci. Technol. 36 (2002) 2185–2192.
[61] M. Nicolas, O. Ramalho, F. Maupetit, Reactions between ozone and building products: impact on primary and secondary emissions, Atmos. Env. 41 (2007) 3129–3138.
[62] D.G. Poppendieck, H.F. Hubbard, C.J. Weschler, R.L. Corsi, Formation and emissions of carbonyls during and following gas-phase ozonation of indoor materials, Atmos. Env. 41 (2007) 7614–7626.
[63] H. Wang, G.C. Morrison, Ozone-surface reactions in five homes: surface reaction probabilities, aldehyde yields, and trends, Indoor Air. 20 (2010) 224–234.
[64] W.W. Nazaroff, G.R. Cass, Mathematical modeling of chemically reactive pollutants in indoor air, Environ. Sci. Technol. 20 (1986) 924–934.
[65] W. Yang, K. Lee, M. Chung, Characterization of indoor air quality using multiple measurements of nitrogen dioxide, Indoor Air. 14 (2004) 105–111.
[66] T. Grøntoft, M.R. Raychaudhuri, Compilation of tables of surface deposition velocities for O3, NO2 and SO2 to a range of indoor surfaces, Atmos. Env. 38 (2004) 533–544.
[67] EPA, Introduction to indoor air quality, Environmental Protection Agency - Office of air and radiation, 1991.
[68] J. Chen, C.-S. Poon, Photocatalytic construction and building materials: from fundamentals to applications, Build. Environ. 44 (2009) 1899–1906.
[69] M.R. Hoffmann, S.T. Martin, W. Choi, D.W. Bahnemann, Environmental applications of semiconductor photocatalysis, Chem. Rev. 95 (1995) 69–96.
[70] M.M. Ballari, M. Hunger, G. Hüsken, H.J.H. Brouwers, Modeling and experimental study of the NOx photocatalytic degradation employing concrete pavement with titanium dioxide, Catal. Today. 151 (2010) 71–76.
[71] J. Dalton, P. Janes, N. Jones, J. Nicholson, K. Hallam, G. Allen, Photocatalytic oxidation of NOx gases using TiO2: a surface spectroscopic approach, Environ. Pollut. 120 (2002) 415–422.
[72] Y. Ohko, Y. Nakamura, N. Negishi, S. Matsuzawa, K. Takeuchi, Photocatalytic oxidation of nitrogen monoxide using TiO2 thin films under continuous UV light illumination, J. Photochem. Photobiol., A. 205 (2009) 28–33.
[73] T. Maggos, J.G. Bartzis, P. Leva, D. Kotzias, Application of photocatalytic technology for NOx removal, Appl. Phys. a: Mater. Sci. Process. 89 (2007) 81–84.
[74] M.M. Ballari, Q.L. Yu, H.J.H. Brouwers, Experimental study of the NO and NO2 degradation by photocatalytically active concrete, Catal. Today. 161 (2011) 175–180.
[75] Y. Murata, K. Kamitani, K. Takeuchi, Air purifying blocks based on photocatalysis, in: JIPEA World Congress, 2000: pp. 570–578.
[76] N. Bengtsson, M. Castellote, Photocatalytic activity for NO degradation by

construction materials: parametric study and multivariable correlations, J. Adv. Oxid. Technol. 13 (2010) 341–349.
[77] S. Devahasdin, C. Fan, K. Li, D.H. Chen, TiO2 photocatalytic oxidation of nitric oxide: transient behavior and reaction kinetics, J. Photochem. Photobiol., A. 156 (2003) 161–170.
[78] T. Lim, S. Jeong, S. Kim, J. Gyenis, Photocatalytic decomposition of NO by TiO2 particles, J. Photochem. Photobiol., A. 134 (2000) 209–217.
[79] Y.-M. Lin, Y.-H. Tseng, J.-H. Huang, C.C. Chao, C.-C. Chen, I. Wang, Photocatalytic activity for degradation of nitrogen oxides over visible light responsive titania-based photocatalysts, Environ. Sci. Technol. 40 (2006) 1616–1621.
[80] M.E. Monge, C. George, B. D'Anna, J.-F. Doussin, A. Jammoul, J. Wang, et al., Ozone formation from illuminated titanium dioxide surfaces, J. Am. Ceram. Soc. 132 (2010) 8234–8235.
[81] C.H. Ao, S.C. Lee, J.Z. Yu, J.H. Xu, Photodegradation of formaldehyde by photocatalyst TiO2: effects on the presences of NO, SO2 and VOCs, Appl. Catal., B. 54 (2004) 41–50.
[82] S. Poulston, M.V. Twigg, A.P. Walker, The effect of nitric oxide on the photocatalytic oxidation of small hydrocarbons over titania, Appl. Catal., B. 89 (2009) 335–341.
[83] A.C. Tamhane, Statistical analysis of designed experiments, A John Wiley & Sons, Inc., Publication, 2009.
[84] R.W. Mee, A comprehensive guide to factorial two-level experimentation, Springer, 2009.
[85] D.G. Poppendieck, E.K. Darling, E. McDonald Buller, Y. Kimura, R.L. Corsi, Dry deposition of ozone to built environment surfaces, Center for Energy and Environmental Resources, University of Texas at Austin, 2011.
[86] K. Asano, Mass transfer: from fundamentals to modern industrial applications, Wiley-VCH, 2007.
[87] ASTM, Standard guide for small-scale environmental chamber determinations of organic emissions from indoor materials/products, ASTM International, West Conshohocken, PA, 2010.
[88] P. Guerrero, R.L. Corsi, Emissions of p-dichlorobenzene and naphthalene from consumer products, J. Air Waste Manage. Assoc. 62 (2012) 1075–1089.
[89] A.L. Terpeluk, Effects of photocatalysis on concrete surfaces, University of Texas at Austin, Civil Engineering, 2012.
[90] B.E. Poling, J.M. Prausnitz, J.P. O'Connell, The properties of gases and liquids, Fifth edition, McGraw-Hill, New York, NY, USA, 2000.
[91] D.G. Poppendieck, H.F. Hubbard, M. Ward, C.J. Weschler, R.L. Corsi, Ozone reactions with indoor materials during building disinfection, Atmos. Env. 41 (2007) 3166–3176.
[92] J.A. Cano-Ruiz, D. Kong, R. Balas, W.W. Nazaroff, Removal of reactive gases

at indoor surfaces: combining mass transport and surface kinetics, Atmos. Env. 27 (1993) 2039–2050.
[93] H.S. Judeikis, A.G. Wren, Laboratory Measurements of NO and NO2 depositions onto soil and cement surfaces, Atmos. Env. 12 (1978) 2315–2319.
[94] G.C. Morrison, P. Zhao, L. Kasthuri, The spatial distribution of pollutant transport to and from indoor surfaces, Atmos. Env. 40 (2006) 3677–3685.
[95] J. Sadowska, B. Johansson, E. Johannessen, R. Friman, L. Bronlarz-Press, J.B. Rosenholm, Characterization of ozonated vegetable oils by spectroscopic and chromatographic methods, Chem. Phys. Lipids. 151 (2008) 85–91.
[96] L.J. Lo, A. Novoselac, Cross ventilation with small openings: measurements in a multi-zone test building, Build. Environ. 57 (2012) 377–386.
[97] TCEQ, ed., Hourly air pollution data, (n.d.).
[98] D. Rim, A. Novoselac, G.C. Morrison, The influence of chemical interactions at the human surface on breathing zone levels of reactants and products, Indoor Air. 19 (2009) 324–334.
[99] A.K. Persily, S.R. Martin, A modeling study of ventilation in manufactured houses, NIST, Gaithersburg, MD, USA, 2000.
[100] K. Lee, J. Vallarino, T. Dumyahn, H. Ozkaynak, J.D. Spengler, Ozone decay rates in residences, J. Air Waste Manage. Assoc. 49 (1999) 1238–1244.
[101] P. Zhao, J.A. Siegel, R.L. Corsi, Ozone removal by HVAC filters, Atmos. Env. 41 (2007) 3151–3160.
[102] G.C. Morrison, W.W. Nazaroff, J.A. Cano-Ruiz, A.T. Hodgson, M.P. Modera, Indoor air quality impacts of ventilation ducts: ozone removal and emissions of volatile organic compounds, J. Air Waste Manage. Assoc. 48 (1998) 941–952.
[103] N. Moussiopoulos, P. Barmpas, I. Ossanlis, J. Bartzis, Comparison of numerical and experimental results for the evaluation of the depollution effectiveness of photocatalytic coverings in street canyons, Environ. Model. Assess. 13 (2007) 357–368.
[104] Y.J. Wang, A. DenBleyker, E. McDonald Buller, D. Allen, K.M. Zhang, Modeling the chemical evolution of nitrogen oxides near roadways, Atmos. Env. 45 (2011) 43–52.
[105] T.N.H. Chung, C.-H. Liu, Large-eddy simulation of reactive pollutant dispersion for the spatial instability of photostationary state over idealized 2D urban street canyons, in: 14th Conference on Harmonisation Within Atmospheric Dispersion Modeling for Regulatory Puroposes, Kos, Greece, 2011.
[106] G.R. McGaughey, N.R. Desai, D.T. Allen, R.L. Seila, W.A. Lonneman, M.P. Fraser, et al., Analysis of motor vehicle emissions in a Houston tunnel during the Texas Air Quality Study 2000, Atmos. Env. 38 (2004) 3363–3372.

Vita

Clément Cros was born in Paris, France on October 13, 1986, to Catherine and René Cros. He studied at Lycée Saint Louis and École Centrale de Lille from which he received his undergraduate degree in June 2008. In the fall of 2008, Clément joined the Environmental & Water Resources graduate program at the University of Texas at Austin. He obtained his Master's degree in May 2010 and pursued his Ph.D. immediately afterwards.

Permanent email: clement.cros@gmail.com

This dissertation was typed by Clément Cros